JPL #5.

[redacted]

THERMO ELECTRON

ENGINEERING CORPORATION

Thermo Electron Engineering Corporation, 85 First Avenue, Waltham, Massachusetts 02154

65-355

Report No. TE67-65

THIRD QUARTERLY PROGRESS REPORT FOR TASK IV (RESEARCH) OF THE SOLAR ENERGY THERMIONIC (SET) CONVERSION DEVELOPMENT PROGRAM

Contract No. 950671

1 December 1964 to 28 February 1965

by

F. Rufeh
N. S. Rasor
D. Lieb
J. H. Weinstein
S. S. Kitrilakis

This work was performed for the Jet Propulsion Laboratory, California Institute of Technology, sponsored by the National Aeronautics and Space Administration under Contract NAS7-100.

Approved by: S. Kitrilakis

S. S. Kitrilakis
Research Manager

TABLE OF CONTENTS

TABLE OF CONTENTS (continued)

LIST OF FIGURES

CHAPTER I

INTRODUCTION AND SUMMARY

The purpose of this experimental program is to generate detailed and highly accurate data on the important parameters involved in the operation of a thermionic converter. This data is being taken over a very broad range of parametric variation, so that it will have general validity for future hardware designs, and so that it may be used for insight and substantiation in analytical work leading to a thorough understanding of the physics involved in the conversion process itself. Such understanding will in turn allow further design optimization of hardware converters and provide the guide lines for future experimentation in thermionics and related fields.

Thermo Electron has performed substantial parametric experimentation in the past,[1,2,3,4] and each study has helped point the way to increased converter performance and to further experimentation. At the same time each program has indicated the need for improved test vehicles and measuring equipment to provide greater accuracy and flexibility in experimentation.

---

1. Annual Technical Summary Report for the Thermionic Emitter Materials Research Program. Report No. TE 2-63, S. S. Kitrilakis, M. E. Meeker, N. S. Rasor.
2. Second Annual Technical Summary Report for the Thermionic Emitter Materials Research Program. Report No. TE 27-64, S. S. Kitrilakis, J. H. Weinstein.
3. Additive Converter Studies, Technical Documentary Report. Report No. TE 35-64, S. S. Kitrilakis, J. H. Weinstein.
4. Emitter Crystal Structure Study, Final Technical Report, Report No. TE 36-64, G. Miskolczy, S. S. Kitrilakis, L. van Someren, J. H. Weinstein.

The present program follows this same course, and calls for making full use of recently developed technology and theoretical knowledge to improve the test vehicle and associated equipment, and to plan a whole series of carefully controlled experiments which allow the isolation and study of each important converter variable. The program should result in a complete set of carefully correlated data and a detailed quantitative description of the conversion process.

During the first two quarters the design, development and fabrication of the two types of converters (cesium only and cesium plus cesium fluoride) were accomplished, as were the design, development and fabrication of the associated test equipment. The result has been shown during operation to provide small interelectrode spacing, increased test vehicle versatility, and an order-of-magnitude increase in the accuracy of the data.

At the same time both tungsten and rhenium emitters were carefully prepared and documented, and an exploratory analysis was performed of ignited-mode operation in preparation for the taking of parametric data on the test vehicle. Finally, the initial experimental work, which consisted primarily of taking emitter and collector work function data and of establishing the reproducibility of the data, was performed. In conjunction with those experiments an analysis of the dependence of collector work function on spacing was also performed.

Significant progress is herein reported for the third quarter. Rapid strides have been made in analysis and correlation. This work, which is reported in Chapter II, is based upon a substantial volume of experimental

data taken during the third quarter. It is the availability of this higher quality of experimentally obtained electrical output characteristics, and identification of the various modes of operation by direct visual observation in a magnetic scanning device, which has permitted the formulation of a greatly improved analytical model of the cesium vapor diode. The relations which correlate the diode variables were obtained by considering the basic processes. These relations are shown to describe the form of the electrical characteristics satisfactorily under a variety of conditions. The constants which yield quantitative agreement with experimental data are also shown to be in good agreement with values computed from the atomic properties of cesium.

Chapter III describes the equations and techniques used in the preparation of a preliminary computer formulation for the parametric analysis. It also shows sample computer runs, computer output summaries, and samples of the graphical tabulations to which the computer output was reduced. The purpose of this work was to provide a frame of reference for taking and reducing data, setting the limits of the most useful areas for parametric studies, and tabulating predicted points with which data can be easily compared to establish first-order validity.

Chapter IV reports the initial additive data and preliminary reduction of results. This series of experiments is known as the fluoride-only phase. That is, only cesium fluoride has been released into the tube while the cesium is held in a capsule for later release. The purpose is to examine the behavior of the tungsten emitter surface as the cesium fluoride coverage is varied by variation in the additive reservoir temperature, and from

this to prepare a map summarizing the relationship between emitter work function, emitter surface temperature and additive reservoir temperature. A very preliminary examination of the data indicates that the relationship between work function and coverage is somewhat more complex with cesium fluoride than with cesium.

The rate of data output, from the three test vehicles, is expected to be very high during the fourth quarter, and data reduction and analysis will be conducted concurrently. For the final report it is expected that a complete set of maps for the cesium-only on rhenium case will be complete, and a much better understanding of the additive case will have been achieved.

CHAPTER II

ANALYTICAL CORRELATION OF CONVERTER PHENOMENOLOGY

I. Introduction

The analysis described here has a practical phenomenological basis; i.e., it springs from a body of data obtained by systematically varying all primary converter variables over the range of values giving practically useful output power densities. This large quantity of data is reduced to a series of parametric plots which facilitate access to the data, but which are independent of interpretation. As illustrated in Figure II-1, such parametric representations of the data are directly useful for engineering design purposes, and indeed have been of significant value in hardware projects. During the course of parametric analysis, correlations among the variables have become apparent. These correlations can be used to reduce the number of variables necessary to represent the data, and thereby simplify the parametric representation without affecting its generality.

Theoretical inquiry into the basic origin of such correlations also has given critical insight into the nature of fundamental processes which dominate converter operation for conditions of practical importance.[1,2] The choice among various possible analytical models is greatly narrowed by the restriction that the model must be consistent with observed converter phenomenology over a great variety of conditions, as well as being self-consistent. In effect, the converter itself serves as an accurate, self-programming analog computer in this approach. Emphasis is placed on defining a coherent reference framework for gaging the implications of existing data, and for intercomparison of various analytical models and sources of data.

During the past few months, due to the availability of data from improved experimental apparatus, rapid progress has been made in synthesizing a coherent physical model which is consistent both with the qualitative visual phenomenology of the discharge and with the quantitative electrical output characteristics, over a wide variety of conditions. Furthermore, the constants relating to the observed data to the analytical model are in much better agreement with probable values of the atomic properties of cesium than for the earlier models.

Since the analysis and the comparison with data are not yet complete, only the most important features will be outlined and illustrated with representative data here. A more complete and qualified description will be presented in the forthcoming Annual Summary Report.

II. Saturation Mode of the Cesium Diode Discharge

A. Analytical Model - The region AB of the electrical output characteristic in Figure II-2 is designated as the "saturation mode", and the corresponding motive diagram is shown in Figure 3a. The stream of electrons from the emitter, equal to the saturation current density J_s, gains an energy V_e as it is accelerated across the emitter sheath, and this energy is dissipated in the plasma a short but finite distance from the emitter. The resulting average electron temperature in this region T_ϵ is sufficiently high to produce the ions required to sustain the plasma. Assuming a neutral plasma of width d much greater than the electron mean-free-path, it is shown in Appendix A that the current density of electrons reaching the collector is given by

$$J = \frac{J_s}{1 + \exp\left(-V_e/kT_{\epsilon e}\right)\left[\frac{3}{4}\frac{d}{\lambda} + R\right]} \qquad \text{for } V<V^* \qquad (1)$$

where

$$R = \exp\left(V_c/kT_{\epsilon e}\right) - 1 \tag{2}$$

$T_{\epsilon e}$ and $T_{\epsilon c}$ are the respective electron temperatures at the emitter and collector edges of the plasma, and V_c is the potential energy drop across the collector sheath.

The physical significance of Eq. 1 is that the current $J_s - J$ returning to the emitter from the plasma is made up of two components: R is the fraction of J which is reflected by the collector sheath barrier V_c, and $\frac{3}{4}\frac{d}{\lambda}$ is the fraction which is reflected by the plasma. The fraction of these reflected currents which then surmounts the emitter sheath barrier is $\exp\left(-V_e/kT_{\epsilon e}\right)$.

It is shown in Appendix B that for $d \gg \lambda$ the transport of energy across the plasma requires

$$kT_{\epsilon c} = kT_{\epsilon e} - V_c/2 \tag{3}$$

Also, as may be seen in Fig. 3a,

$$V_e = \phi_e - \phi_c + V_c - eV \tag{4}$$

Thus, Eqs. 1-4 prescribe the electrical output characteristics J(V) in the saturation mode.

B. Analysis of Data. To facilitate comparison with experimental data, Eqs. 1-4 combine to give

$$\frac{J_s}{J} = 1 + A\,(pd + D)\,\exp\left[\frac{eV}{kT_{\epsilon e}}\right] \tag{5}$$

where the quantities

$$A = \frac{3}{4(p\lambda)} \exp\left[-\frac{\phi_e - \phi_c + V_c}{kT_{\epsilon e}}\right] \tag{6}$$

and

$$D = \frac{4}{3}(p\lambda) \exp\left(V_c/kT_{\epsilon c} - 1\right) \tag{7}$$

should be essentially constant under conditions where $T_{\epsilon e}$ does not change appreciably.

Figure II-4 is a family of output characteristics in which only the electrode spacing is changed; all other experimental variables are held constant. In Fig. 5 it may be seen that the data gives a linear relationship between $\frac{1}{J}$ and pd for constant values of $V > V^*$.

These lines converge at a single point which, according to Eq. 5, defines the values of J_s and D. Furthermore according to Eq. 5, the slope of these curves is given by

$$\frac{d\left(\frac{J_s}{J}\right)}{d(pd)} = A \exp\left[\frac{eV}{kT_{\epsilon e}}\right] \tag{8}$$

so that A is the slope of the curve for V = 0.

Using the value of J_s in Fig. 5, the output characteristics of Fig. 4 can be plotted as in Fig. 6, where Eq. 5 becomes a linear equation in V of the form

$$\ell n\left[\frac{J_s}{J} - 1\right] = \left[\ell n\, A(pd+D)\right] + \frac{eV}{kT_{\epsilon e}} \tag{9}$$

Since the slope of each curve in Fig. 6 is $1/kT_{\epsilon e}$, it is possible to obtain the dependence of electron temperature on pd as shown in Fig. 7.

The value of ϕ_e can be computed from the value of J_s obtained in Fig. 5 using the Richardson equation

$$\phi_e = kT_e \ell n\left(\frac{AT_e^2}{J_s}\right) \tag{10}$$

and ϕ_c is known from independent data.[4] Thus, with these known values of ϕ_e and ϕ_c, and using the values of $kT_{\epsilon e}$ in Fig. 7, the values of A and D obtained from Fig. 5 can be used to compute V_c and $(p\lambda)$ from Eqs. 6 and 7. Since it is not possible to solve explicitly for these quantities, Fig. 8 is a plot of the combination of Eqs. 6 and 7 from which the value of V_c can be obtained easily.

Inspection of Figs. 5 - 7 shows that Eq. 5 describes the data in Fig. 4 for the following set of values:

$J_s = 21.1 \text{ amp/cm}^2$

$A = 0.025 \text{ (mil-torr)}^{-1}$

$D = 14 \text{ mil-torr}$

$kT_{\epsilon e} \approx 0.4 \text{ eV}$ (or, more precisely, from Fig. 7)

which are consistent with Eqs. 6, 7 and 9 for the values

$T_e = 1800°K$, $T_c = 700°K$, $T_R = 580°K$ $(p = 2.25 \text{ torr})$

$\phi_e = 2.60 \text{ eV}$, $\phi_c = 1.90 \text{ eV}$, $V_c = 0.38 \text{ eV}$

$(p\lambda) = 2.0 \text{ mil-torr}$

C. Comparison with Basic Physical Constants - The foregoing has shown that the analytical model satisfactorily correlates the experimental variables. A more critical test of the model is the extent of quantitative agreement of the correlation constants with those computed from the physical properties of the cesium atom.

1. Electron Mean Free Path λ - Table I compares the value of $(p\lambda)$ obtained here, and the associated electron-atom collision cross-section $\sigma = kT_o/(p\lambda)$, with values reported or estimated by others[5] for the same region of electron temperatures.

TABLE I

Source	σ ($\mathring{A}^2$)	$p\lambda$ (mil-torr)
Present value	500	2.0
Nottingham[a]	400	1.6
Warner & Hansen[a]	400	1.6
Boekner & Mohler[b]	300	1.2
Stone & Reitz[c]	450	1.8
Robinson[c]	500	2.0
Garret & Mann[c]	650	2.6

a = estimated most probable value

b = experimental

c = theoretical

As may be seen, the value $(p\lambda) = 2.0$ mil-torr is quite close to the most probable value, and falls well within the region of uncertainty.

2. Collector Sheath Height V_c - It is shown in Appendix C that V_c should

be approximately proportional to electron temperature $T_{\epsilon c}$. The values of V_c = 0.38 eV and $T_{\epsilon e} \approx 0.4$ eV observed here imply, through Eqs. 3 and C-3, that the effective thickness of the collector sheath remains constant at about N = 2 Debye lengths, a quite satisfactory result.

3. Electron Temperature $T_{\epsilon e}$ - It is shown in Appendix D that the electron temperature required to produce the ions diffusing out of the plasma is independent of current J_s as observed in Fig. 6. Furthermore, the required electron temperatures, computed using the probable values[7] of the ionization and diffusion cross sections, agree well with those observed here, and approximate the observed dependence on pd.

In view of this agreement, it appears that for practical purposes the electrode spacing d can be identified with the width of the ion generation region d^*, and the electron temperature $T_{\epsilon e}$ with T_ϵ. Accordingly, the electron temperature can be eliminated from Eq. 1 since, using Eq. D-3,

$$\exp\left(V_e/kT_{\epsilon e}\right) = \left(B_s\, pd\right)^{2\, V_e/V_i} \qquad (11)$$

III. Obstructed Mode of the Discharge

A. Analytical Model - The power input to the plasma is $J(V_e + 2kT_e)$. As V is increased, V_e is decreased, and this power must eventually fall below that required to maintain the high electron temperature sustaining the plasma under the conditions in Fig. 3a. It is evident from observed data such as Fig. 4, and from the energy balance considered in Appendix E, that the plasma can continue to exist through impact ionization at still higher V only if a certain minimum

emitter sheat height V_e^* is maintained.[1] This results in the situation in Fig. 3c, where a space charge barrier exists at the emitter of sufficient height to maintain this minimum value of V_e^* for $V>V^* = \phi_e - \phi_c + V_c - V_e^*$. The region BC of Fig. 2, where this barrier exists and thus limits the electron emission current from the emitter, is designated as the "obstructed mode".

In the obstructed mode, the saturation electron emission current J_s in Eq. 1 is replaced by the current J_s^* emitted over the new barrier of height $V-V^*$, and V_e is replaced by V_e^*; so Eq. 1 becomes

$$J = J^* \exp\left(\frac{V^* - V}{kT_e}\right) \qquad \text{for } V > V^* \qquad (12)$$

where J^* is the value given by Eq. 1 with $V_e = V_e^*$. The transition point V^*, designated B in Fig. 2 and illustrated in Fig. 3b, is of considerable practical significance since maximum power output typically occurs there. It usually is readily identified in experimental output characteristics as a point of inflection.

B. Analysis of Data - Values of V_e^* are most easily obtained from such directly observed values of V^*. A more precise method is to plot the J-V characteristics on a log plot and identify V^* as the point of intersection between a linear extrpolation of the obstructed mode (slope = $\frac{1}{kT_e}$) and of the saturation mode (slope $\approx \frac{1}{kT_\epsilon}$). Values of V_e^* obtained from the data in Fig. 4, using the values of ϕ_e, ϕ_c and V_c determined in Section II-C-3, are shown in Fig. 9. Values obtained similarly from other data are included in Fig. 9, showing that V_e^* (pd) is essentially independent of pressure and $\phi_e - \phi_c$.

C. Comparison with Physical Model - The electron energy balance for the plasma is shown in Appendix E to enforce a unique relationship between V_e and pd. In the saturation mode, where V_e is dependent on V, a large part of the energy input to the plasma is returned to the emitter by the electrons back-scattered from the plasma, due to the direct communication between emitter and plasma. As a result, both electron temperature T_ϵ and plasma size d' can remain relatively constant over a wide range of V. In the obstructed mode, however, the dark barrier region between the emitter and bright plasma (Fig. 3c) greatly reduces both the emission into the plasma and the amount of high energy electrons back-reflected to the emitter from the plasma. The value of V_e' which characterizes the obstructed mode, therefore, is independent of current, as given in Eq. E-5, and has the computed dependence on pd shown in Fig. 8, using Eqs. D-3 and D-4.

The value of C which best fits the data in Fig. 8 corresponds to a value for the ratio of excitation and ionization cross section of $K_x/K_i \approx 0.3$, which is far different from the estimated[7] most probable value of 18. While there is considerable uncertainty in this value, the disagreement is well outside the probable range of error. Future work will attempt to determine the cause of this disagreement.

IV. Ball-of-Fire Mode. In the obstructed mode, the energy requirements of the plasma imposed by Eq. E-5 (Fig. 9) are met for $V_e < V_e'$ through the existence of an energy barrier at the emitter of sufficient height to accommodate the required emitter sheath V_e' associated with electrode spacing d. An alternate mode by which the discharge can satisfy E-5 is to exist with an emitter sheath of height $V_e = V_e'$ associated with a smaller d; i.e., the plasma occupies only a small part of the interelectrode space with an effective plasma width of $d' < d$. Visual obser-

vation of the discharge shows that such a condition occurs in the region BE of the output characteristics as shown in Fig. 2. This well-known "ball-of-fire" mode of the discharge is of only academic interest since it occurs in a region of inefficient power generation. Photographic evidence supporting the above description will be given in the forthcoming Annual Report.

V. Extinguished Mode. Eq. 1 has been shown previously[8,9] to also describe the extinguished mode for ion rich emission, as shown in Fig. 3e and identified as region FD in Fig. 2. In this case the emitter sheath height is essentially independent of V and pd, now having the form

$$V_e = kT_e \ln \beta \tag{13}$$

where $\beta = \left(\frac{M}{m}\right)^{\frac{1}{2}} \frac{\mu e}{J_s}$ is the ion richness ratio. The collector sheath height now depends on V to satisfy Eq. 4, and $kT_{\epsilon e} \approx kT_{\epsilon c} \approx kT_e$.

VI. Summary. A coherent formalism has been obtained which describes most of the phenomenology of the cesium diode discharge, and which correlates the variables satisfactorily for the several cases analyzed to date. Furthermore, the correlating constants agree well with those computed from basic physical constants, with a single notable exception. Future work will further test the generality of this formalism over a greater range and variety of experimental variables (e.g. the effect of collector temperature[2]). An attempt also will be made to overcome the weaknesses presently apparent in the analytical model.

REFERENCES

1. S. Kitrilakis, A. Shavit and N. Rasor, Rept. of MIT Physical Electronics Conf. (Mar. 1964) p. 171

2. N. Rasor and S. Kitrilakis, Rept. of Thermionic Conv. Specialist Conf., Cleveland (Oct. 1964) p. 227

4. A. Shavit and S. Kitrilakis, AFCRL-64-721, TE 7-65 (1964)

5. L. Hansen & C. Warner, Rept. of TCSC, Gatlinburg (Oct. 1963) p. 44

6. L. Tonks and I. Langmuir, Phys. Rev. 33 195 (1929)

7. J. Houston, Rept. of TCSC, Cleveland (Oct. 1964)

8. L. Hansen & C. Warner, ibid p. 310

9. A. Shavit and G. Hatsopoulos, ibid p. 206

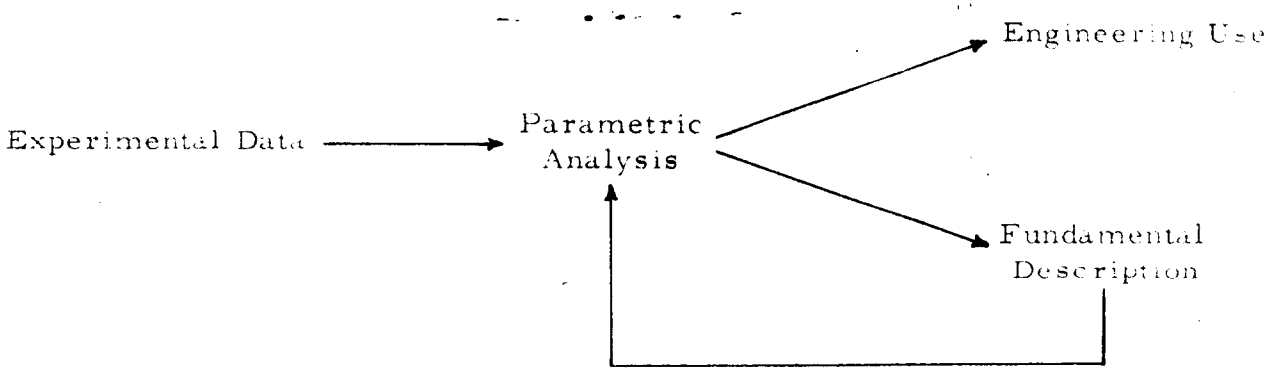

Figure II-1. Phenomenological Approach.

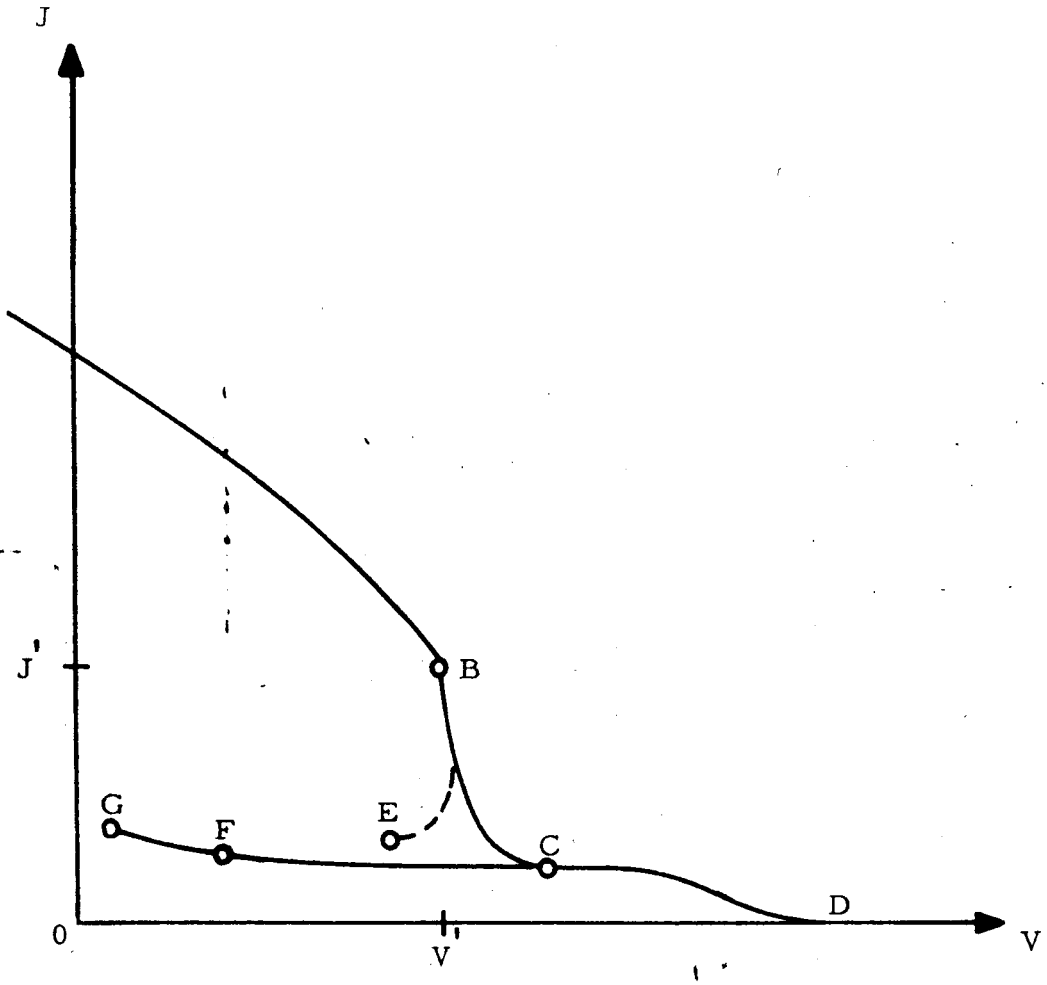

Figure II-2. Identification of Discharge Modes in Electrical-Output Characteristics.

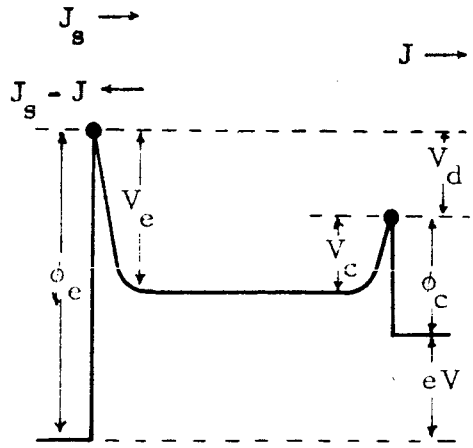

(a)

Saturation Mode (A-B)

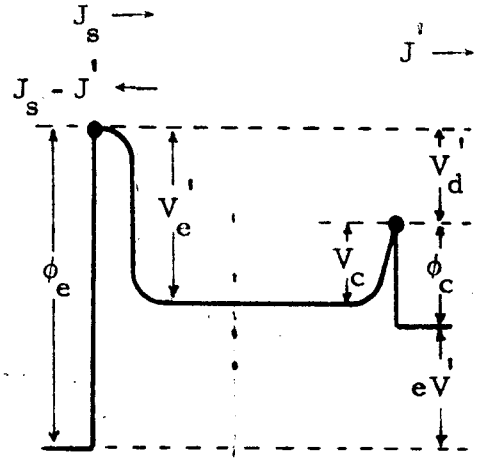

(b)

Transition Point (B)

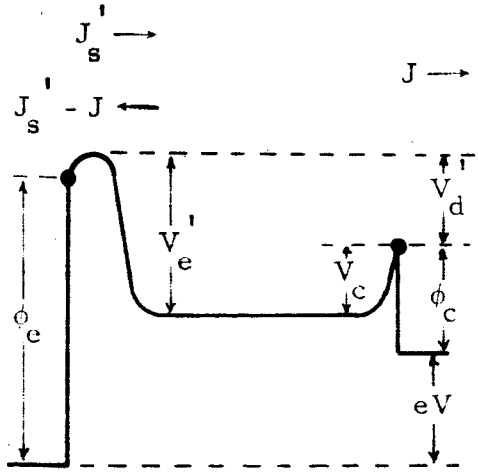

(c)

Obstructed Mode (BC)

Figure II-3. Motive Diagram for Modes of Discharge.

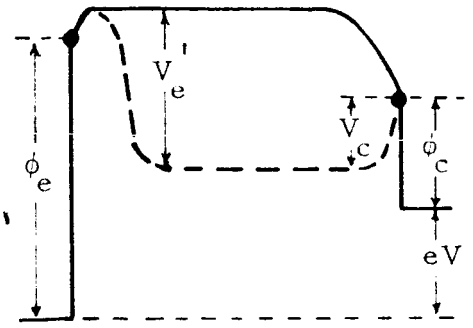

(d)

Ball-of-Fire Mode (BE)

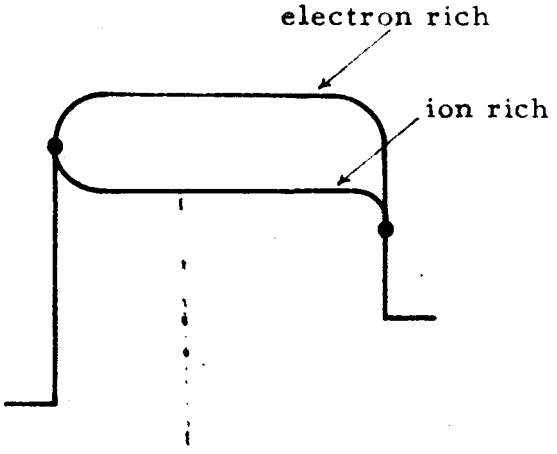

(e)

Extinguished Mode (FD)

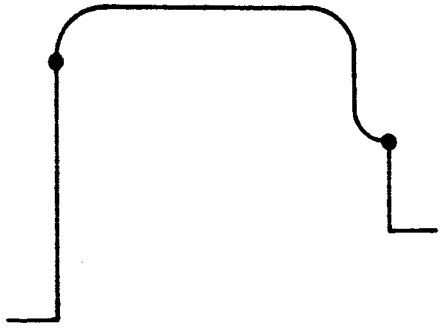

(f)

Collector Glow Mode (FG)

Figure II-3. Motive Diagram for Modes of Discharge.

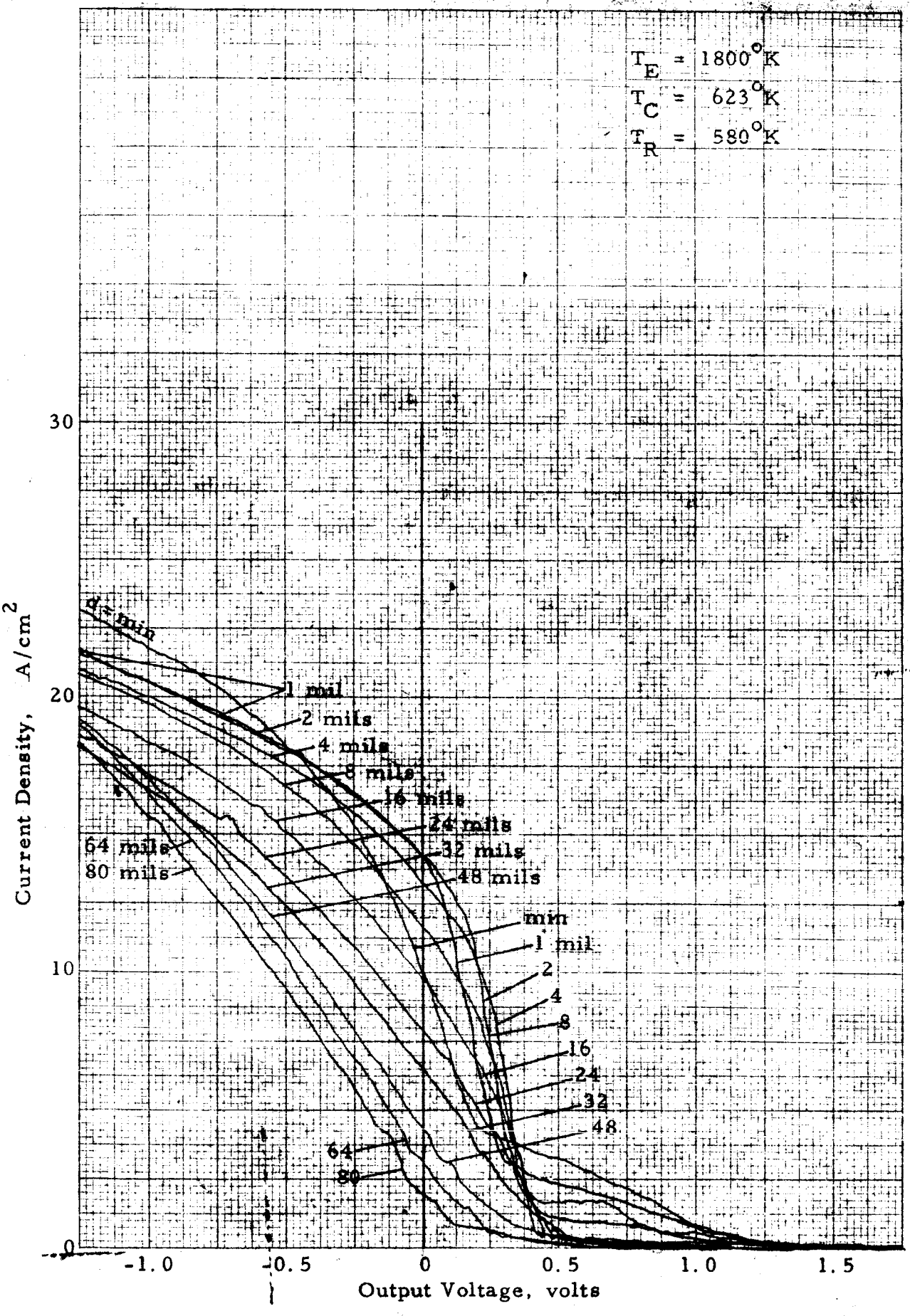

Figure II-4. Typical Variable-Spacing J-V Characteristics.

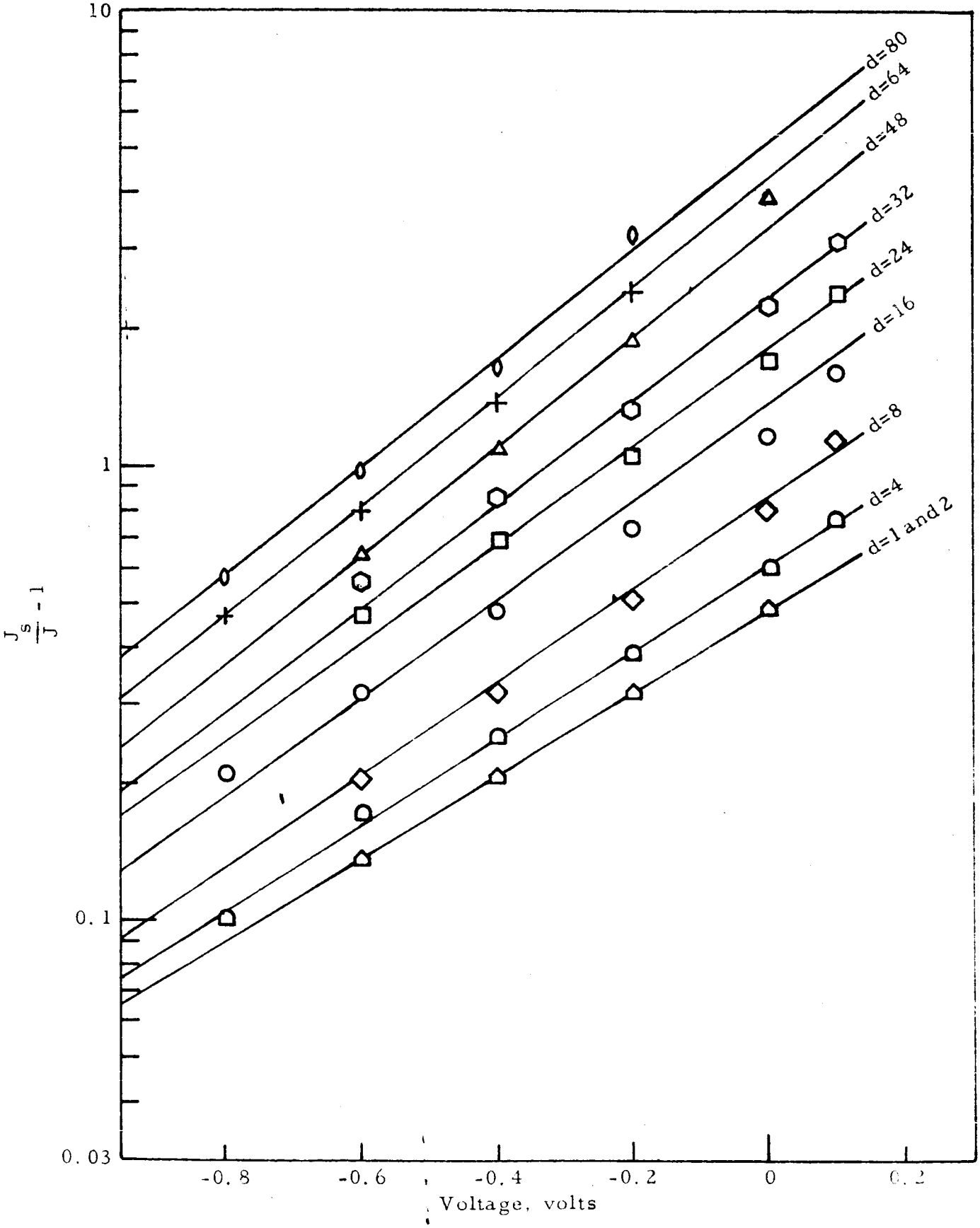

Figure II-6. $\frac{J_s}{J} - 1$ versus Output Voltage.

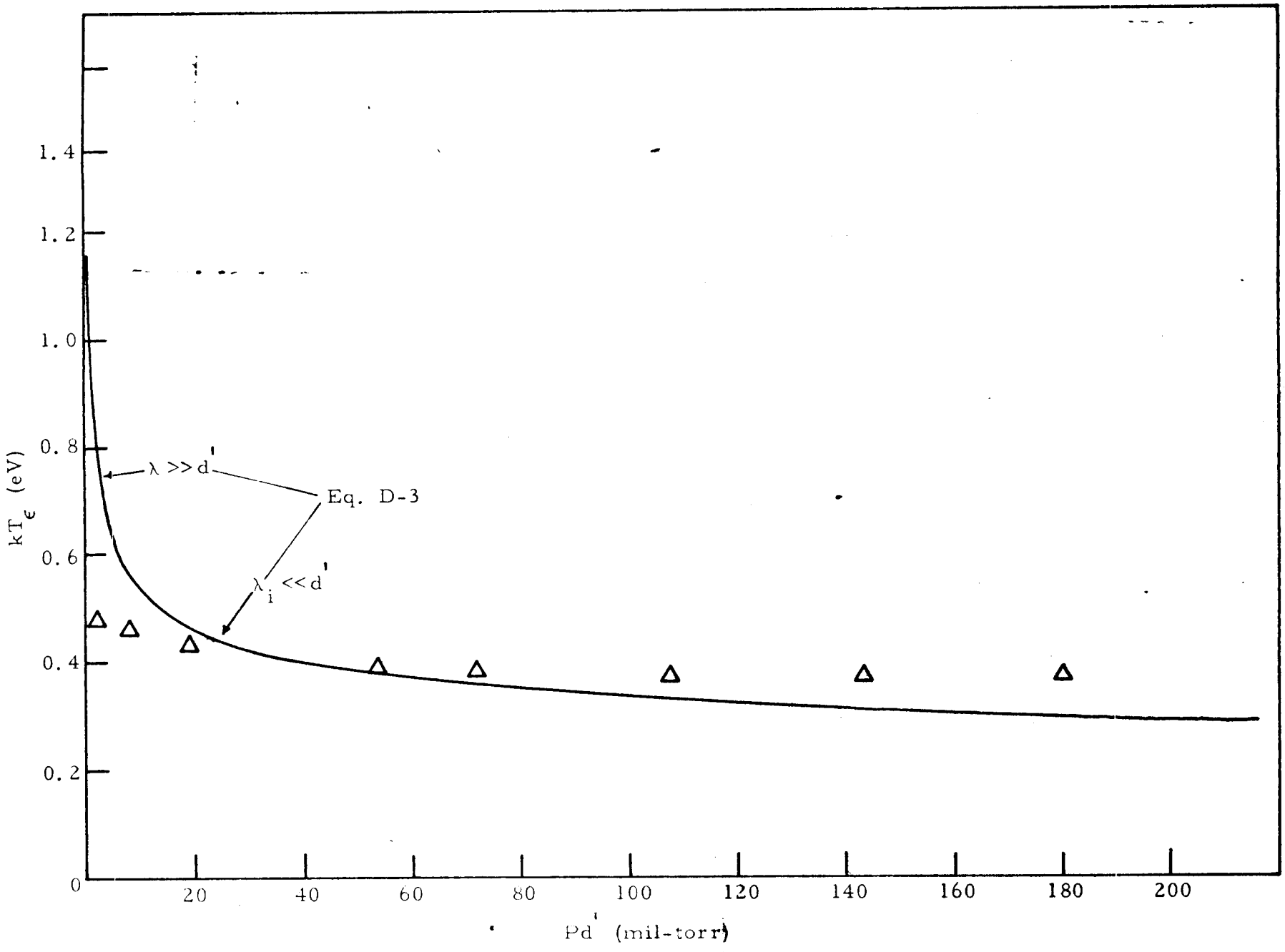

Figure II-7. Comparison of Observed and Computed Electron Temperatures.

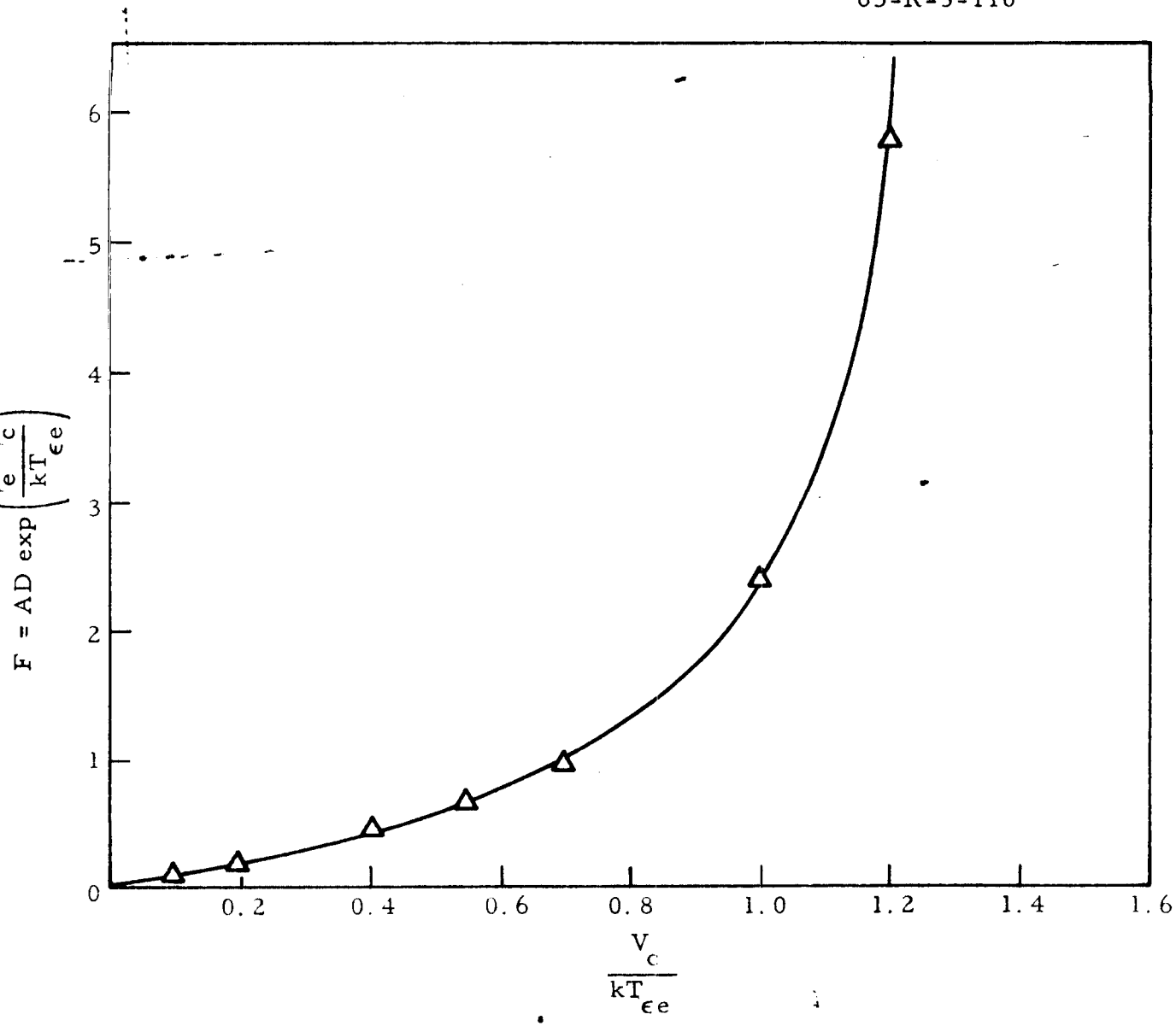

Figure II-8. Graphical Determination of V_c

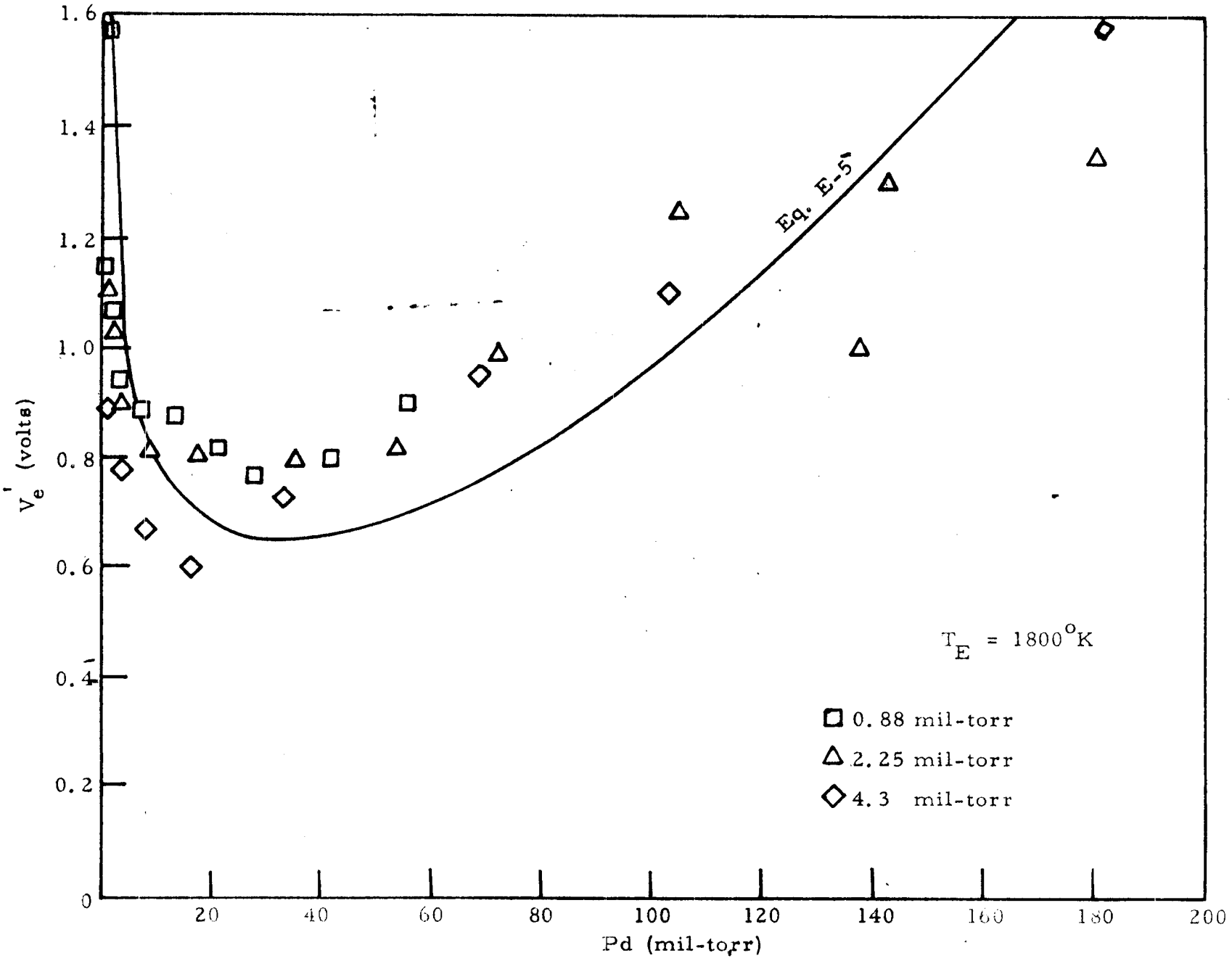

Figure II-9. Comparison of Observed and Computed Emitter Sheath Height

CHAPTER III

PRELIMINARY COMPUTER FORMULATION FOR PARAMETRIC STUDIES

The usefulness of the parametric studies, which form an important part of this program, is greatly enhanced if experimental results can be anticipated to some extent. To put it more directly, it is significantly simpler to formulate a relationship among a number of variables if a rough idea is available of what the relationship is. Based, therefore, on past experience and the guidance of the analytical work of this program, a framework has been constructed which gives a rough idea of what is to be expected from the parametric experiments. This framework has the form of maps of current-voltage characteristics and power characteristics for the rhenium-molybdenum system. These maps are based on the properties of the electrode materials and correlations of the different variables affecting the conversion process. Some of these correlations are quite exact and well-known. Others are rather vague and inaccurate and, in fact, constitute the object of much of the experimental work that is carried on in this program. The result, however, is that at least an order-of-magnitude answer is available with which to gauge experimental results that are obtained, and also to anticipate trends and dependencies among the variables.

To construct these performance maps, the following relationships were used:

The work function of the rhenium surface in therms of the ratio of surface to reservoir temperature. (See Table of Nomenclature on page III-12.)

$$\phi_e = -.106\ T_e/T_R\ (T_e/T_R - 19.86) - 2.821$$

This equation is a fit of the data shown in Figure III-1.

The cesium pressure is given in terms of the reservoir temperature by:

$$P = \frac{2.45 \times 10^8}{\sqrt{T_R}}\ e^{-\frac{8.91 \times 10^3}{T_R}}$$

The output current is given in terms of work function and emitter temperature by:

$$J_m = 120\ T_C^2\ \exp\left(-\frac{11.6 \times 10^3\ \phi_e}{T_e}\right) \times \frac{1}{2}$$

The cesium gas conduction is given in terms of emitter temperature, collector temperature, spacing, and cesium pressure by:

$$Q_{cs} = \frac{5.25 \times 10^{-2}\ (T_e - T_c)}{2.5d + \frac{1.15 \times 10^{-2}(T_e + T_c)}{P}}$$

The internal voltage drop is given in terms of the product Pd by:

$$V_d = \{[(Pd - 213)Pd + 8 \times 10^3]\ Pd \times .75 \times 10^{-6}\} + .535$$

The output voltage corresponding to the output current J_m is given by:

$$V = \phi_e - \phi_c - V_d + \frac{T_e}{11.6 \times 10^3} \ln J_m/J_s$$

The power at the electrodes is given by:

$$P_{el} = VJ_m$$

The heat loss other than lead conduction is given by:

$$Q = J_m \phi_e \ln \frac{1}{2} + Q_{rad} + Q_{cs}$$

The efficiency to a first approximation is equal to:

$$\eta = \frac{P_{el}}{Q}$$

The following relationships exist among the electrical and thermal lead losses and converter properties.

$$P_{lead} = S\,C\,J_m$$

$$Q_{lead} = C/S\,J_m$$

$$P_{out} = P_{el} - P_{lead}$$

$$\eta_{opt} = \frac{P_{out}}{Q + Q_{lead}} - \frac{P_{out}}{2}$$

where

$$C = \sqrt{P - k(T_e - T_c)}$$

and

$$S = \frac{\eta}{1 - \eta/2}$$

Based on these relationships, a program was written, and a G. E. 225 computer was used to solve for the unknowns in terms of selected values of the independent variables. The independent variables are: the emitter temperature, collector work function, reservoir temperature, and spacing. The solution is really the constant-spacing envelope; i. e., the maximum current obtainable at a given voltage for fixed spacing and emitter temperature. Figure III-2 is a typical run. At the top of the page the chosen values of emitter temperature and collector work function are shown. Next, cesium reservoir and spacing values are selected. The remaining variables are computed from the relationships previously described. If, however, the product Pd turns out to be less than 10, a minus sign is placed in front of the spacing value to indicate that the computation is invalid, since the internal voltage drop correlation does not hold. Figure III-3 is a summary at each spacing value computed in Figure III-2. The summarizing process consists of selecting the maximum efficiency and power points at each spacing and computing the output characteristics for a Cs pressure above and below the optimum point. Care was exercised to write the program in such a manner that new relationships among the variables, which are expected to develop, can easily be incorporated.

The computer solutions have been plotted in the form of output current versus output voltage. A typical map is shown in Figure III-4. The solid lines are lines of output for a fixed collector work function value. The collector work function values shown range from 1.5 ev to 1.8 eV. The emitter temperature and spacing are fixed for the map and are 2000°K and 2 mils, respectively. Each solid line in the map, corresponding to a work function value, is the maximum output obtainable with a given emitter temperature and spacing, and collector work function, if all other variables are optimized.

To the right of the plot, the cesium reservoir temperature necessary to achieve this output is shown, and, in the form of dotted lines crossing the solid lines, lines of constant collector temperature are shown.

From the data of Figure III-2 the map of Figure III-5 has been constructed. Here, again, the solid lines are lines of constant collector work function. Lines of constant cesium reservoir temperature are shown as dotted lines, and lines of constant collector temperature are identified.

It should be noted that the analysis used in this program is not valid for instances where the Cs pressure-spacing product is below 10 mil-torr. The plots, therefore, are limited to the regions where the product, Pd, has values above 10. Solutions have been obtained for emitter temperatures from 1600°K to 2000°K in 100° steps for spacings of 1, 2, 5, 10 and 20 mils, whenever the pressure-spacing product is above 10.

The collector work function range is from 1.5 to 1.8eV in 0.1-V steps. As parametric power data become available in the program, they will be compared with these solutions. Adjustments will be made in the analysis and in the correlations that resulted in these computer solutions as becomes necessary in the light of the experimental results.

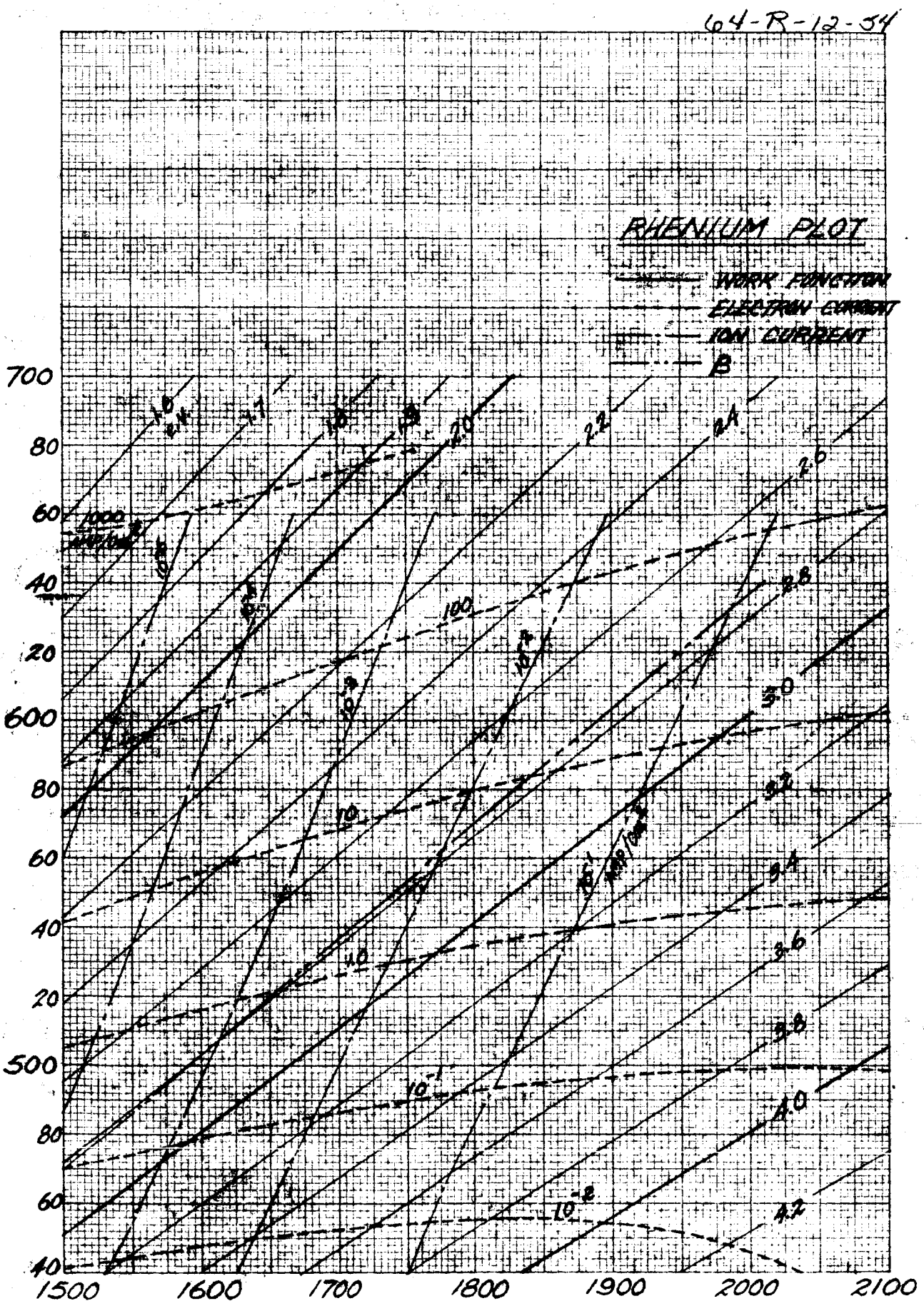

Figure III-1. Rhenium Map.

POWER OUTPUT AND EFFICIENCY CALCULATION

RHENIUM

EMITTER TEMP. 1900 DEG. K , COLLECTOR W.F. 1.70 EV.

TK	D MIL	J A/SQC	V VOLT	P OUT W/SQC	EFF PCT	EMIT EV	VD VOLT	QL W/SQC	P EL W/SQC
630	-1.0	34.5	0.477	13.8	14.5	2.564	0.500	17.0	16.5
640	-1.0	52.7	0.414	17.9	13.2	2.494	0.494	27.2	21.8
650	1.0	79.6	0.352	22.6	11.5	2.427	0.488	44.2	28.0
660	1.0	119.1	0.292	27.4	9.6	2.361	0.482	72.9	34.8
670	1.0	176.5	0.233	31.6	7.5	2.296	0.477	123.1	41.1
680	1.0	259.1	0.174	33.3	5.2	2.234	0.473	217.3	45.0
690	1.0	377.1	0.113	30.0	3.0	2.172	0.472	422.3	42.7
700	1.0	543.9	0.050	17.4	0.9	2.112	0.475	1111.8	27.4
710	1.0	778.1	-0.016			2.05	0.483		-12.7
720	1.0	1104.0	-0.065			2.00	0.498		-97.7
730	1.0	1554.1	-0.168			1.94	0.522		-261.0
740	1.0	2171.2	-0.256			1.89	0.555		-555.5
750	1.0	3011.0	-0.353			1.83	0.598		-1062.5
550	-2.0	0.8	1.076	0.8	5.4	3.186	0.524	0.6	0.8
560	-2.0	1.3	0.994	1.2	7.4	3.101	0.521	0.9	1.3
570	-2.0	2.1	0.915	1.8	9.7	3.018	0.517	1.3	2.0
580	-2.0	3.5	0.839	2.7	11.9	2.938	0.512	1.9	3.0
590	-2.0	5.7	0.766	3.9	14.0	2.859	0.506	2.7	4.4
600	-2.0	9.1	0.696	5.6	15.4	2.782	0.500	4.1	6.3
610	-2.0	14.3	0.628	7.8	16.2	2.708	0.493	6.7	9.0
620	2.0	22.4	0.562	10.7	16.2	2.635	0.487	10.4	12.6
630	2.0	34.5	0.497	14.4	15.5	2.564	0.480	16.4	17.2
640	2.0	52.7	0.433	18.8	14.2	2.494	0.475	26.2	22.8
650	2.0	79.6	0.368	23.7	12.4	2.427	0.472	42.6	29.3
660	2.0	119.1	0.300	28.2	10.1	2.361	0.474	71.1	35.8
670	2.0	176.5	0.228	30.8	7.4	2.296	0.482	124.1	40.3
680	2.0	259.1	0.150	28.2	4.3	2.234	0.497	240.3	38.8
690	2.0	377.1	0.062	15.1	1.2	2.172	0.524	663.4	23.2
700	2.0	543.9	-0.037			2.11	0.563		-20.4
710	2.0	778.1	-0.148			2.05	0.615		-115.3
720	2.0	1104.0	-0.269			2.00	0.678		-296.6
730	2.0	1554.1	-0.392			1.94	0.746		-609.0
740	-2.0	2171.2	-0.503			1.89	0.801		-1091.1
750	-2.0	3011.0	-0.572			1.83	0.817		-1722.5
550	-5.0	0.8	1.090	0.8	5.5	3.186	0.510	0.6	0.8
560	-5.0	1.3	1.012	1.2	7.7	3.101	0.503	0.9	1.3
570	-5.0	2.1	0.936	1.9	10.2	3.018	0.496	1.3	2.0
580	5.0	3.5	0.863	2.8	12.7	2.938	0.488	1.9	3.0
590	5.0	5.7	0.792	4.1	15.0	2.859	0.480	2.7	4.5
600	5.0	9.1	0.721	5.8	16.7	2.782	0.475	4.1	6.6
610	5.0	14.3	0.649	8.1	17.4	2.708	0.472	6.4	9.3
620	5.0	22.4	0.572	10.9	17.1	2.635	0.476	10.1	12.8
630	5.0	34.5	0.488	14.1	15.6	2.564	0.489	16.3	16.8
640	5.0	52.7	0.393	16.9	12.9	2.494	0.515	27.6	20.7
650	5.0	79.6	0.284	17.8	9.1	2.427	0.556	50.2	22.6
660	5.0	119.1	0.158	14.0	4.4	2.361	0.616	109.0	18.9
670	5.0	176.5	0.020	2.0	0.2	2.296	0.690	797.8	3.5
680	5.0	259.1	-0.120			2.23	0.767		-31.1
690	-5.0	377.1	-0.231			2.17	0.817		-87.3
700	-5.0	543.9	-0.256			2.11	0.782		-139.2

APPROX. 111 , CONST.-TC 900 K, F0.15 , J/JS0.50 , RK 3.78E-05 V /DEG

Figure III-2. Typical Run — Output from Computer

POWER OUTPUT AND EFFICIENCY CALCULATION

RHENIUM
EMITTER TEMP. 1900 DEG. K , COLLECTOR W.F. 1.70 EV.

TR K	D MIL	J A/SQC	V VOLT	P OUT W/SQC	EFF PCT	EMIT EV	VD VOLT	QL W/SQC	P EL W/SQC
600	-0.2	9.1	0.665	5.4	14.0	2.782	0.531	4.6	6.0
610	-0.2	14.3	0.591	7.4	14.4	2.708	0.530	7.1	8.5
620	-0.2	22.4	0.520	9.9	14.0	2.635	0.528	11.2	11.6
660	-0.2	119.1	0.254	23.6	7.8	2.361	0.520	81.1	30.3
670	-0.2	176.5	0.192	25.7	5.7	2.296	0.518	141.7	34.0
680	-0.2	259.1	0.133	24.8	3.6	2.234	0.514	264.6	3 .4
600	-0.5	9.1	0.671	5.4	14.3	2.782	0.525	4.5	6.1
610	-0.5	14.3	0.599	7.5	14.8	2.708	0.522	7.0	8.6
620	-0.5	22.4	0.529	10.1	14.5	2.635	0.519	11.0	11.8
670	-0.5	176.5	0.213	28.6	6.6	2.296	0.497	131.6	37.6
680	-0.5	259.1	0.156	29.5	4.5	2.234	0.492	235.6	40.3
690	0.5	377.1	0.100	26.0	2.5	2.172	0.486	465.1	37.6
600	-1.0	9.1	0.680	5.5	14.7	2.782	0.516	4.4	6.2
610	-1.0	14.3	0.610	7.6	15.3	2.708	0.511	6.9	8.7
620	-1.0	22.4	0.542	10.4	15.2	2.635	0.506	10.7	12.1
670	1.0	176.5	0.233	31.6	7.5	2.296	0.477	123.1	41.1
680	1.0	259.1	0.174	33.3	5.2	2.234	0.473	217.3	45.0
690	1.0	377.1	0.113	30.0	3.0	2.172	0.472	422.3	42.7
610	-2.0	14.3	0.628	7.8	16.2	2.708	0.493	6.7	9.0
620	2.0	22.4	0.562	10.7	16.2	2.635	0.487	10.4	12.6
630	2.0	34.5	0.497	14.4	15.5	2.564	0.480	16.4	17.2
660	2.0	119.1	0.300	28.2	10.1	2.361	0.474	71.1	35.8
670	2.0	176.5	0.228	30.8	7.4	2.296	0.482	124.1	40.3
680	2.0	259.1	0.150	28.2	4.3	2.234	0.497	240.3	38.8
740	-5.0	2171.2	4.148	9005.7	315.7	1.885	-3.849	0.0	9005.7
750	-5.0	3011.0	8.546	25732.5	670.4	1.832	-8.301	0.0	25732.5
760	-5.0	-0.0	-2.121			-0.00	0.535		0.0
740	-5.0	2171.2	4.148	9005.7	315.7	1.885	-3.849	0.0	9005.7
750	-5.0	3011.0	8.546	25732.5	670.4	1.832	-8.301	0.0	25732.5
760	-5.0	-0.0	-2.121			-0.00	0.535		0.0

APPROX. 111 , CONST.-TC 900 K, F0.15 , J/JS0.50 , RK 3.78E-05 VV/DEG

Figure III-3. Typical Data Summary from Computer

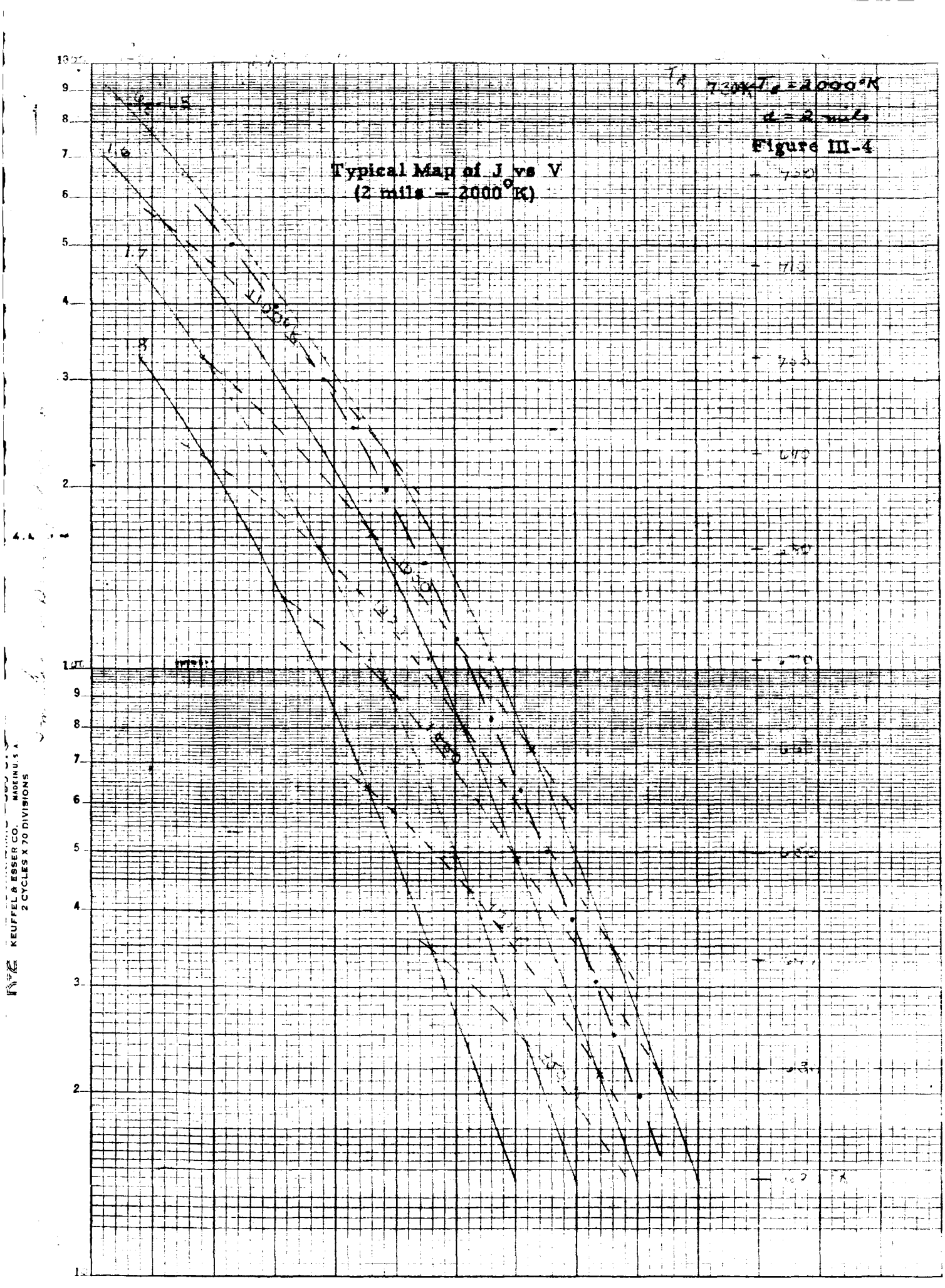
Typical Map of J vs V
(2 mils – 2000°K)
1.6
1.7
1.8
KEUFFEL & ESSER CO. MADE IN U.S.A.
2 CYCLES X 70 DIVISIONS

Figure III-4

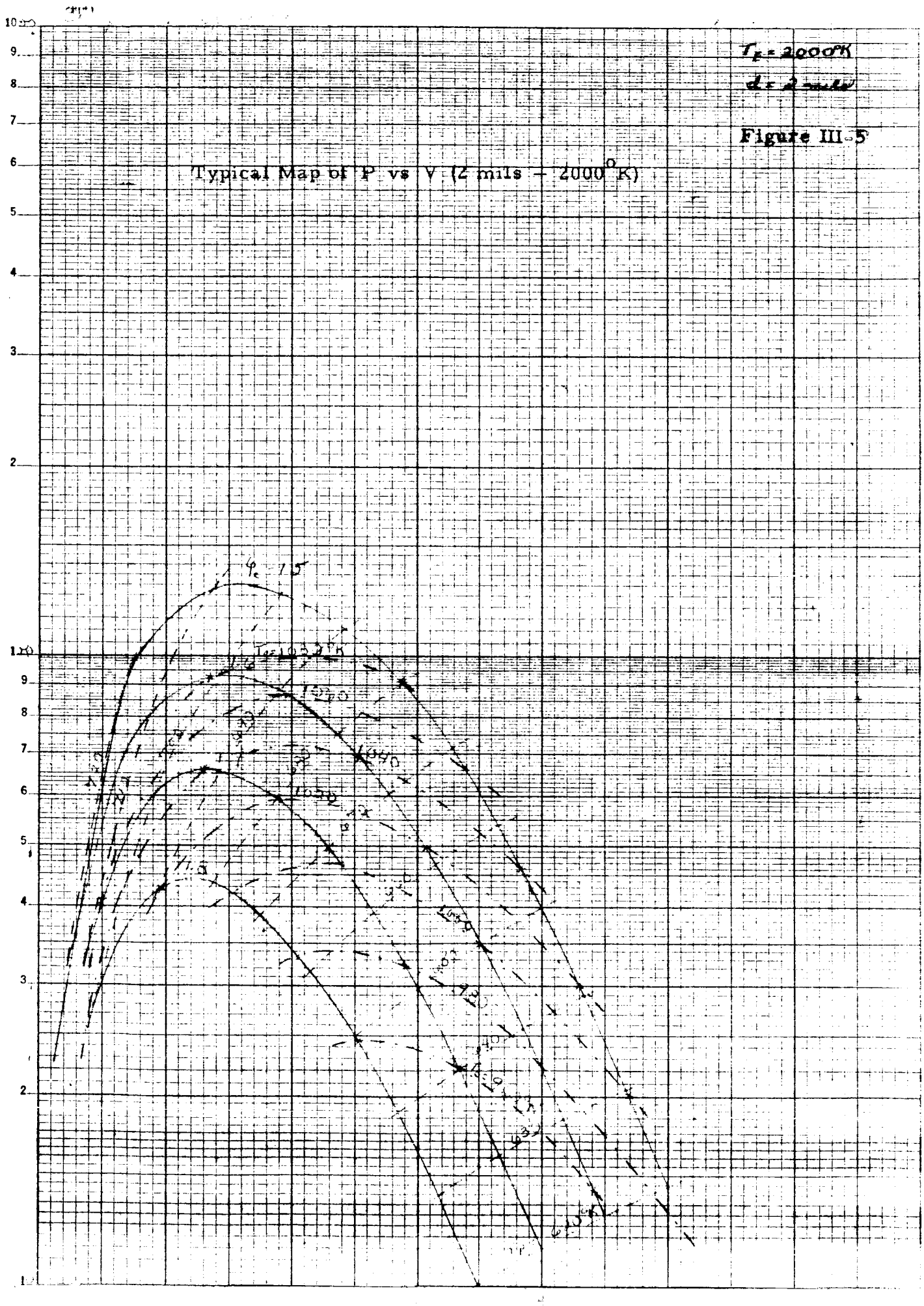

Figure III-5

Typical Map of P vs V (2 mils - 2000°K)

CHAPTER IV

EXPERIMENTS WITH CESIUM FLUORIDE

The work reported in this chapter is the first experimental phase of the additive program which will attempt to thoroughly document the effect of a "surface" additive upon the performance of a cesium thermionic converter.

This series of experiments examines the behavior of the work function of a tungsten emitter surface as the coverage of the surface by cesium fluoride (in the absence of cesium) is varied by controlling the temperature of the cesium fluoride reservoir. The experimental work is to provide sufficient data for the development of a graphical represenation of the relationship between the work function of the surface (ϕ_E), the surface temperature (T_E) and the temperature of the additive (T_A). Similar maps have been developed for the cesium only system.

This documentation should make it possible to predict the emission properties of the surface when covered by both cesium and cesium fluoride. Such prediction would, of course, make use of the cesium only data as well as the cesium fluoride data. Further experiments using cesium plus cesium fluoride in the converter will then be performed to verify the predictions.

In addition to the "equilibrium" experiments described above, a study of time dependent phenomena has shown that appreciable delays in work function change occur with certain variations in surface and additive temperatures. Such effects severely limit the extent of experimental data which can be obtained in a given period and may be a very significant

area of investigation.

EXPERIMENTAL PROCEDURE

Test Vehicle

The test vehicle with molybdenum collectors and tungsten emitter used in these experiments has been described in the second quarterly report. However, the outgassing schedule was modified to eliminate any possible contamination due to water contained in the cesium fluoride pellets. Two test outgassing setups, Figure IV-1, were constructed and the pressure, temperature, and time characteristics of the pellets were determined. The first sample was apparently sucked into the vacuum system as no pellets were found in the pinched-off tube. In the second sample, with the outgassing profile shown in Figure IV-2, the fluoride was heated to over 300°C to be sure all the water was driven off. Considerable outgassing was observed even above 100°C. When the pressure remained steady at 10^{-6} torr, the copper tubing with the pellets was pinched off. The pellets were then transferred to a glass jar and examined for any loss in volume. Since they appeared to be intact except for a brownish discoloration, this schedule was adopted for the outgassing.

In charging the test vehicle with the cesium fluoride, a flow of argon was maintained down through the cesium tubulation, through the vehicle, and out the fluoride reservoir. The pellets were dropped into the reservoir and the tubulation was connected to the ion pump. At this time the cesium tubulation was pinched off and the vacuum pump started, thus minimizing the exposure of the fluoride to air. Outgassing then proceeded with the cesium fluoride reservoir at 300°C and the cesium

reservoir at 400°C to be sure that all gasses were cleaned up. The converter was then pinched off and set up for testing.

Testing

To serve as a control for the additive experiments, the "bare" work function of the tungsten emitter surface was determined at several temperatures. These runs were made while keeping the collector and guard at 200°C and the cesium and cesium fluoride reservoirs at 140°C. The J versus V curves were measured using the guarded collector work function instrumentation, which has been described in the second quarterly. This equipment made it possible to measure currents as low as 0.5 μa with an emitter temperature of 1700°K. Because of the guarding the effects of stray leakages were eliminated from the measurements.

The additive was introduced into the test vehicle by raising its reservoir temperature and maintaining the collector and guard at an equal or greater temperature. Because of the low vapor pressure of cesium fluoride considerable delay was expected in establishing the desired pressure throughout the device. To speed up this process the entire collector-guard structure was treated as the reservoir and maintained at nearly the fluoride temperature. Any time effects in current value were monitored on a strip chart recorder. J-V curves were traced for several different emitter temperatures at each of several reservoir temperatures. Traces were also obtained at various times during the attainment of equilibrium. From these curves, shown in Appendix G, the work functions for the various conditions may be calculated using the Richardson equation.

RESULTS

Steady State

The work function data obtained from these experiments are summarized in Figure IV-3. The supposedly bare data is shown by the solid dots; but as indicated by the changing values with temperature, some additive is probably present. The values shown have considerable scatter and only a slight trend towards higher work functions with increased additive coverage (represented by higher values of T_A and/or lower values of T_E) can be seen. On the figure all values were plotted regardless of time effects. Taking only those points corresponding to long equilibrating times produced the results shown in Figure IV-4. Here a definite trend is visible and indicates a strong correlation between additive coverage and work function. The two lower emitter temperature points for 773°K reservoir temperature coincide with those for 673°K reservoir indicating that equilibrium may not have been reached since these points were taken only a few hours after the reservoir temperature was raised. Additional experiments will be necessary to clarify the behavior for this reservoir temperature. Figure IV-5 shows the data of Figure IV-4 replotted with T_E/T_A as the abscissa. These points do not form a single curve, indicating that the dependence of work function on fluoride temperature is not as simple a relationship as the one for cesium. However, with the limited data at this point no definite conclusion can be reached.

Time Effects

During testing, whenever emitter or reservoir temperatures were

changed, a significant delay time appeared before the J-V curves became stabilized. Several series of such delays are indicated on Figure IV-3 as vertical sets of points at constant T_E.

To give added confidence in the conditions and data on time effects the following check was made. The additive reservoir temperature was held at a low value and the emitter temperature was raised. I-V curves for surface work function were then taken at intervals until equilibrium was reached. Calculation of the work function for these runs shows that the values of ϕ were initially high but as time passed and the surface approached the "bare" condition, the value of ϕ tended to fall between 4.6 and 4.9 which is the range expected for bare tungsten.

Some of the time delay characteristics are shown in Figure IV-6, IV-7 and IV-8 as calculated work function versus time. After additive coverage is increased, either by raising the reservoir temperature or lowering the emitter temperature, there is an approximately exponential approach to the final equilibrium work function value. In Figure IV-6 which shows data following an increase in additive temperature at time zero and at constant T_E, ϕ is initially low and comparable to the bare value. It then becomes higher as the additive pressure in the tube increases and the surface becomes covered. The reverse process is illustrated in Figure IV-7 where T_E was rapidly increased at time zero and the fluoride forced to leave the surface. At first, ϕ is high and then approaches a lower value. Figure IV-8 is similar to IV-6 except that a reduction in T_E was made at time zero and the additive pressure maintained constant. The effects in the two figures are similar.

Figure IV-9 is a semi-log plot illustrating the relative time constants of the work function changes. In most cases a straight line has been obtained indicating an exponential behavior.

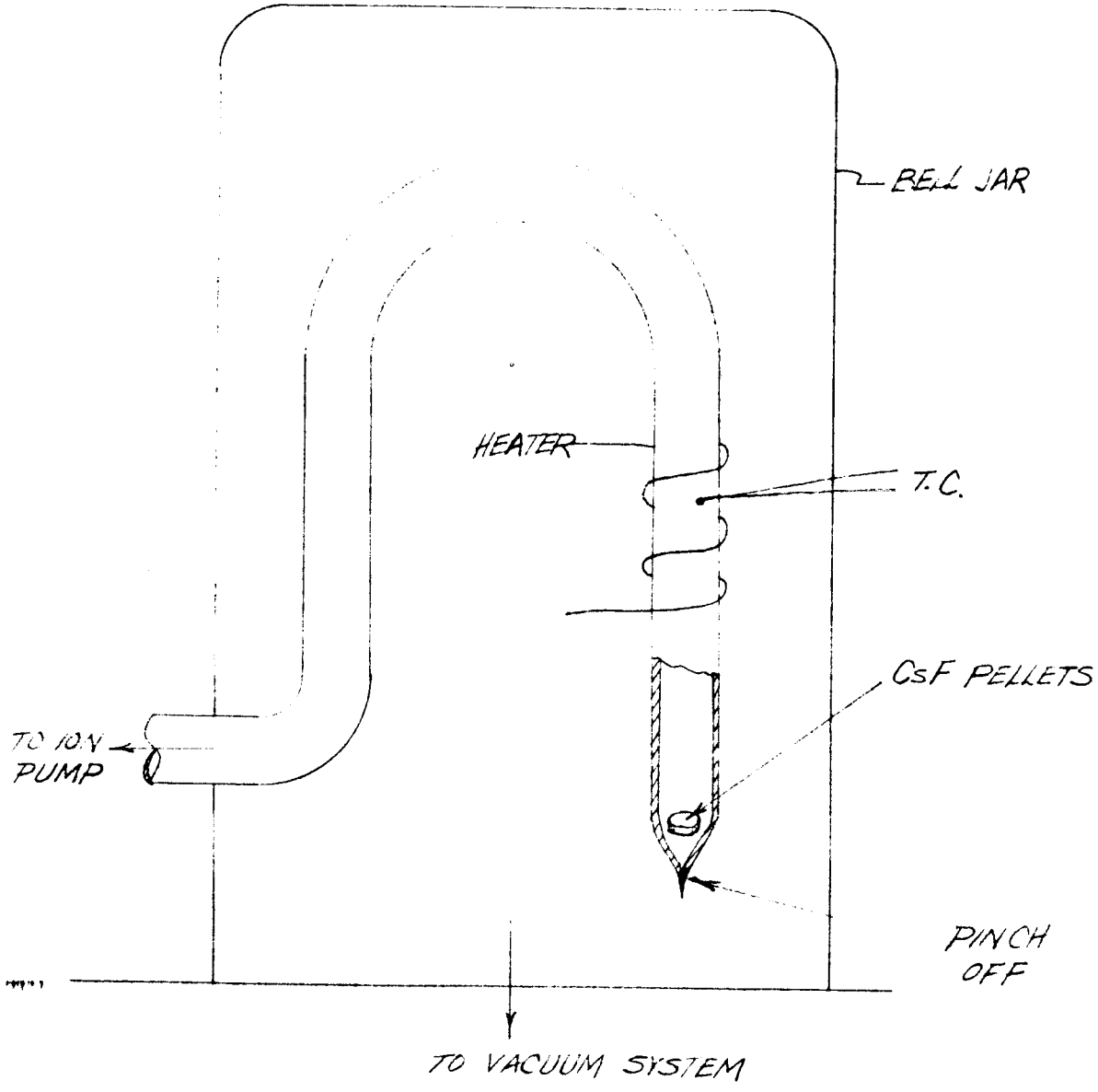

Figure IV-1. Outgassing setup for cesium fluoride

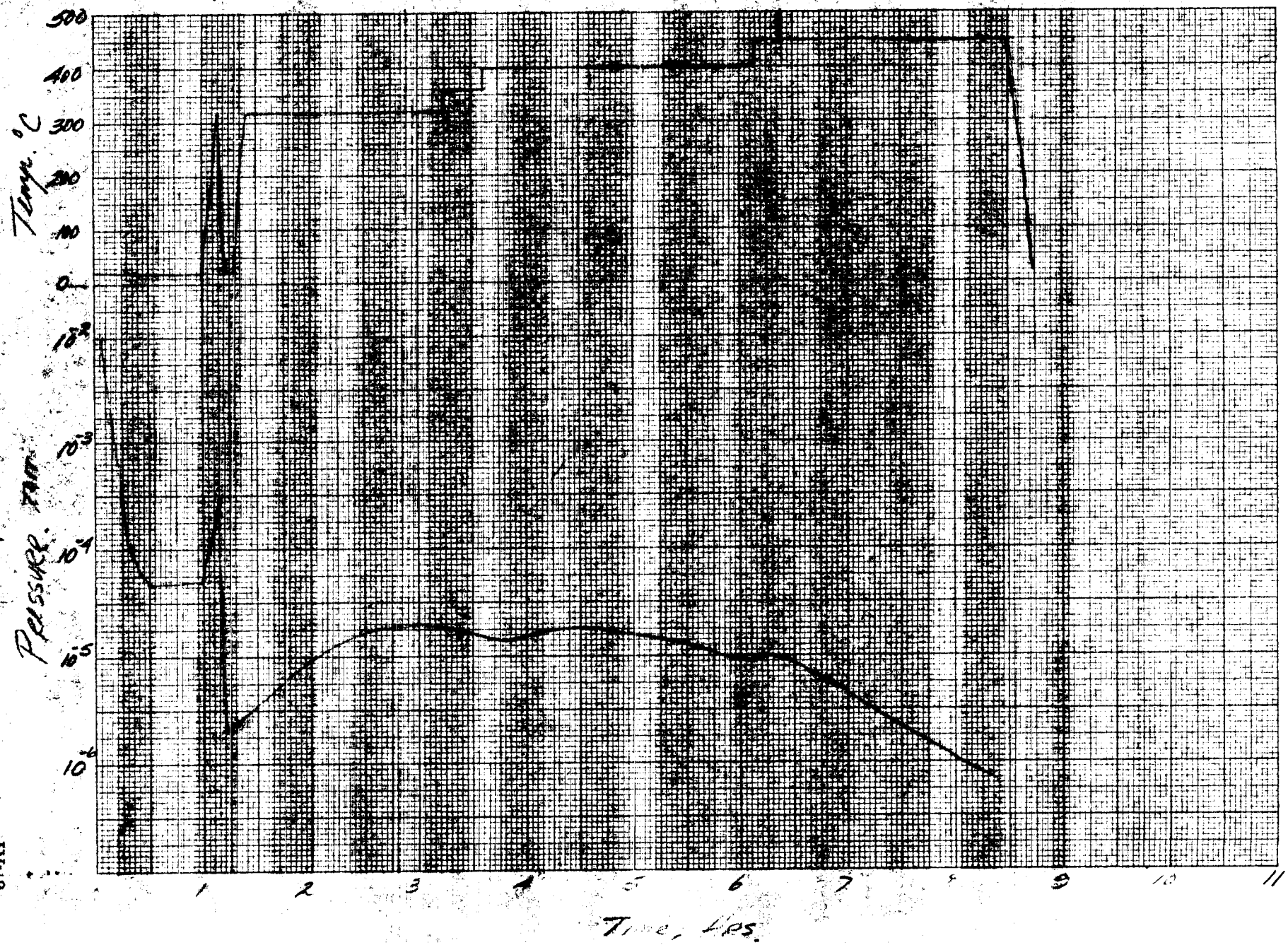

Figure IV-2. Outgassing Plot for Cesium Fluoride.

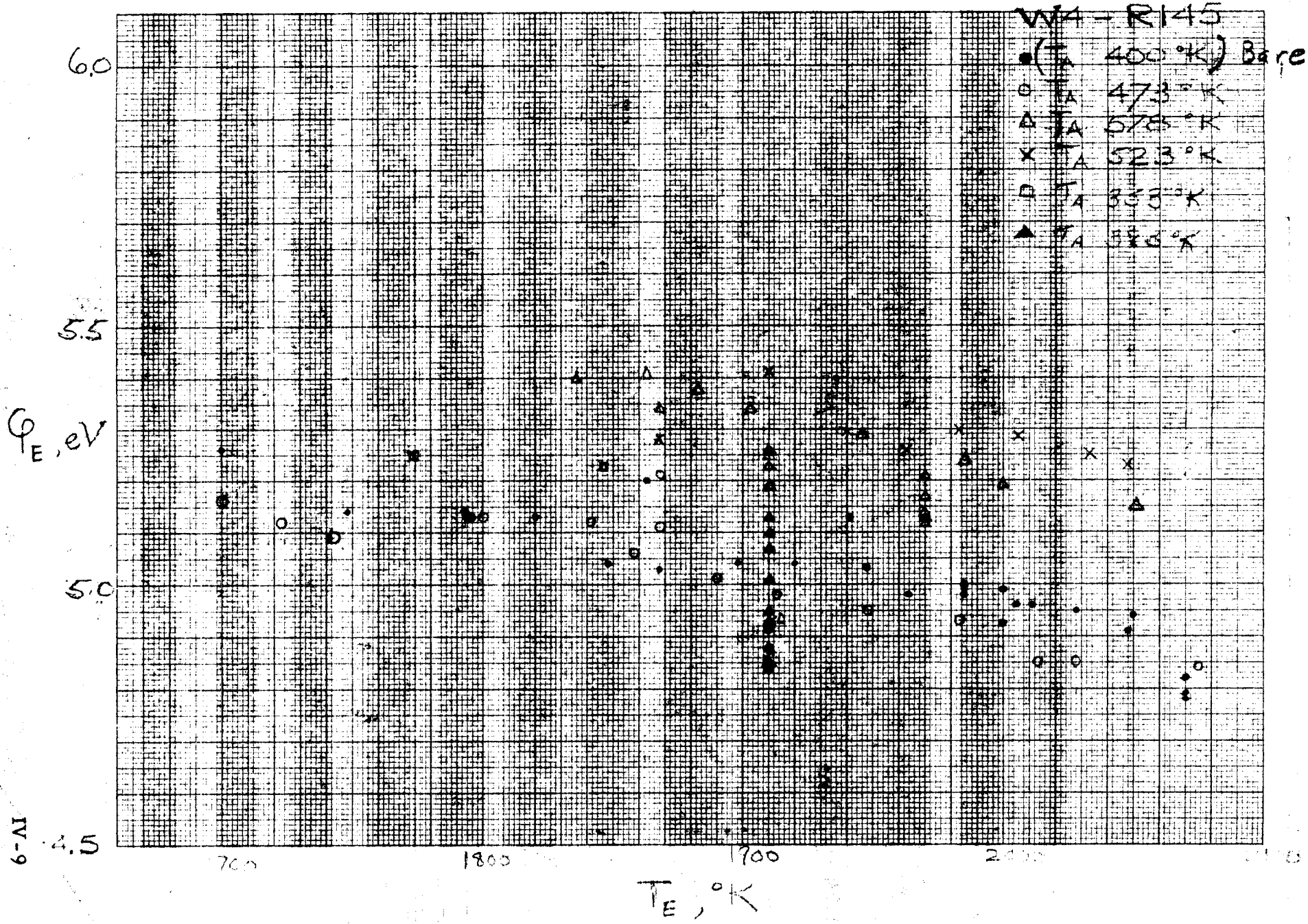

Figure IV-3. Summary ϕ vs T.

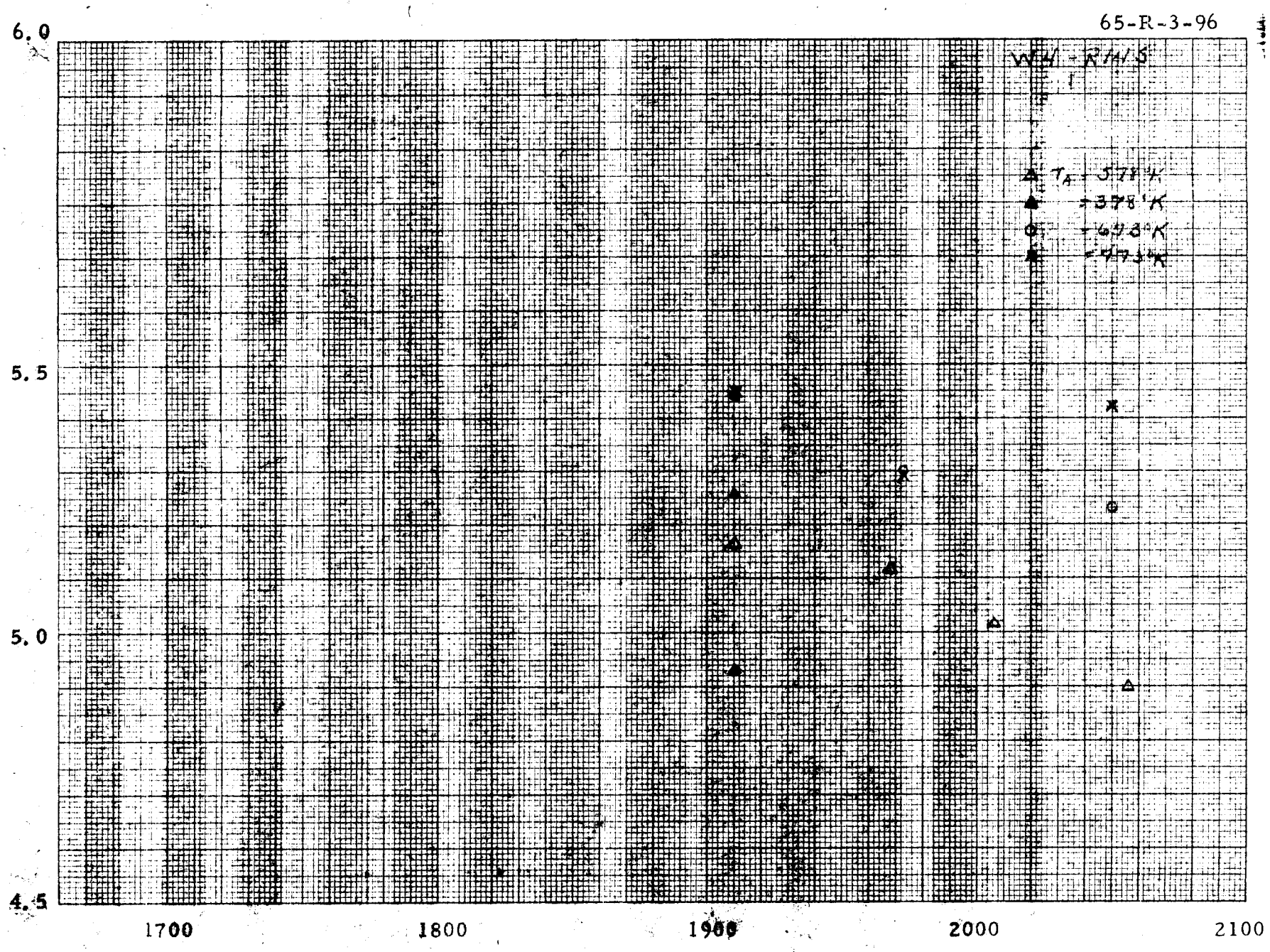

Figure IV-4. Equilibrium ϕ vs T.

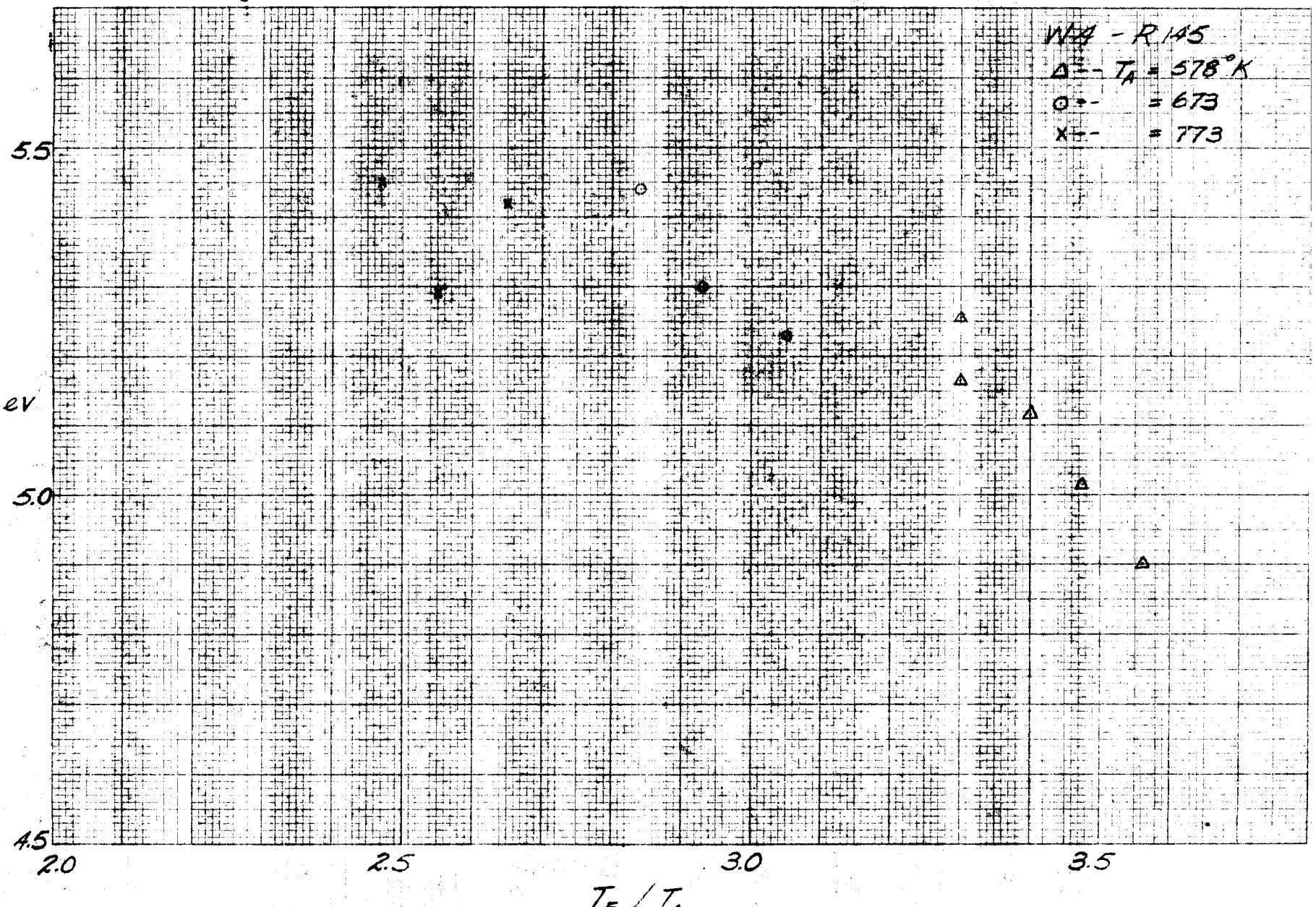

Figure IV-5. φ vs T/T_R.

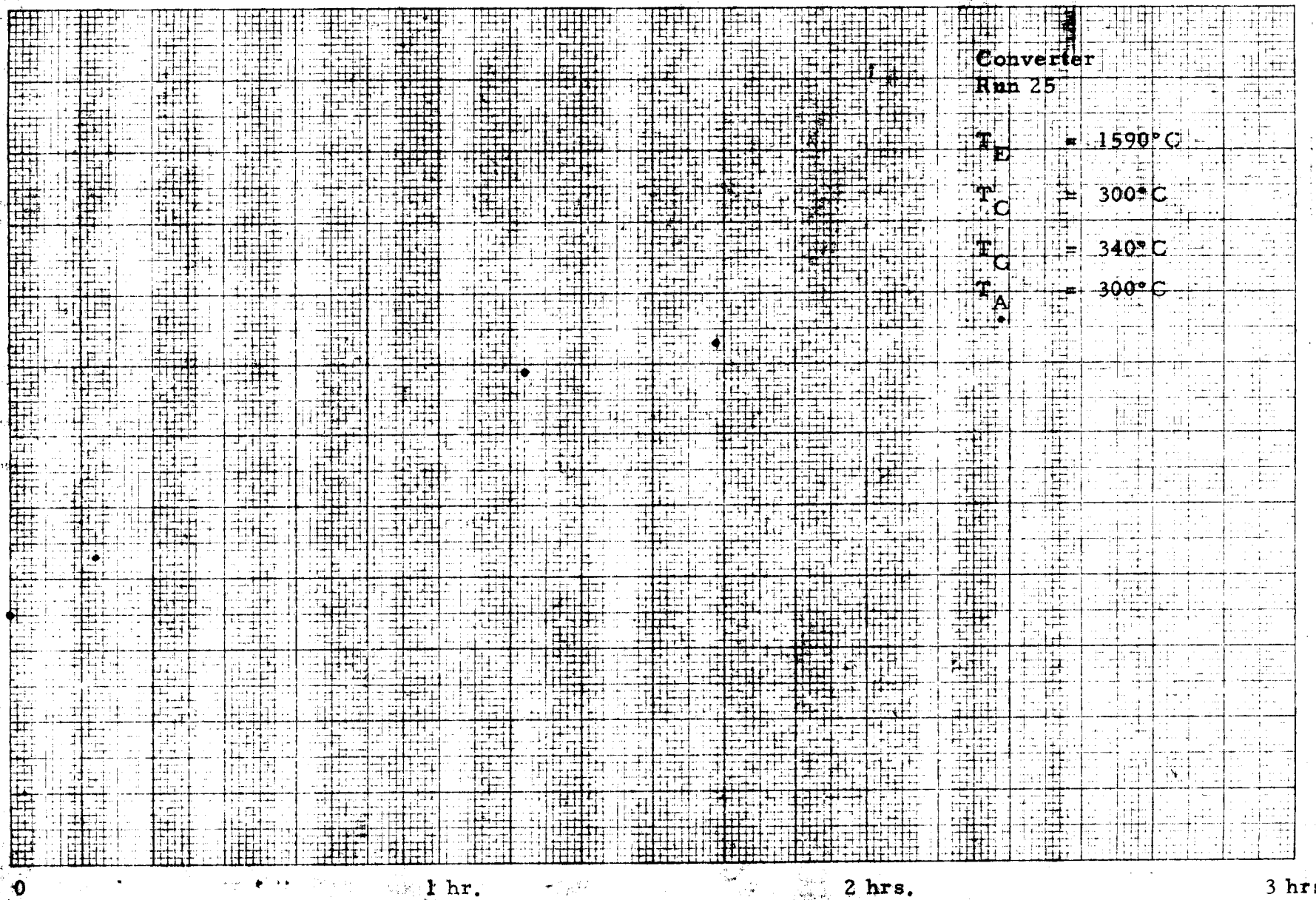

Figure IV-6. Run 25 — ϕ vs Time.

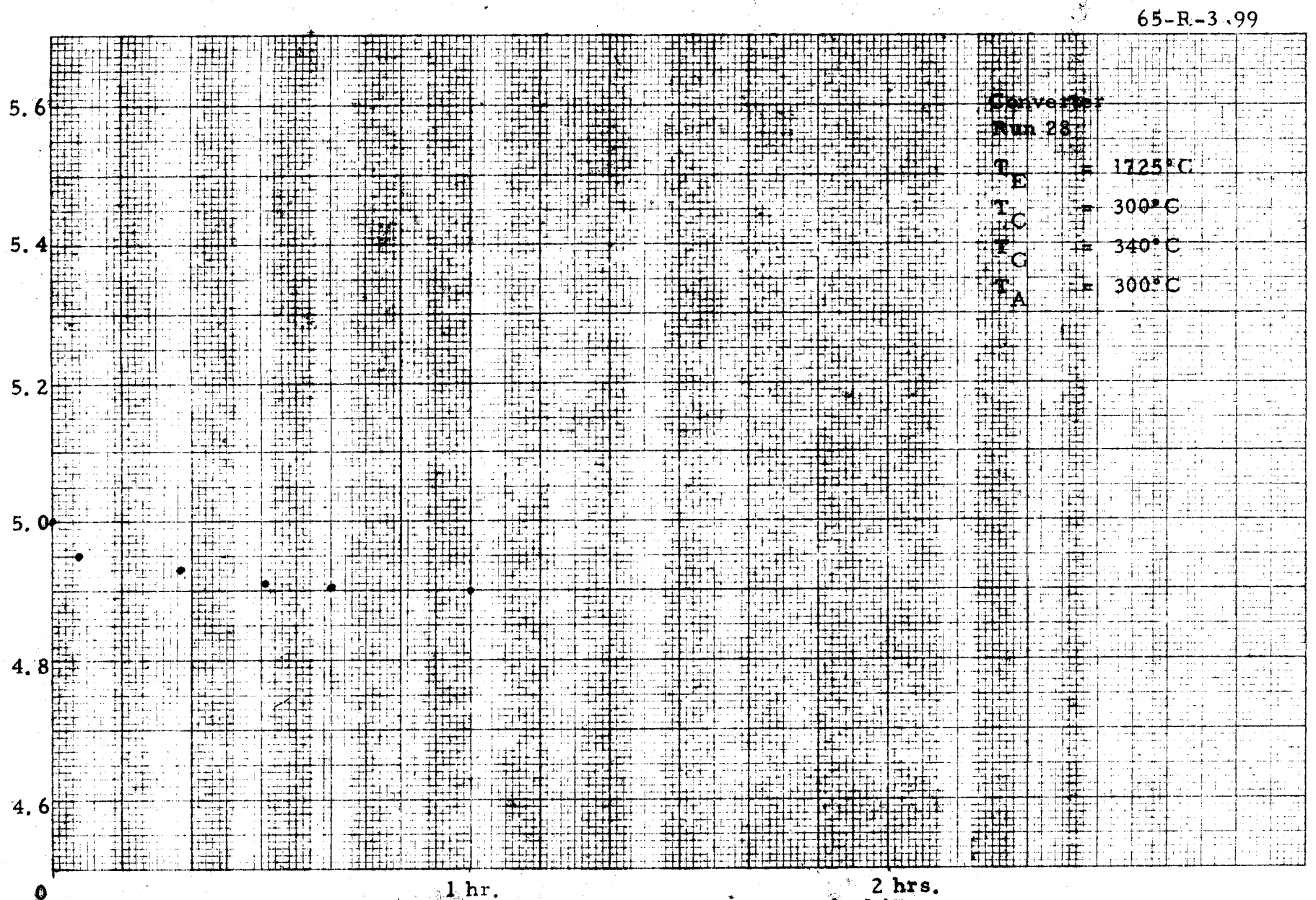

Figure IV-7. Run 28 — ϕ vs. Time.

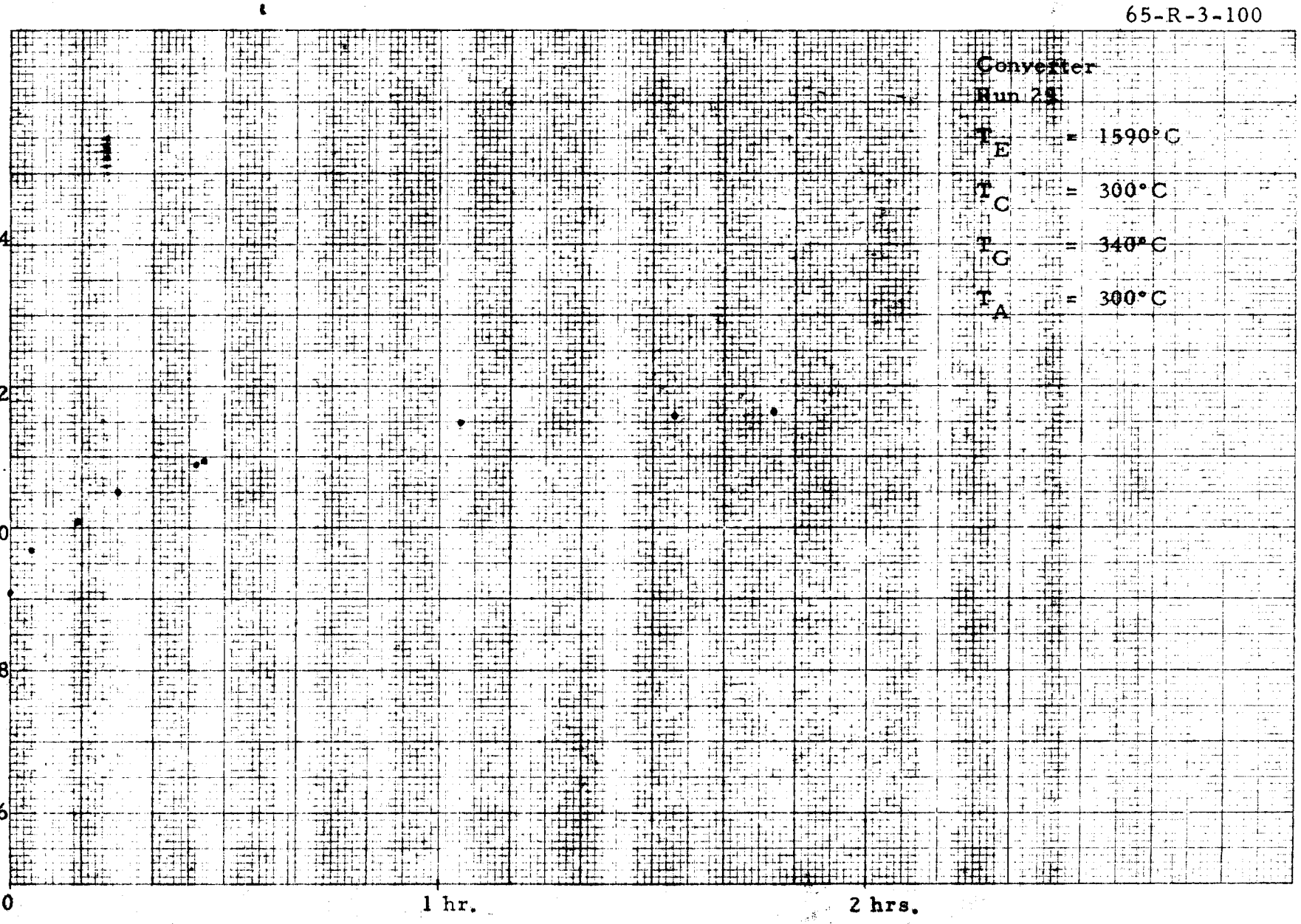

Figure IV-8. Run 29 — ϕ vs Time.

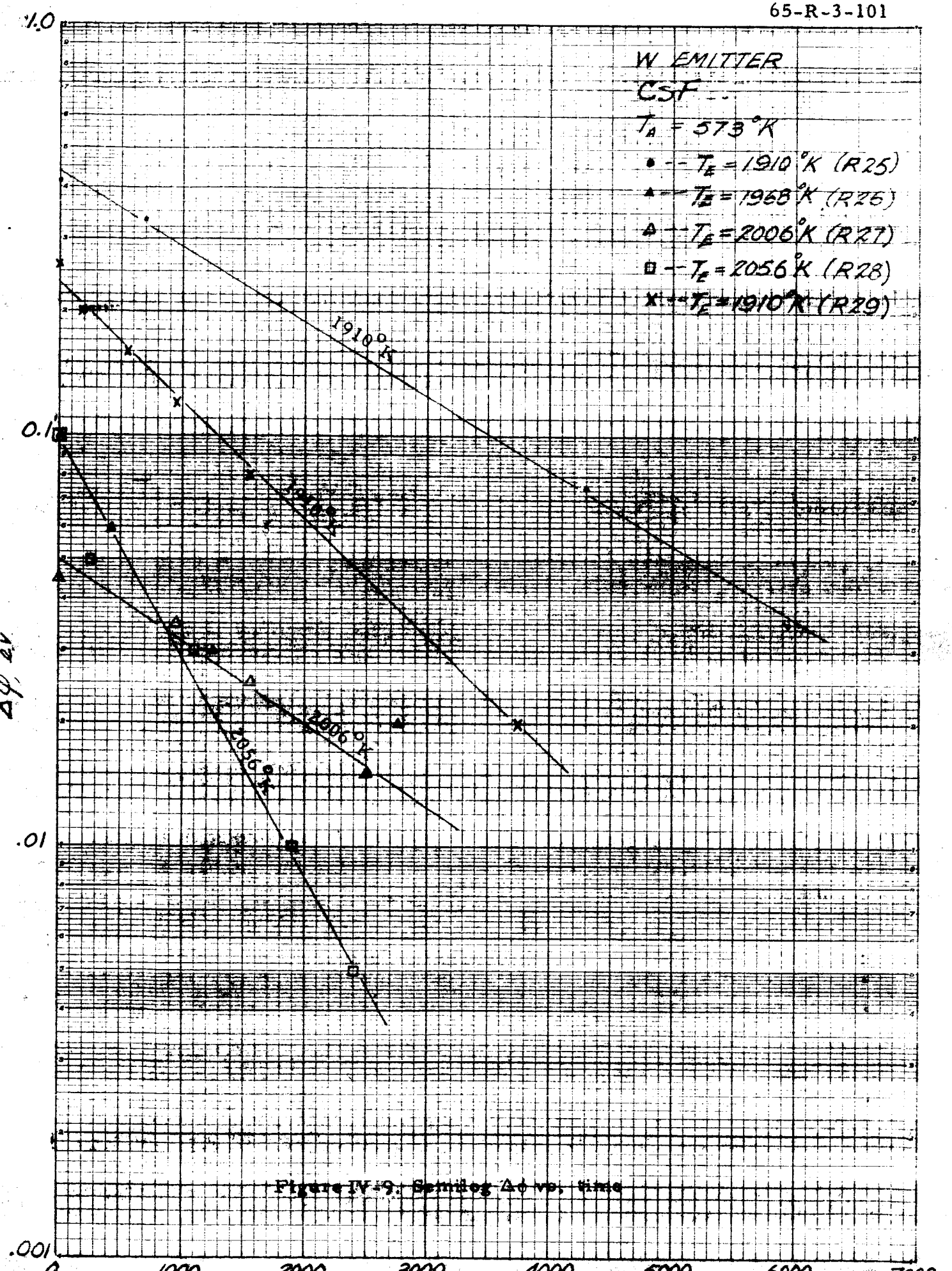

Figure IV-9. Semilog Δφ vs. time

APPENDIX A

DIFFUSION OF ELECTRONS THROUGH PLASMA

This treatment is similar to that by C. Warner[8] for the extinguished mode.

A neutral field-free plasma, bounded by the emitter and collector sheaths of height V_e and V_c as in Fig. 3a, is assumed. Since no significant source or sink of electrons exists in the plasma

$$\frac{d^2n}{dx^2} = 0 \tag{A-1}$$

where n is the density of electrons at a distance x from the emitter side of the plasma. The solution of Eq. A-1 is

$$n = Mx + N \tag{A-2}$$

where M and N are constants determined by the boundary conditions.

At the emitter side of the plasma (x= 0) the electron current entering the plasma is

$$\frac{n_e\bar{v}}{4} + \frac{J}{2} = J_s + \left(\frac{n_e\bar{v}}{4} - \frac{J}{2}\right)\left(1 - \exp\left[-V_e/kT_{\epsilon e}\right]\right) \tag{A-3}$$

Similarly, at the collector side (x= d),

$$\frac{n_c\bar{v}}{4} - \frac{J}{2} = J_{cs} + \left(\frac{n_c\bar{v}}{4} + \frac{J}{2}\right)\left(1 - \exp\left[-V_c/kT_{\epsilon c}\right]\right) \tag{A-4}$$

where n_e and n_c are the respective electron densities at the emitter and collector edges of the plasma, $\bar{v}$ is the average electron velocity, J_s and J_{cs} are the respective saturation emission currents from the emitter and collector, J is the net electron current received by the collector, $T_{\epsilon e}$ and $T_{\epsilon c}$ are the respective electron temperatures at the emitter and collector edges of the plasma, and k is Boltzmann's constant. The variation of $\bar{v}$ with the electron temperature is neglected for simplicity here.

The diffusion of the net electron current J through the plasma is required by Fick's law to be

$$J = -\frac{\bar{v}\lambda}{3}\frac{dn}{dx} \tag{A-5}$$

where λ is the electron mean-free-path.

Combining Eqs. A-2 through A-5 gives

$$\frac{J_s}{J} = a + b\left(\frac{d}{\lambda}\right) \tag{A-6}$$

where
$$a = \frac{\exp\left(V_e/kT_{\epsilon e}\right) + \exp\left(V_c/kT_{\epsilon c}\right) - 1}{\exp\left(V_e/kT_{\epsilon e}\right) - \frac{J_{cs}}{J}\exp\left(V_c/kT_{\epsilon c}\right)}$$

$$b = \frac{3/4}{\exp\left(V_e/kT_{\epsilon e}\right) - \frac{J_{cs}}{J_s}\exp\left(V_c/kT_{\epsilon c}\right)}$$

If the collector emission is negligible, Eq. A-6 simplifies to the form given as Eq. 1 in the text.

APPENDIX B

ELECTRON TEMPERATURE DROP ACROSS PLASMA

A general consequence of electron flow through a plasma is an electron temperature gradient. In analogy with the well-known electron heating and cooling effects at electrode surfaces, a large heat flux is similarly introduced into the emitter side of the plasma by the incoming electrons, and a large fraction of this heat is removed from the collector side by the outgoing electrons. For any distance x from the emitter side, where the electron temperature is T_ϵ, continuity of heat flow requires that

$$J\left(V_c + 2kT_{\epsilon c}\right) = 2kT_\epsilon + K_\epsilon \left(dT_\epsilon/dx\right) \tag{B-1}$$

This equation states that the electron cooling of the plasma at the collector side equals the heat of transport $2kT_\epsilon J$ due to the net electron flow plus the thermal conduction down a temperature gradient in the electron gas of thermal conductivity K_ϵ. Elementary kinetic theory gives $K_\epsilon = 2k\lambda J_r$ for $d \gg \lambda$, where J_r is the random electron current density. Integration of Eq. B-1 and substitution for K_ϵ gives

$$T_{\epsilon e} - T_{\epsilon c} = \frac{V_c}{2k}\left(1 - \exp\left[-\frac{J}{J_r}\frac{d}{\lambda}\right]\right) \tag{B-2}$$

Therefore, for small d/λ the electron temperature approaches uniformity. However, as d/λ exceeds J_r/J, the electron temperature drop across the plasma approaches $V_c/2k$.

The heat removed by excitation, and the x-dependence of J_r are neglected in this simplified treatment.

APPENDIX C

HEIGHT OF COLLECTOR SHEATH

If $\exp(-V_c/kT_{\epsilon c}) \ll 1$, positive ion space charge predominates over most of the collector sheath. Assuming that ion scattering is insignificant in the sheath itself, the Langmuir-Child space charge equation gives

$$J_{ic} = en_{ic}\left(\frac{2kT_c}{\pi M}\right)^{\frac{1}{2}} = \frac{1}{9\pi e}\left(\frac{2}{M}\right)^{\frac{1}{2}} \frac{V_c^{\frac{3}{2}}}{w^2} \qquad \text{(C-1)}$$

where T_c is the temperature of the collector, w is the thickness of the collector sheath, and n_{ic} is the ion density at the collector edge of the plasma. Since the collector sheath thickness cannot greatly exceed the Debye length h, it is convenient to express w in terms of h,

$$w = Nh = N\left(\frac{kT_{\epsilon c}}{4\pi n_{ic} e^2}\right)^{\frac{1}{2}} \qquad \text{(C-2)}$$

where N is the number of Debye lengths in the sheath, Eqs. C-1 and C-2 combine to give

$$\frac{V_c}{kT_{\epsilon c}} = \frac{1}{\pi^{\frac{1}{3}}}\left(\frac{3}{2}\right)^{\frac{4}{3}}\left(\frac{T_c}{T_{\epsilon c}}\right)^{\frac{1}{3}} N^{\frac{4}{3}} = 1.17\left(\frac{T_c}{T_{\epsilon c}}\right)^{\frac{1}{3}} N^{\frac{4}{3}} \qquad \text{(C-3)}$$

For present plasma conditions ($T_c \simeq 700°K$ and $T_{\epsilon c} \simeq 2500°K$), $\frac{V_c}{KT_{\epsilon c}} \simeq 0.8\, N^{\frac{4}{3}}$, and N should be near unity.

APPENDIX D

ELECTRON TEMPERATURE REQUIRED TO SUSTAIN THE IGNITED MODE

The rate at which ions are produced in a gas from impact ionization by an electron gas at temperature T_ϵ is

$$\frac{dn_i}{dt} = n_\epsilon\, p\, K_i \left(2+\frac{V_i}{kT_\epsilon}\right)\left(\frac{T_\epsilon}{T_o}\right)^{\frac{1}{2}}\left(\frac{M}{m}\right)^{\frac{1}{2}}\left(\frac{kT_o}{2\pi M}\right)^{\frac{1}{2}} \exp\left(-\frac{V_i}{kT_\epsilon}\right) \qquad \text{(D-1)}$$

where n_i and n_ϵ are respectively the ion and electron densities; p, T_o, M and V_i are respectively the pressure, temperature, atomic mass and ionization energy of the gas; m is the electron mass; K_i is the initial rate of increase of ionization cross section σ_i with electron energy U above the threshold, i.e., $K_i = \left(d\sigma_i/dU\right)_{U=V_i}$. This equation assumes that the density of excited atoms is much less than the gas density. The rate at which ions leave unit area of such a plasma, for a symmetrical one-dimensional system, has been shown to be[6]

$$\left.\begin{aligned} \mu_{iL} &= 0.345\, n_\epsilon \left(\frac{2kT_\epsilon}{M}\right)^{\frac{1}{2}} && \text{for } \lambda_i \gg d' \\ \mu_{is} &= 0.895\, \pi \frac{n_\epsilon}{pq}\left(\frac{kT_o}{M}\right)^{\frac{1}{2}} \frac{kT_\epsilon}{d'} && \text{for } \lambda_i \ll d' \end{aligned}\right\} \qquad \text{(D-2)}$$

Where λ_i is the ion mean-free-path, q is the cross section for ion diffusion

through the plasma, and d^* is the effective width of the ion generation region.

Because of the large electron temperature drop across the plasma (Appendix B), most of the ions are produced on the emitter side of the plasma, so it is assumed that most ions leave the plasma at the emitter side. Accordingly, at steady state, the rate at which ions leave the plasma at the emitter, μ_{iL} or μ_{is}, must equal the total rate of ion production per unit area of plasma, $\left(\frac{dn_i}{dt}\right) d^*$. Therefore, Eqs. D-1 and D-2 combine to give

$$kT_\epsilon = \frac{V_i}{\ell n (B_L p d^*)} \qquad \text{for } \lambda_i \gg d^* \tag{D-3}$$

or

$$kT_\epsilon = \frac{V_i}{2\ell n (B_s p d^*)} \qquad \text{for } \lambda_i \ll d^*$$

where

$$B_L = 3.2 \left(\frac{M}{m}\right)^{\frac{1}{2}} \left(2 + \frac{V_i}{kT_\epsilon}\right) \frac{T_\epsilon}{T_o} \quad K_i \approx 60 \text{ (mil-torr)}^{-1} \tag{D-4}$$

$$B_s = 0.75 \left(\frac{M}{m}\right)^{\frac{1}{4}} \left(2 + \frac{V_i}{kT_\epsilon}\right)^{\frac{1}{2}} \left(\frac{T_\epsilon}{T_o}\right)^{\frac{3}{4}} \left(\frac{K_i q}{kT_\epsilon}\right)^{\frac{1}{2}} \approx 3.6 \text{ (mil-torr)}^{-1}$$

The value $K_i = 4 \text{ Å}^2/\text{eV}$ and $q = 1200 \text{ Å}^2$, used to compute the values of B_L and B_s shown, have been estimated by Houston[7] to be the most probable. The uncertainties introduced by the unsymmetrical plasma, the non-uniform electron temperature, and the relation of d to d^*, are probably no greater than the combined uncertainties in these values. In any event, the computed electron temperature is quite insensitive to the value of B_s or d^* for $pd^* \gg 10$ mil-torr.

APPENDIX E

ENERGY BALANCE FOR PLASMA

Equating energy input and energy loss for the plasma gives

$$J_s (V_e+2kT_e) = J (V_c+2kT_{\epsilon c}) + (J_s-J)(V_e+2kT_{\epsilon e}) + e\mu_x V_x \qquad (E-1)$$

The first three terms are the energies carried into and out of the plasma by the electron currents identified in Fig. 3a. The last term is the energy removed from the plasma by the current of excited atoms μ_x or their decay photons, where V_x is the excitation energy. The rate of production of excited atoms is given by Eq. D-1 with V_x substituted in place of V_i, and the analogous quantity K_x for K_i. Accordingly,

$$\frac{\mu_x}{\mu_i} = \frac{K_x}{K_i} \frac{2+\frac{V_x}{kT_\epsilon}}{2+\frac{V_i}{kT_\epsilon}} \exp\left(\frac{V_i - V_x}{kT_\epsilon}\right) \qquad (E-2)$$

If the Langmuir double sheath relation holds at the emitter

$$J = \left(\frac{M}{m}\right)^{\frac{1}{2}} \mu_i e \qquad (E-3)$$

Eqs. E-1 to E-3 combine to give

$$V_e = (2kT_{\epsilon e} - 2kT_{\epsilon}) \frac{J_s}{J} + C \left[B_s \, pd^* \right]^{2\left(1 - \frac{V_x}{V_i}\right)} \qquad (E-4)$$

where $$C = V_x \left(\frac{m}{M}\right)^{\frac{1}{2}} \frac{K_x}{K_i} \frac{2 + \frac{V_x}{kT_{\epsilon}}}{2 + \frac{V_i}{kT_{\epsilon}}}$$

and B_s and d^* are defined in Appendix D (Eq. D-4). In view of the relations in Eqs. 1, 3, and 11, Eq. E-4 enforces a unique relationship between V_e and pd^*.

For the obstructed mode, as discussed in the text, the fraction of back-reflected current from the bright plasma which reaches the emitter becomes negligibly small, eliminating the term in $J_s - J$ in Eq. E-1. Eq. E-4 then becomes

$$V_e^* = 2kT_{\epsilon} - 2kT_e + C \left(Bpd^* \right)^{2\left(1 - \frac{V_x}{V_i}\right)} \qquad (E-5)$$

APPENDIX F

SELECTED FAMILIES OF I-V CHARACTERISTICS

The program calls for a large number of I-V families, and a substantial number have been taken during the third quarter. We include here a sample set of data for three families of I-V characteristics taken with spacing as the primary variable. The conditions for each family are listed below. All data is for the tube containing emitter R16.

Family #	T_E	T_C	T_R	Spacing
	°C	°C	°C	mils
2	1485	350	272	1, 2, 4, 8, 16, 24, 32, 48, 64, 80
3	1485	400	333	1, 2, 4, 8, 16, 24, 32, 48, 64, 80
4	1600	400	308	1, 2, 4, 8, 16, 24, 32, 64, 80

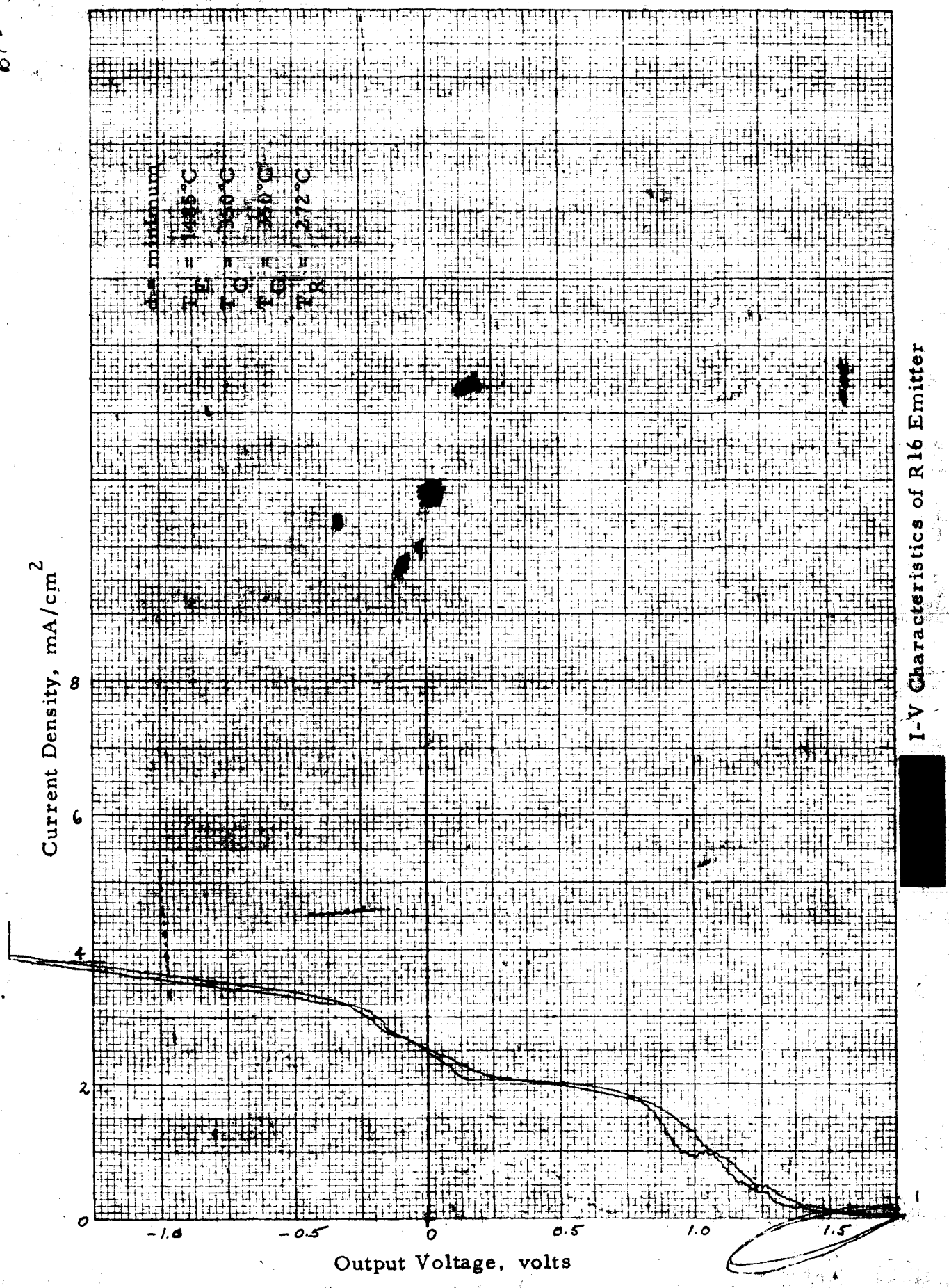

I-V Characteristics of R16 Emitter

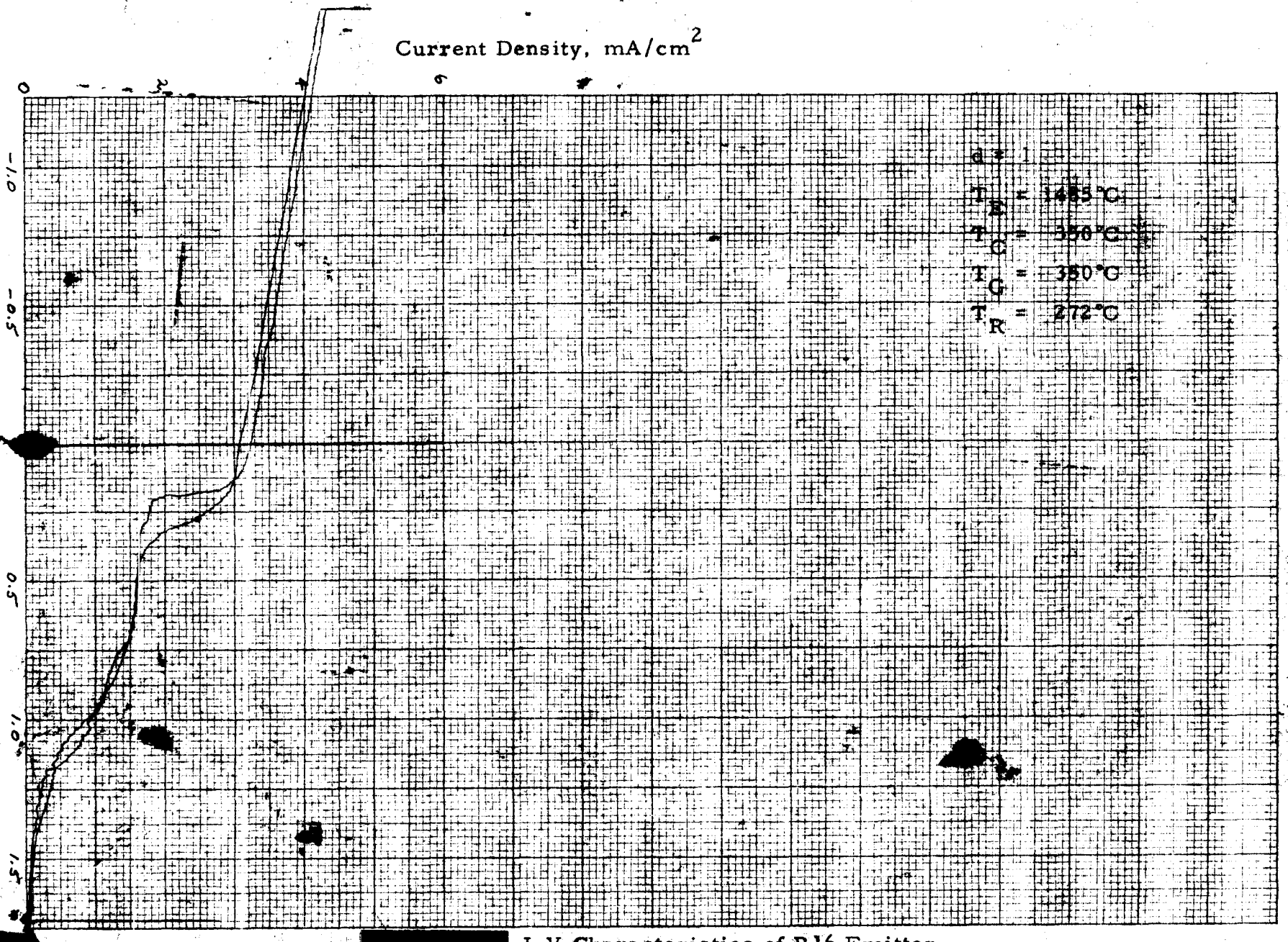

I-V Characteristics of R16 Emitter

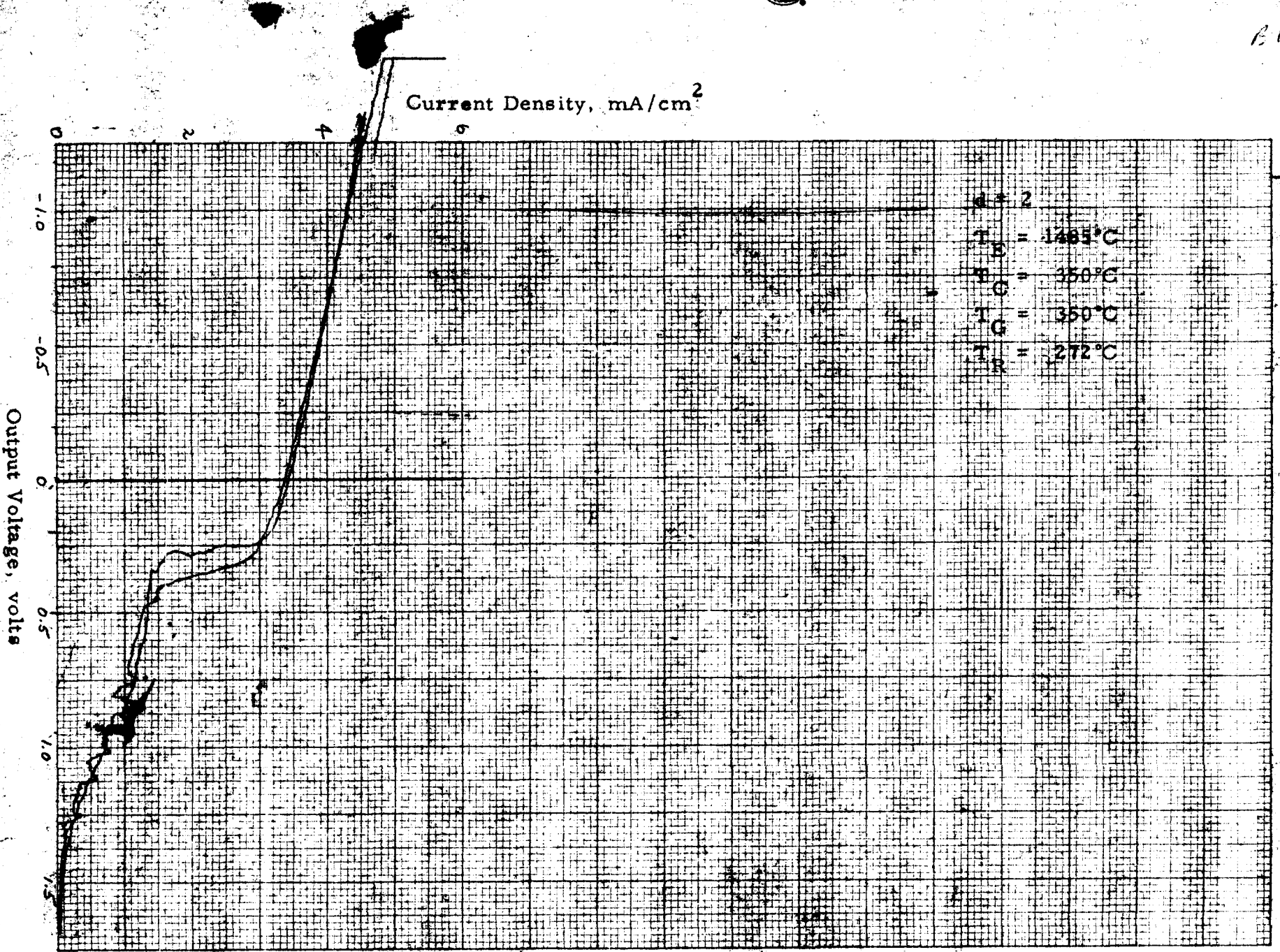

[redacted] I-V Characteristics of R16 Emitter

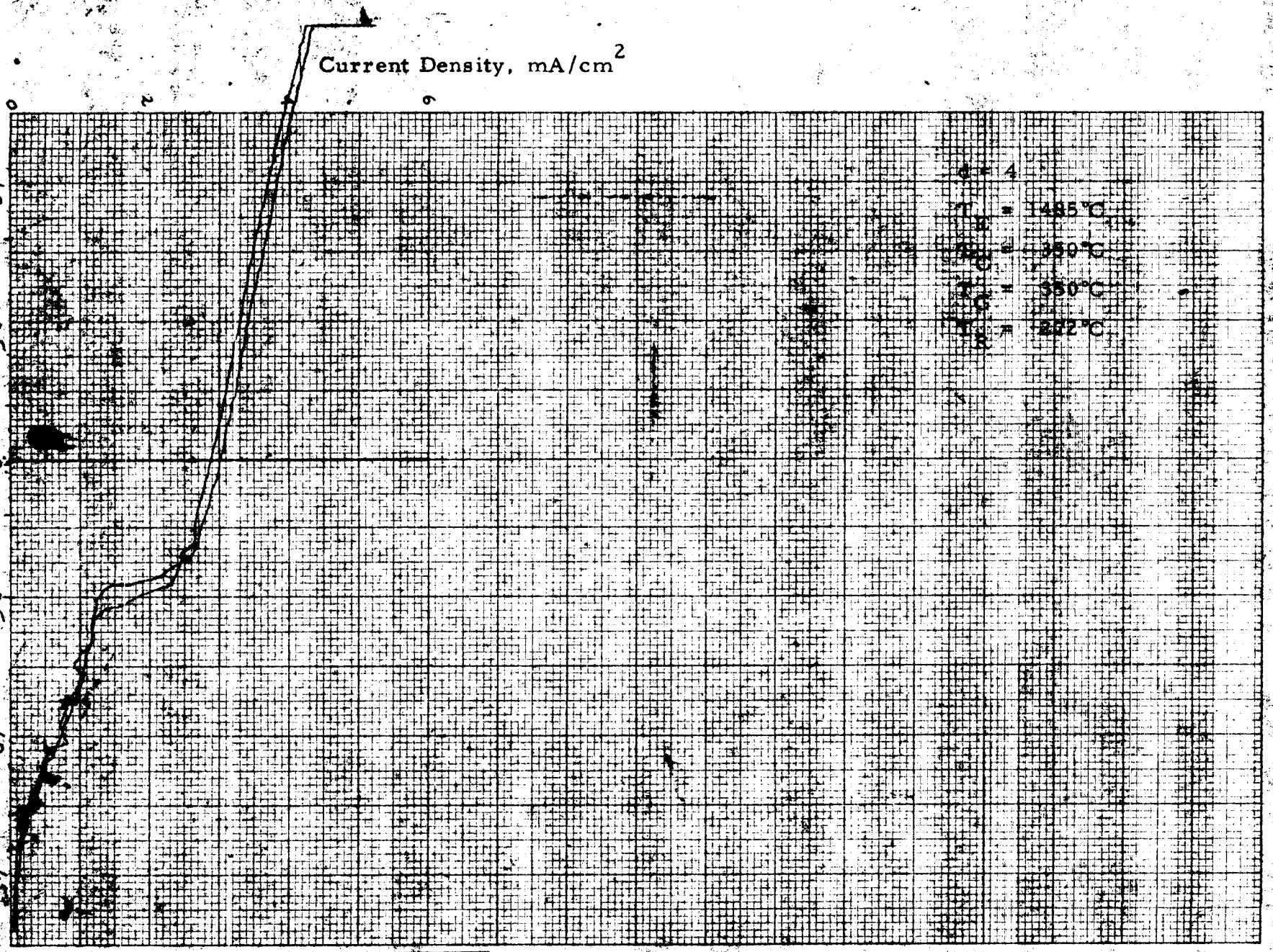

[redacted] I-V Characteristics of R16 Emitter

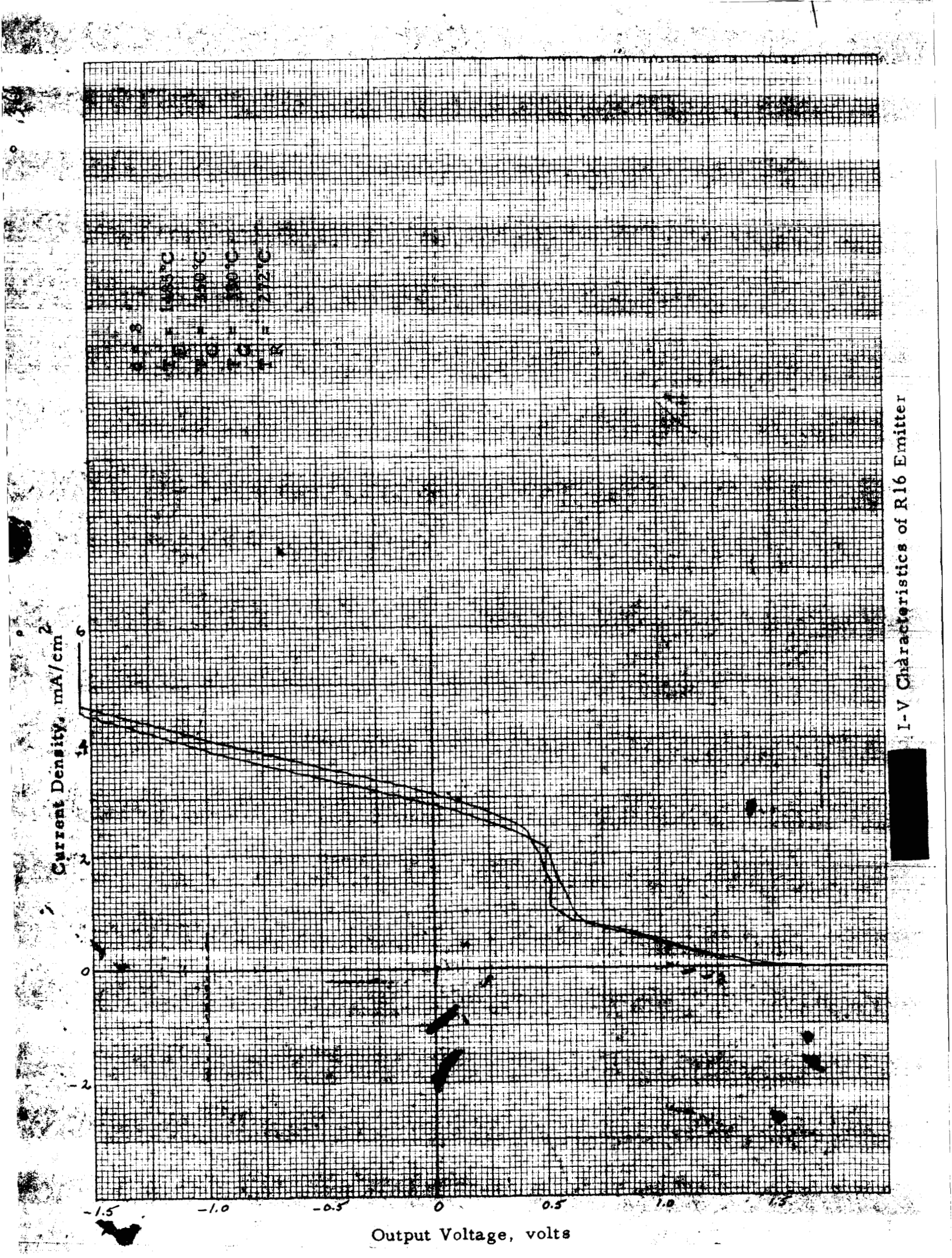
I-V Characteristics of R16 Emitter
Current Density, mA/cm²
6
4
2
0
-2
-1.5
-1.0
-0.5
0
0.5
1.0
1.5
Output Voltage, volts

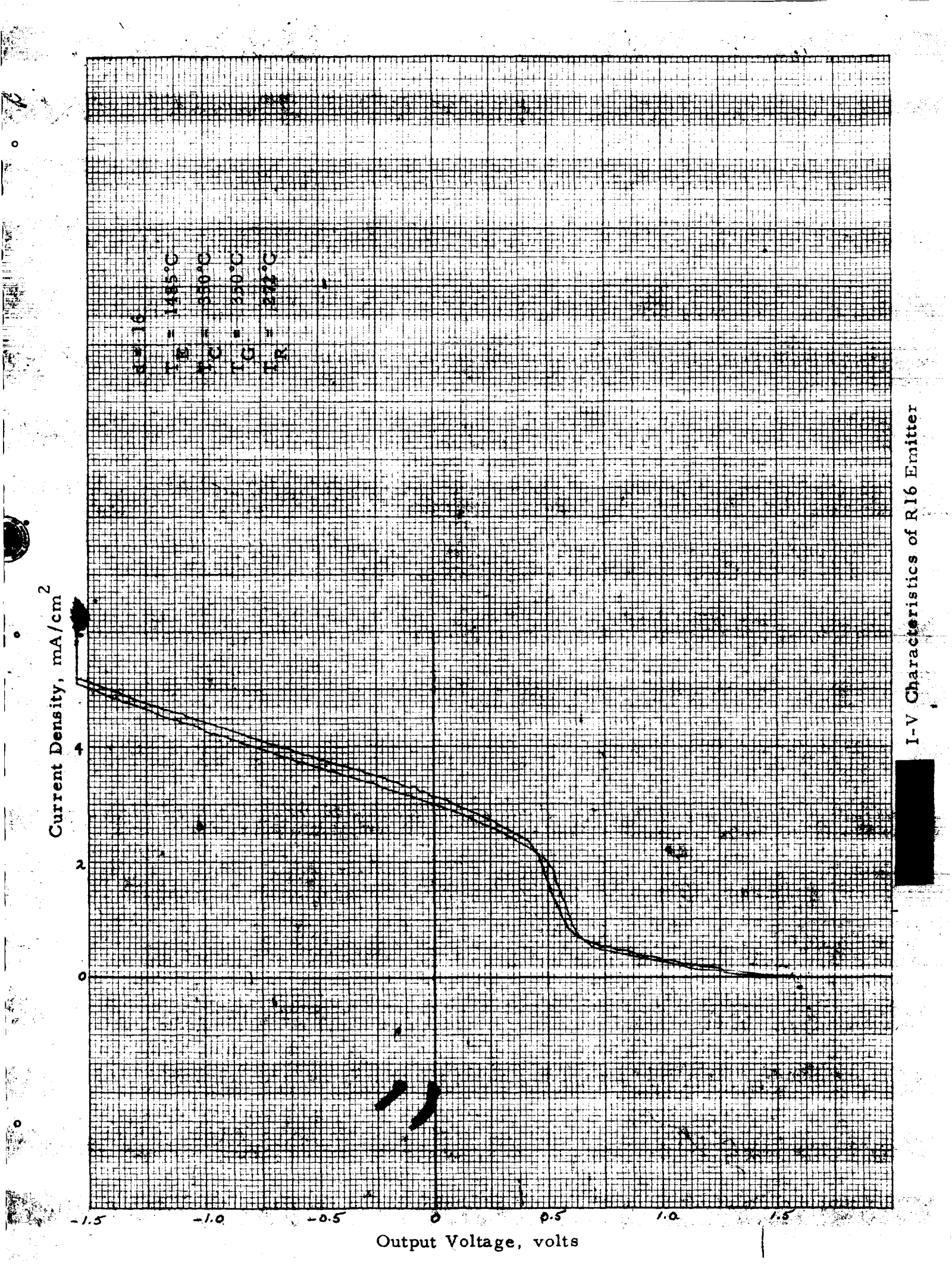

I-V Characteristics of R16 Emitter

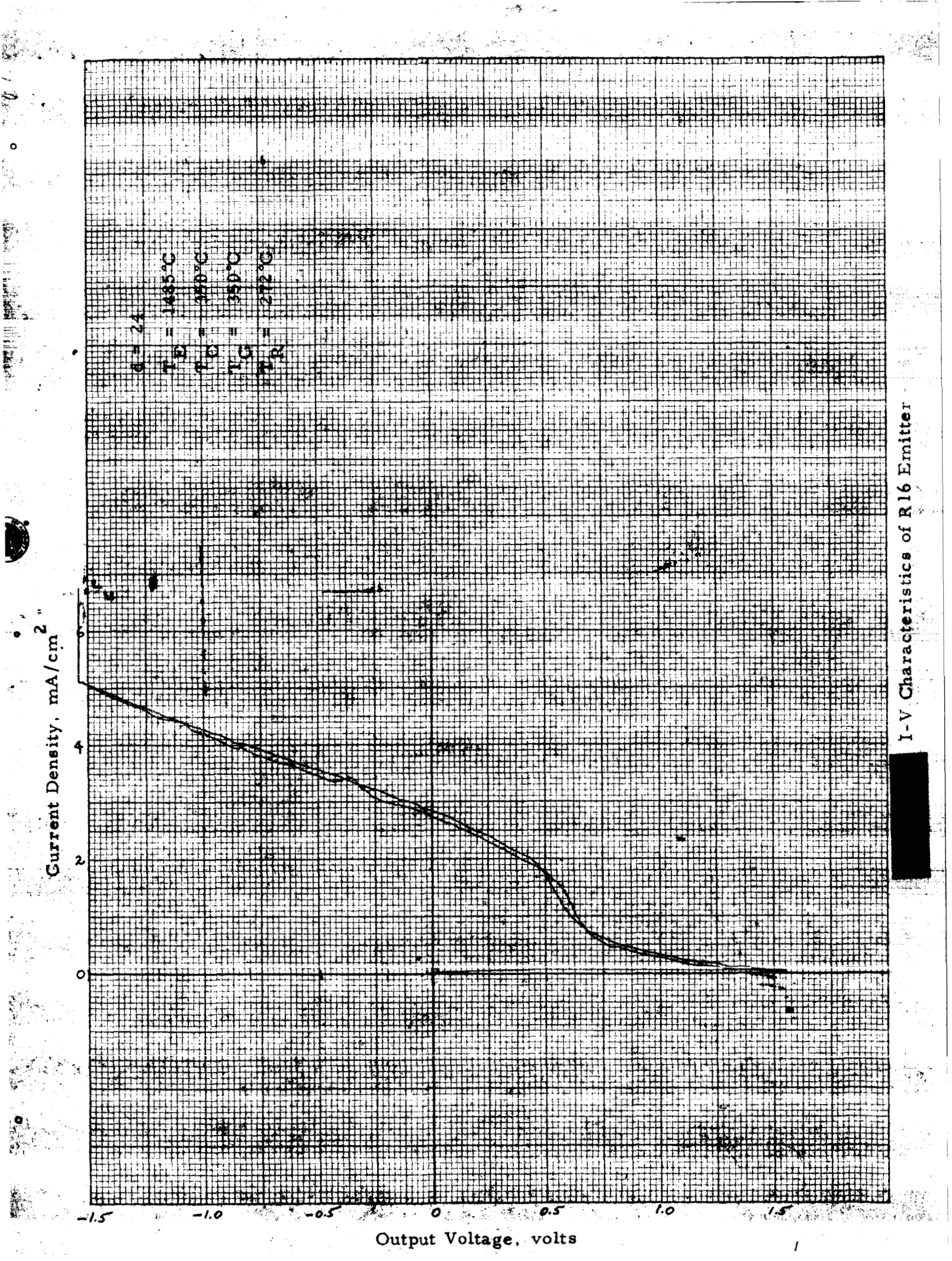

I-V Characteristics of R16 Emitter

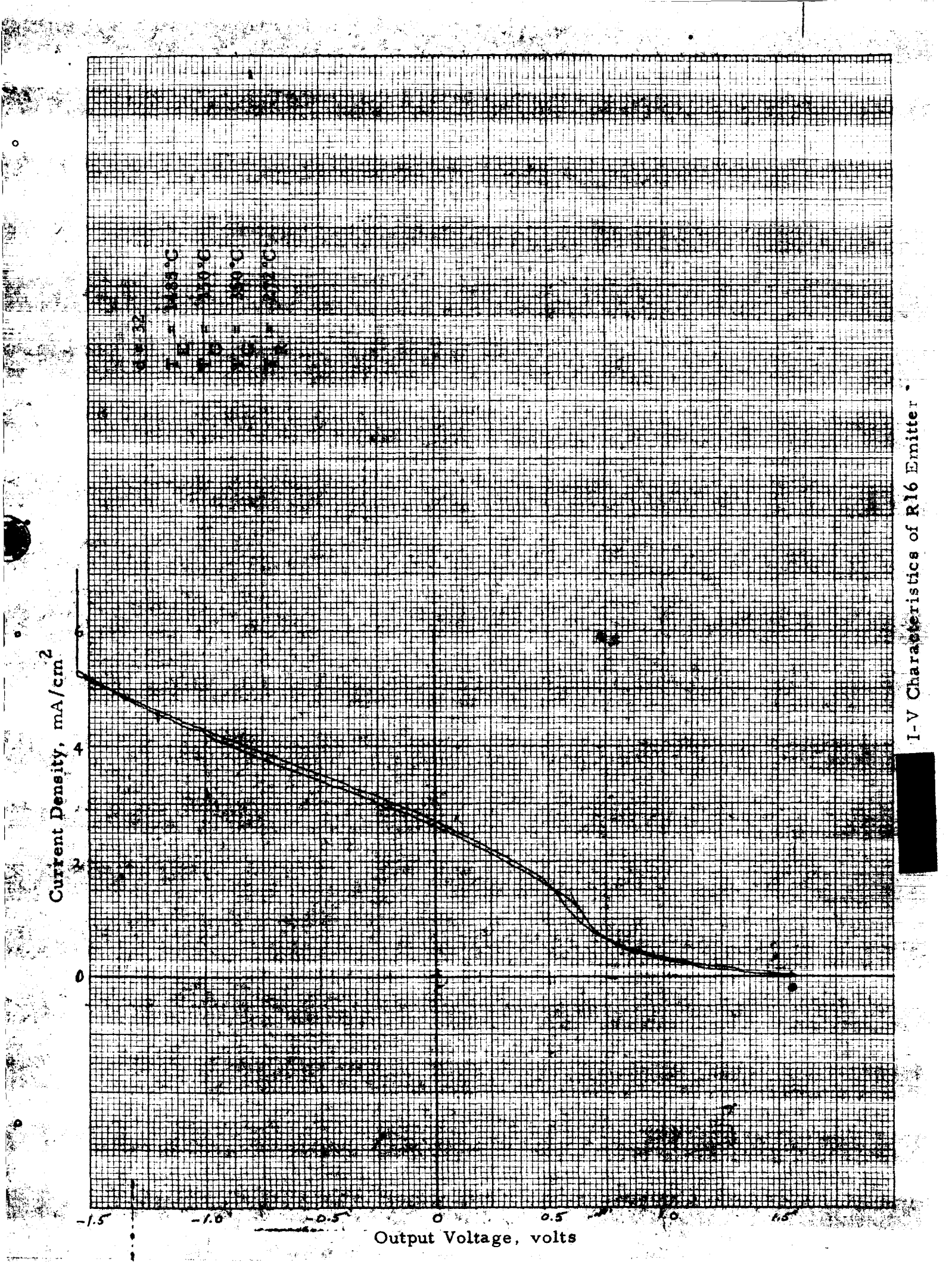

I-V Characteristics of R16 Emitter

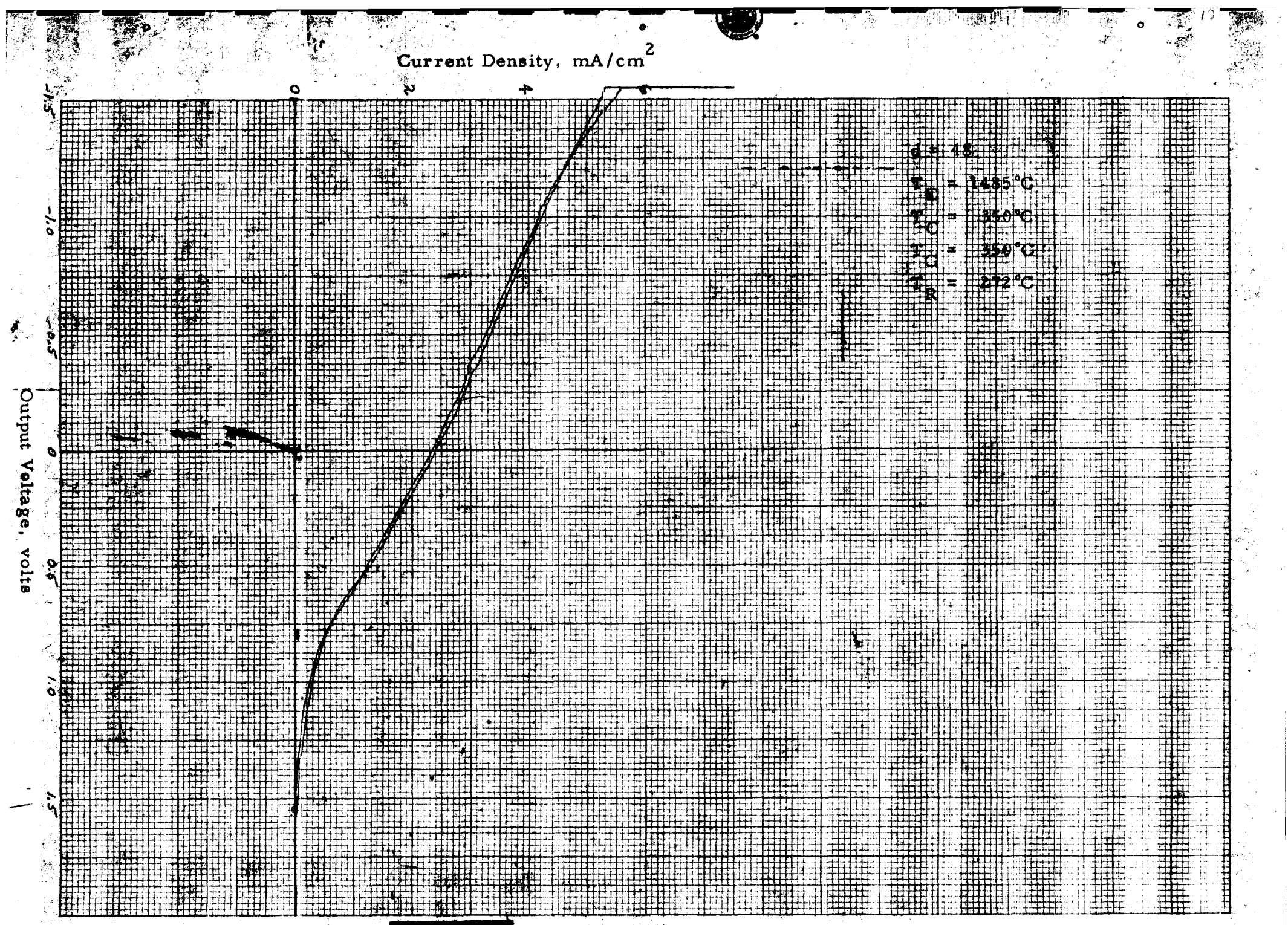

I-V Characteristics of R16 Emitter

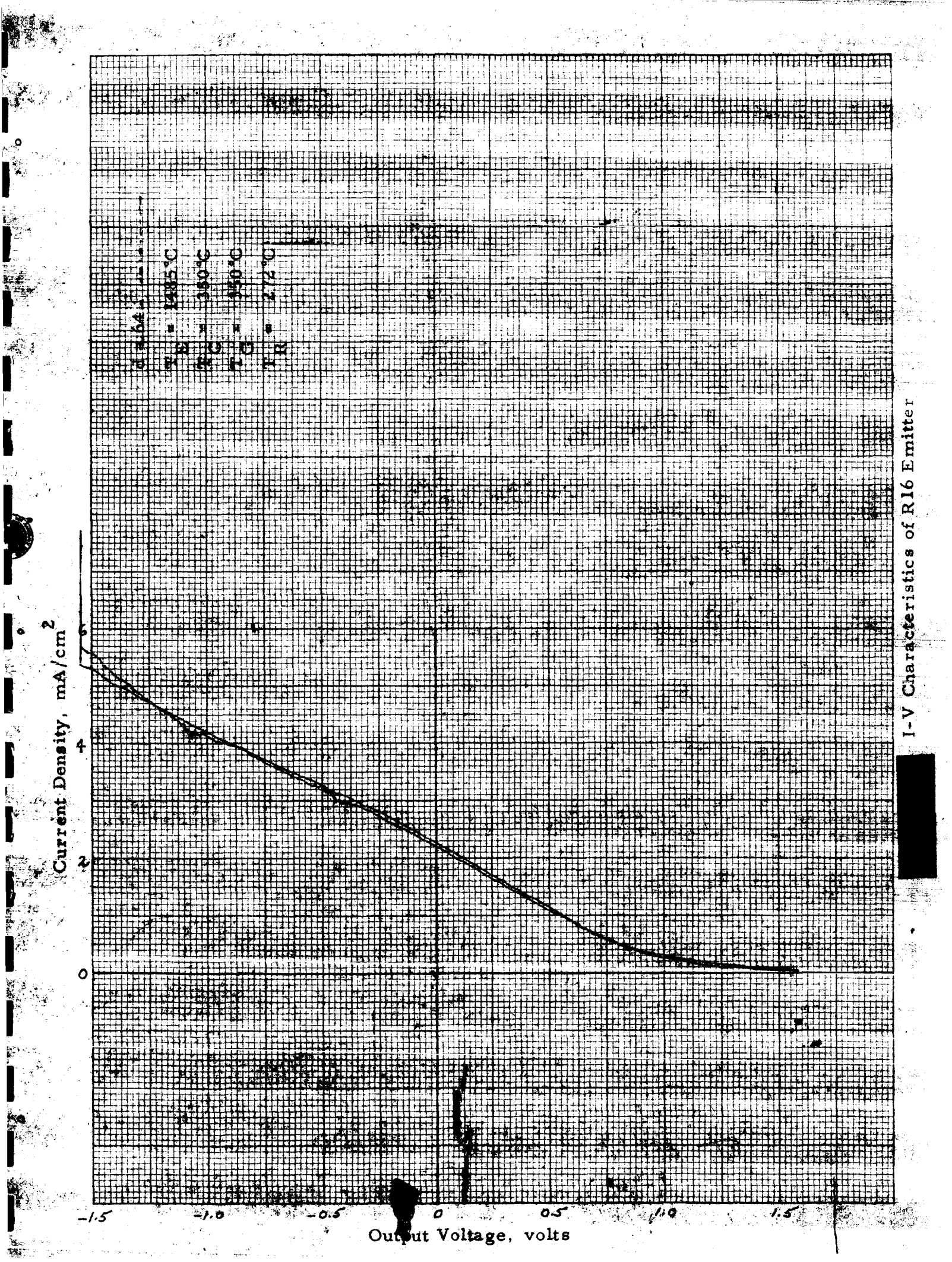

I-V Characteristics of R16 Emitter

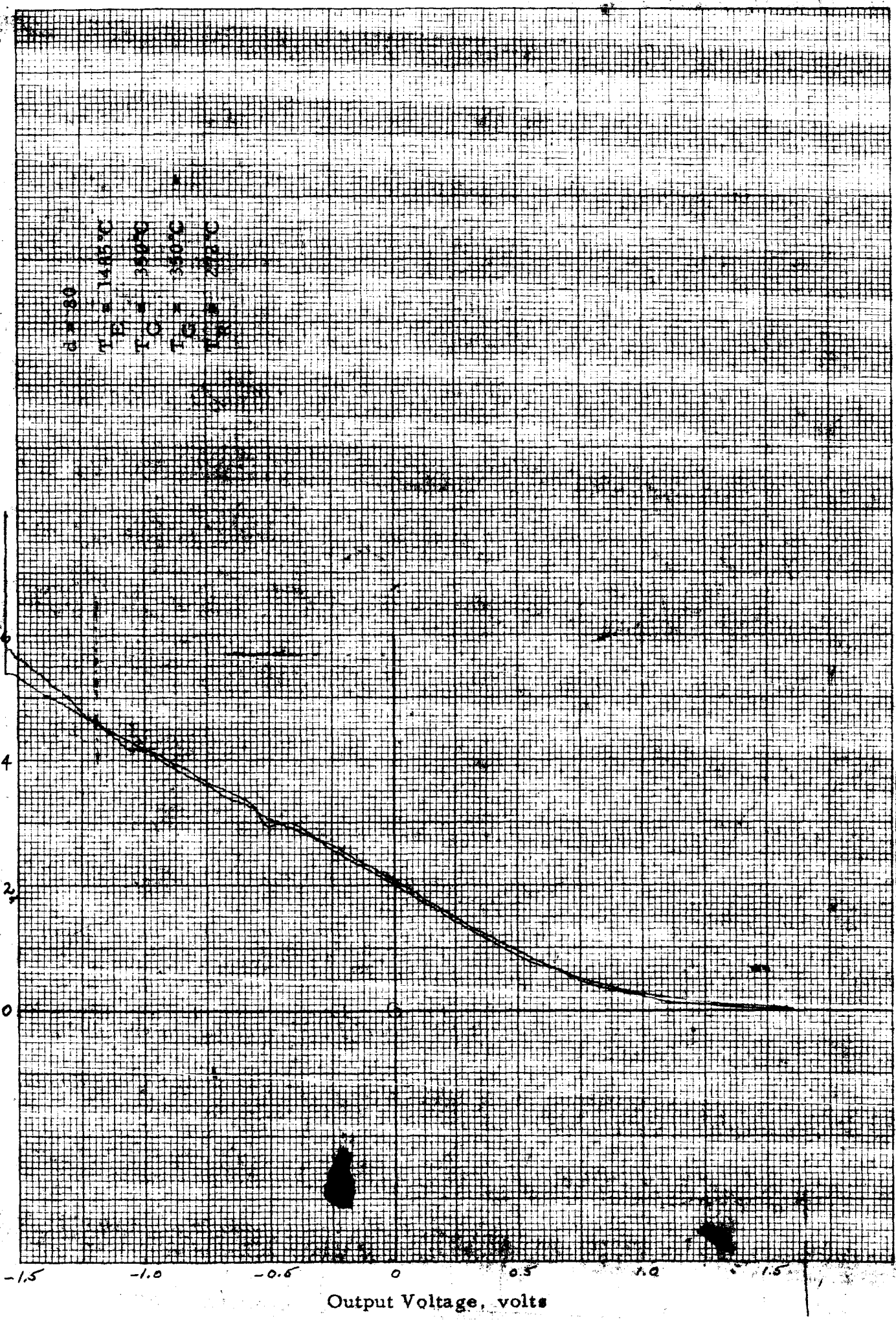

I-V Characteristics of R16 Emitter

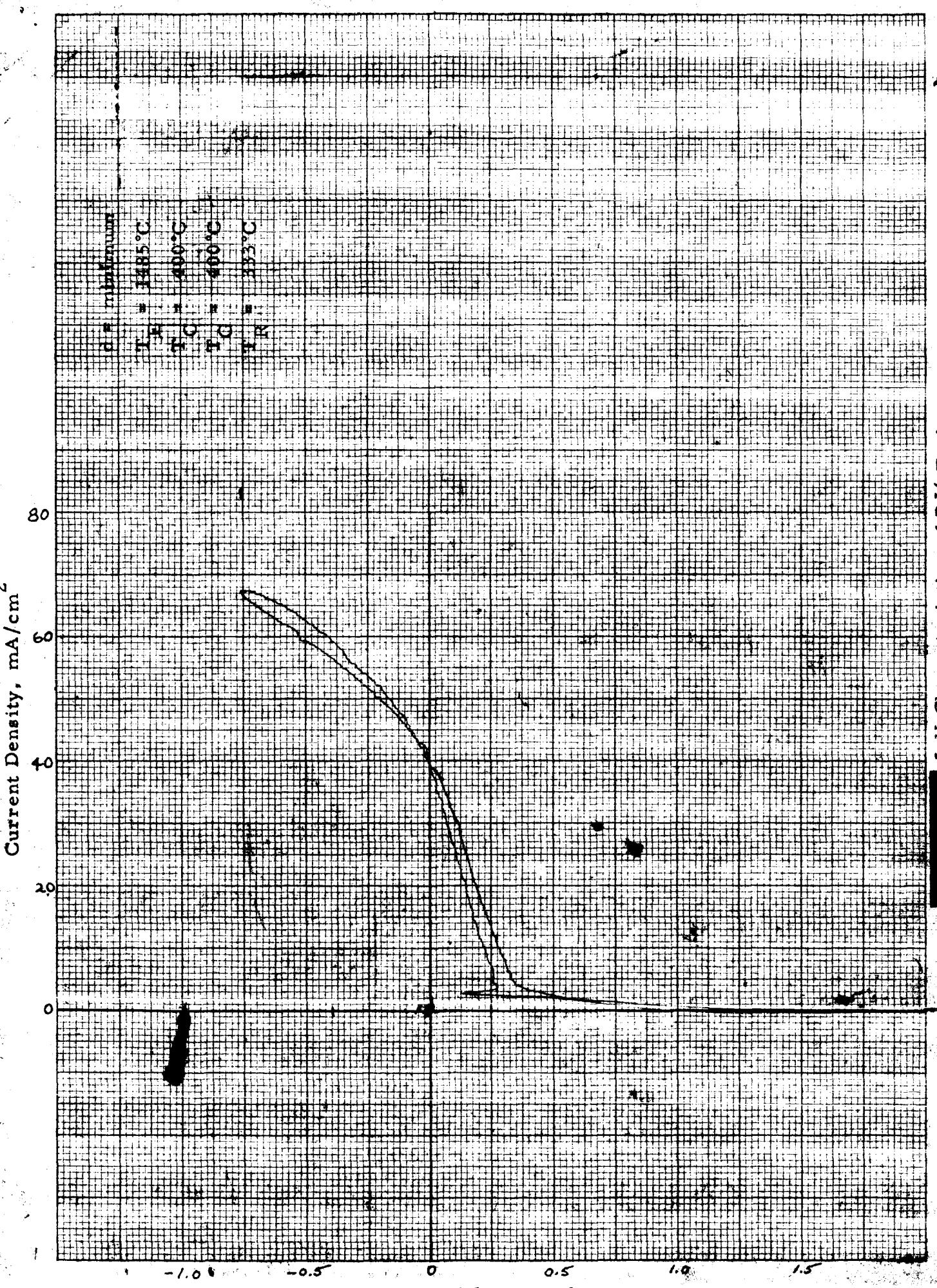

I-V Characteristics of R16 Emitter

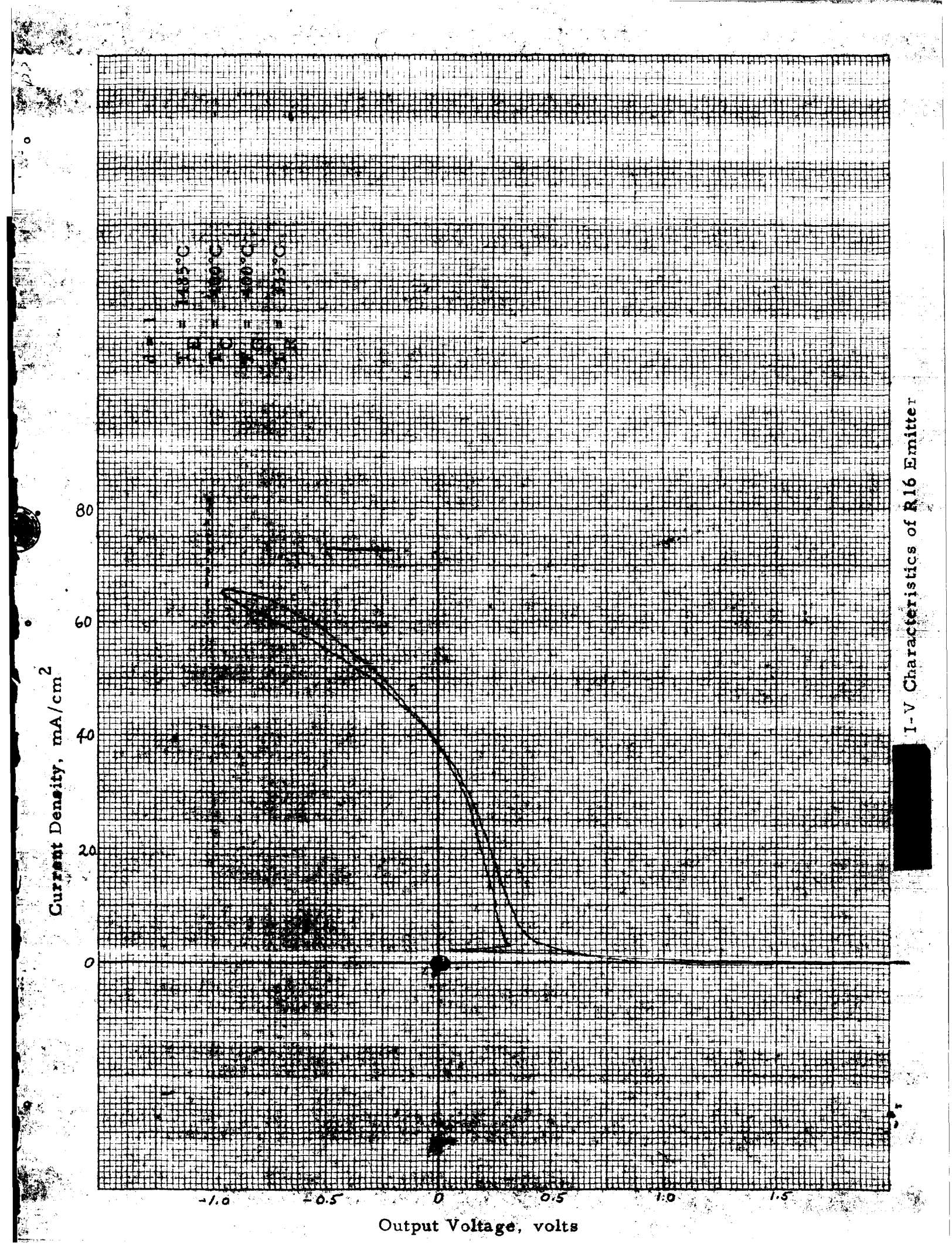
I-V Characteristics of R16 Emitter
Current Density, mA/cm^2
80
60
40
20
0
-1.0
-0.5
0
0.5
1.0
1.5
Output Voltage, volts

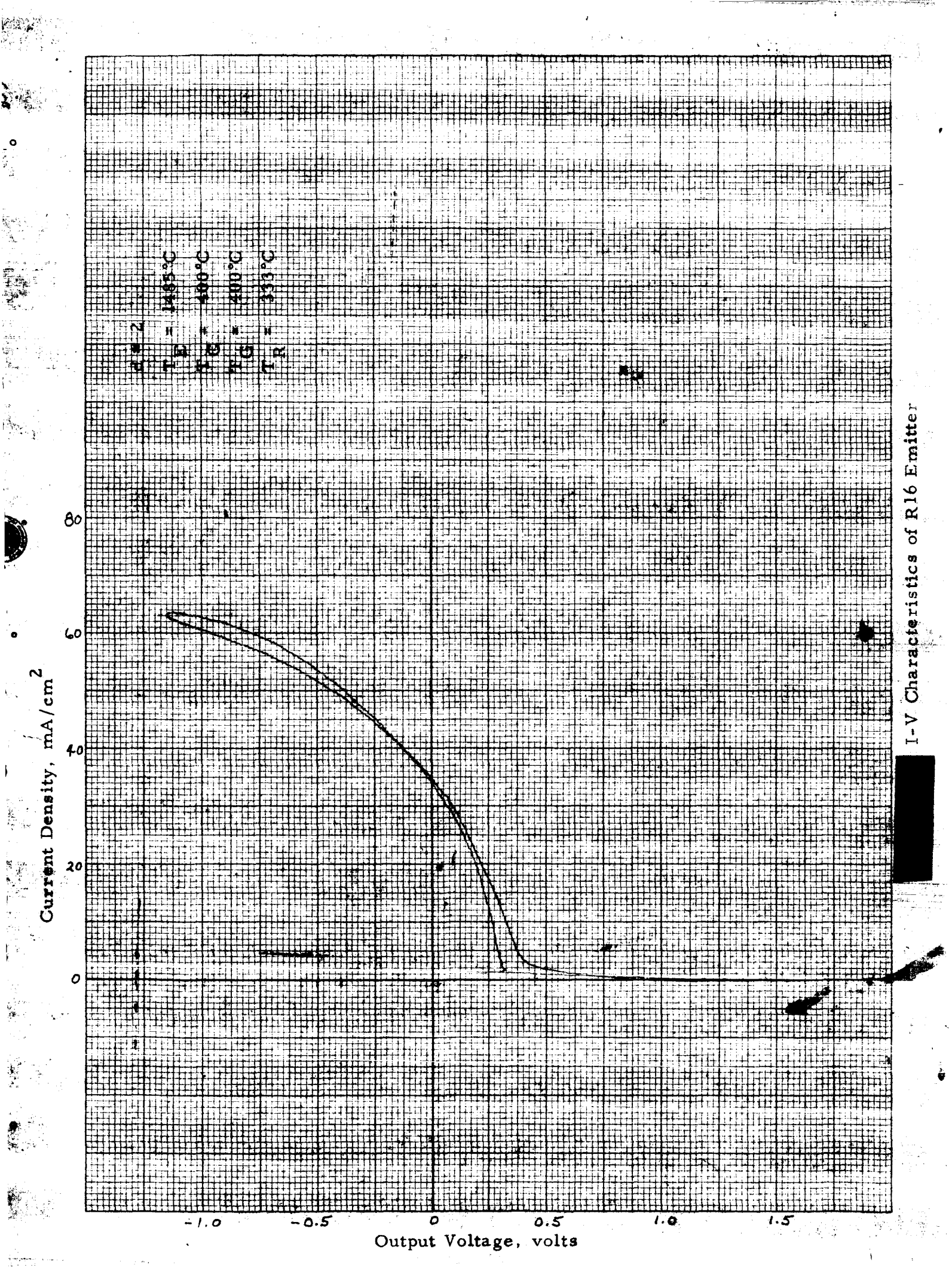
d = 2
T_B = 146°C
T_E = 400°C
T_C = 400°C
T_R = 333°C
80
60
40
20
0
Current Density, mA/cm²
-1.0
-0.5
0
0.5
1.0
1.5
Output Voltage, volts
I-V Characteristics of R16 Emitter

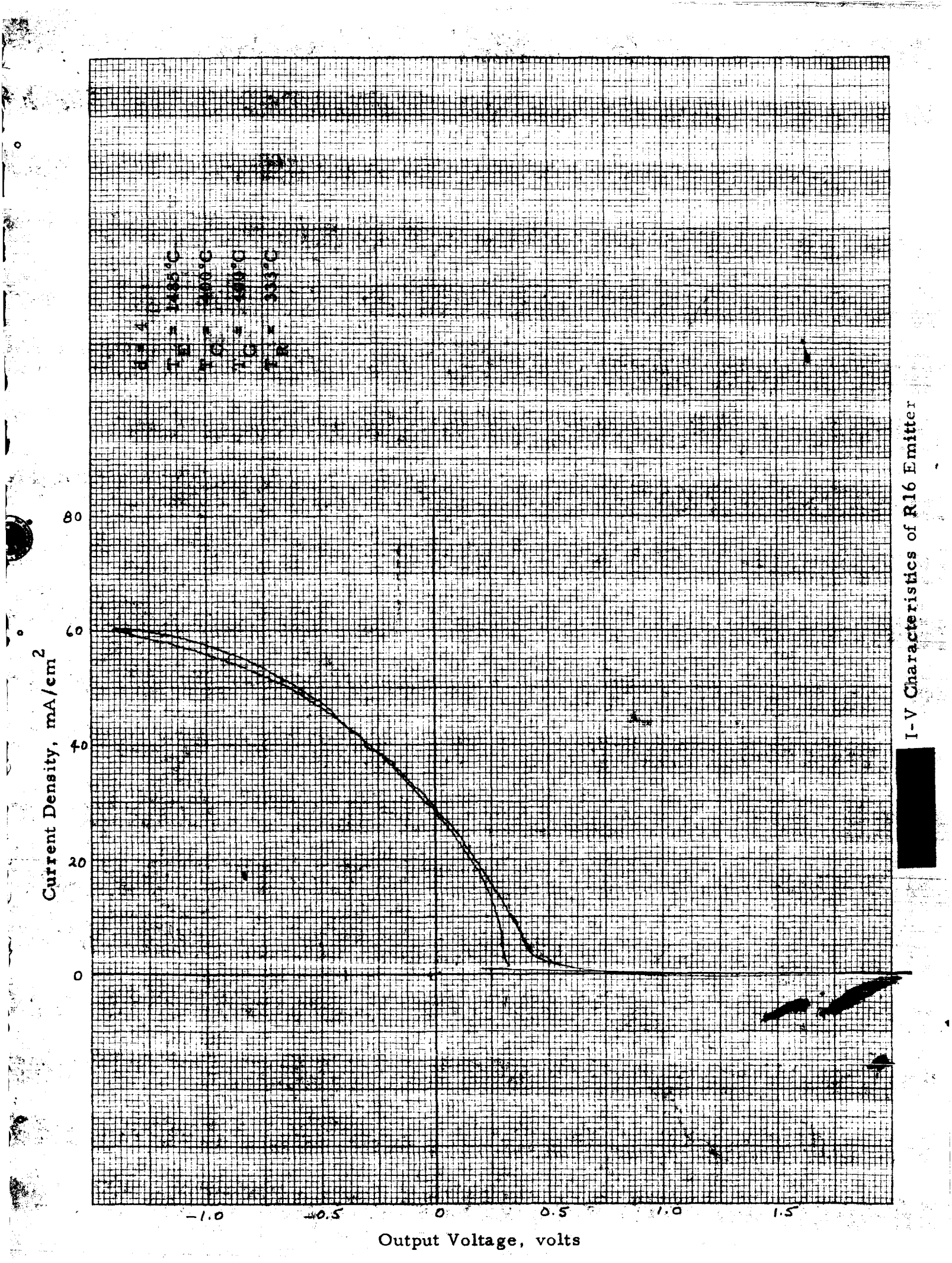
I-V Characteristics of R16 Emitter
Current Density, mA/cm^2
80
60
40
20
0
-1.0
-0.5
0
0.5
1.0
1.5
Output Voltage, volts

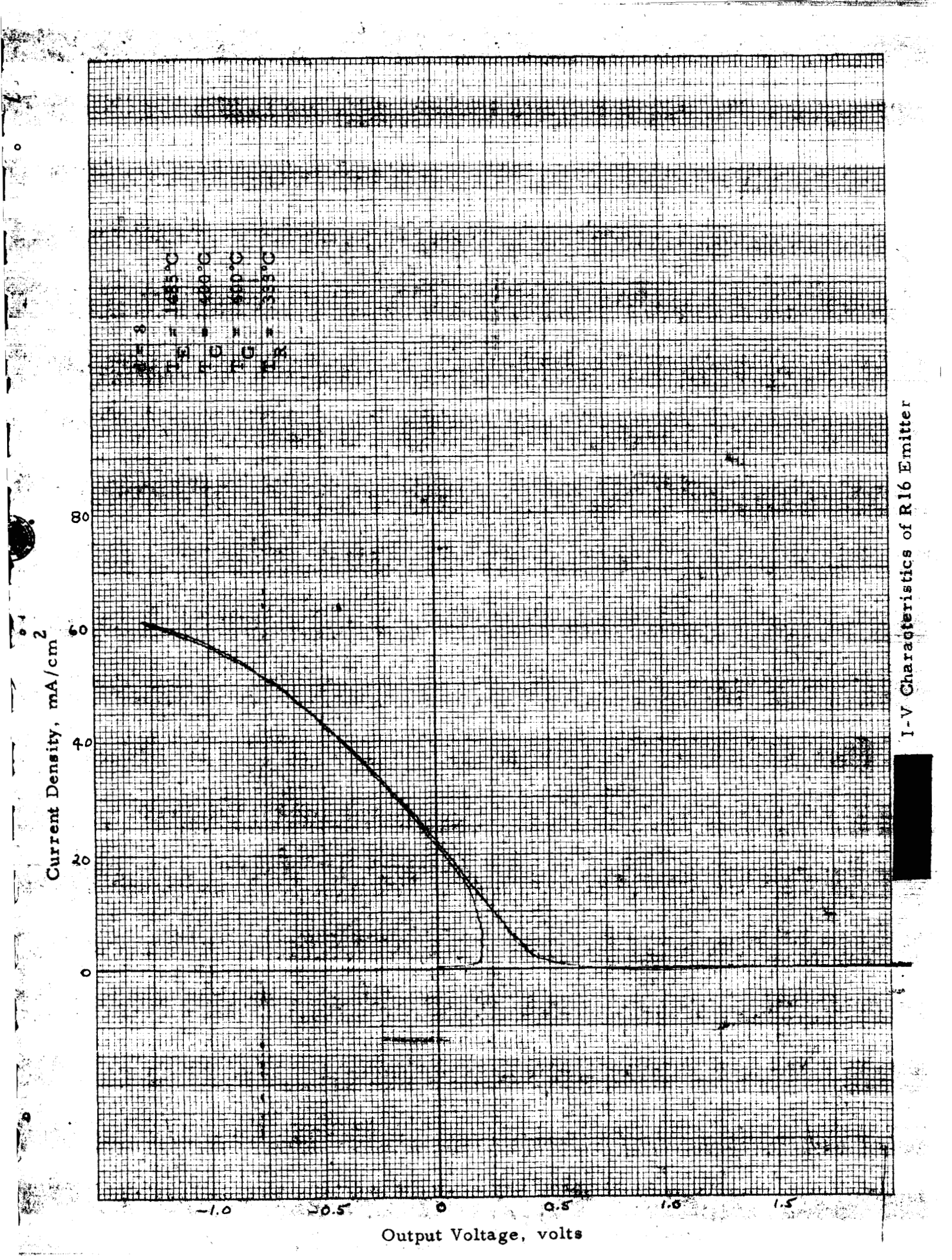
Current Density, mA/cm^2
80
60
40
20
0
-1.0
-0.5
0
0.5
1.0
1.5
Output Voltage, volts
I-V Characteristics of R16 Emitter

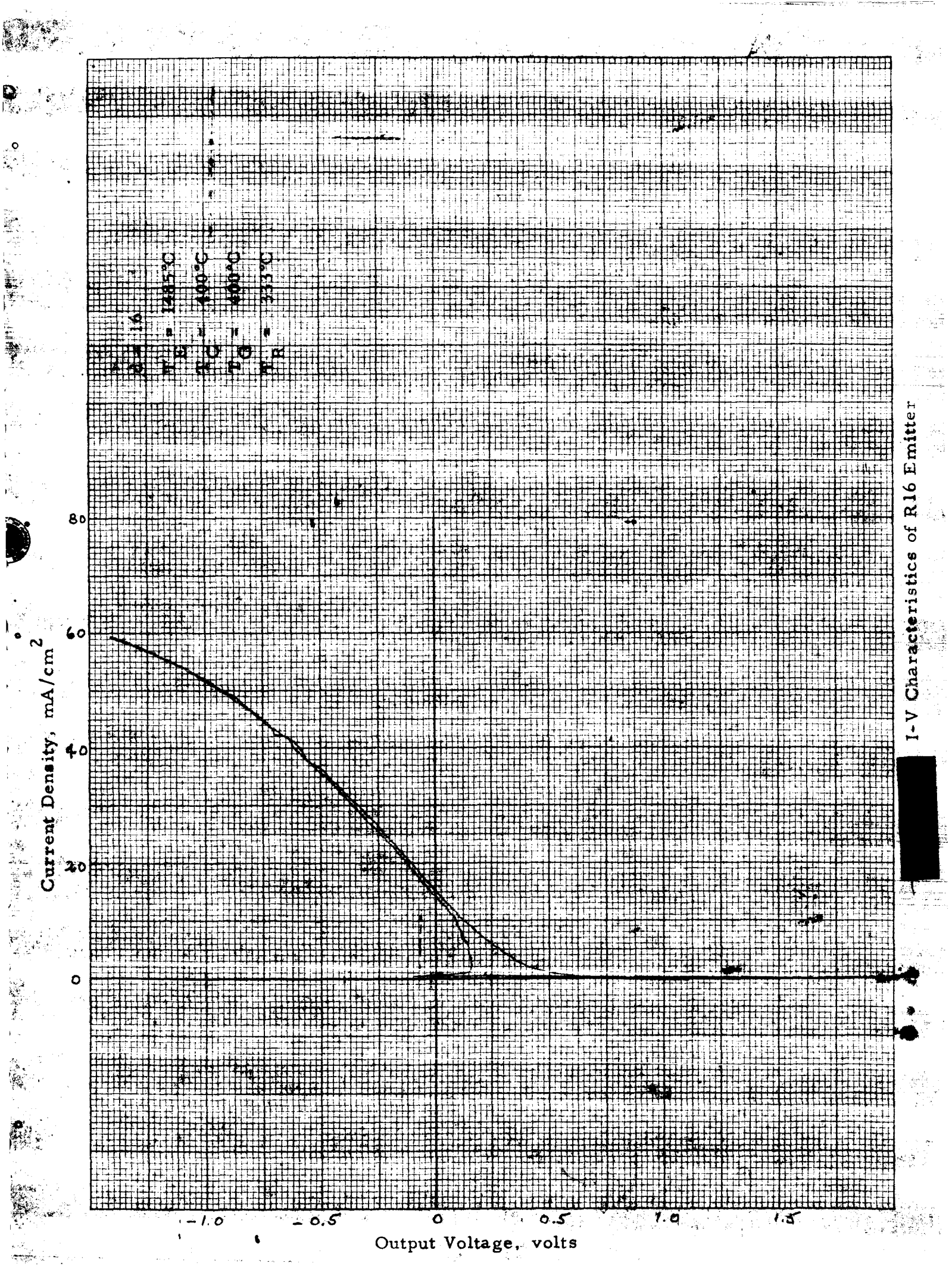

I-V Characteristics of R16 Emitter

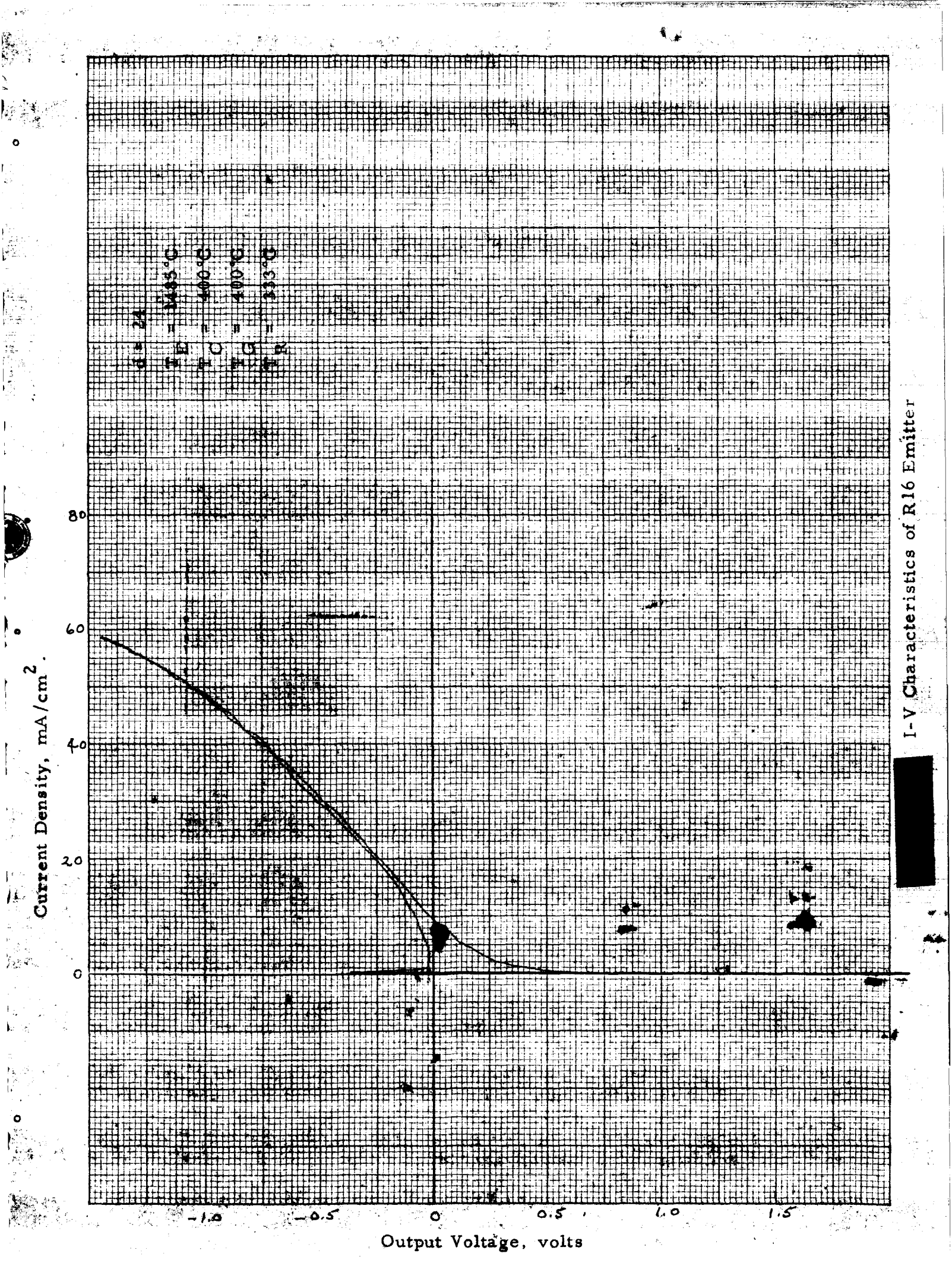

I-V Characteristics of R16 Emitter

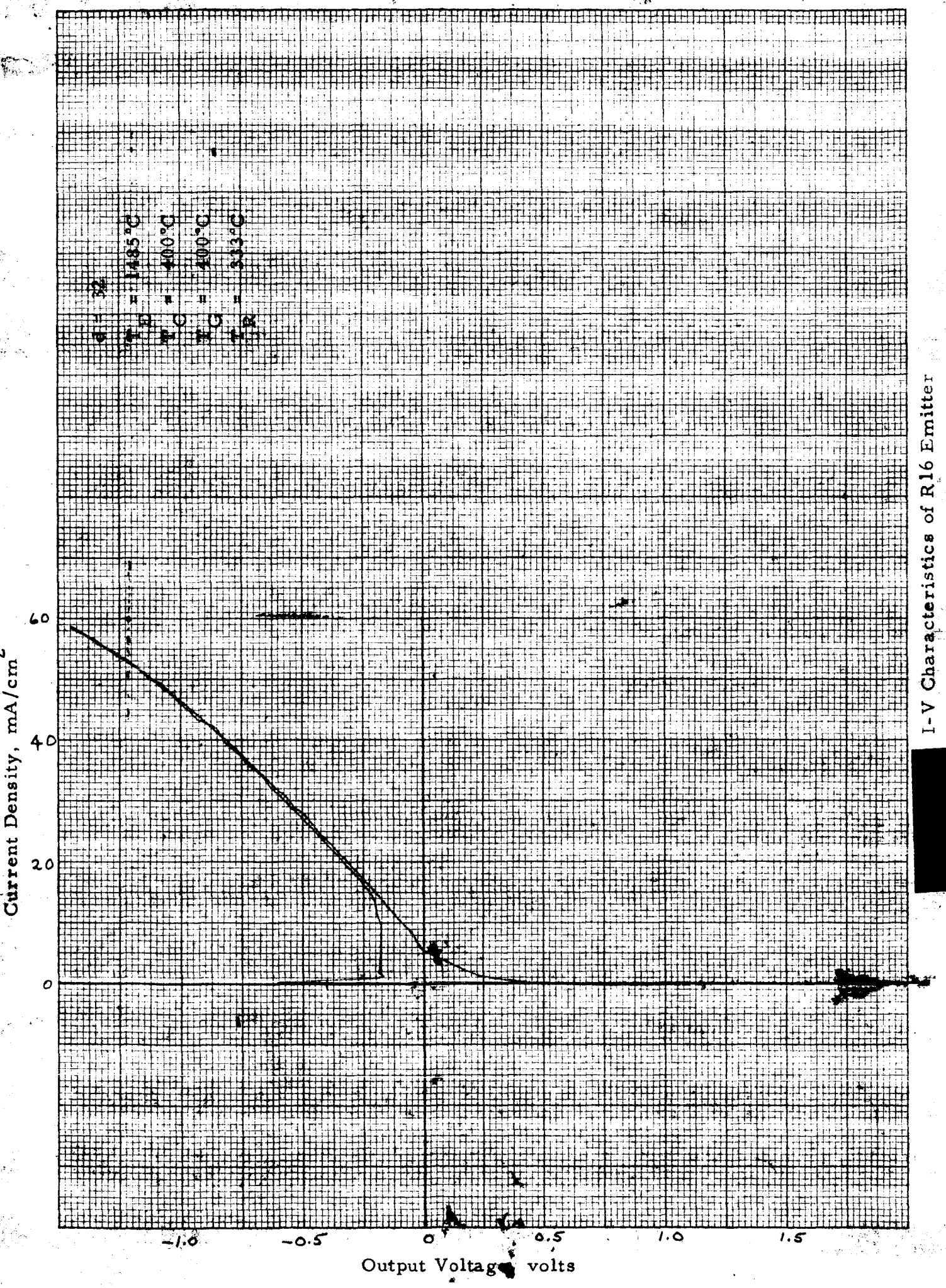

I-V Characteristics of R16 Emitter

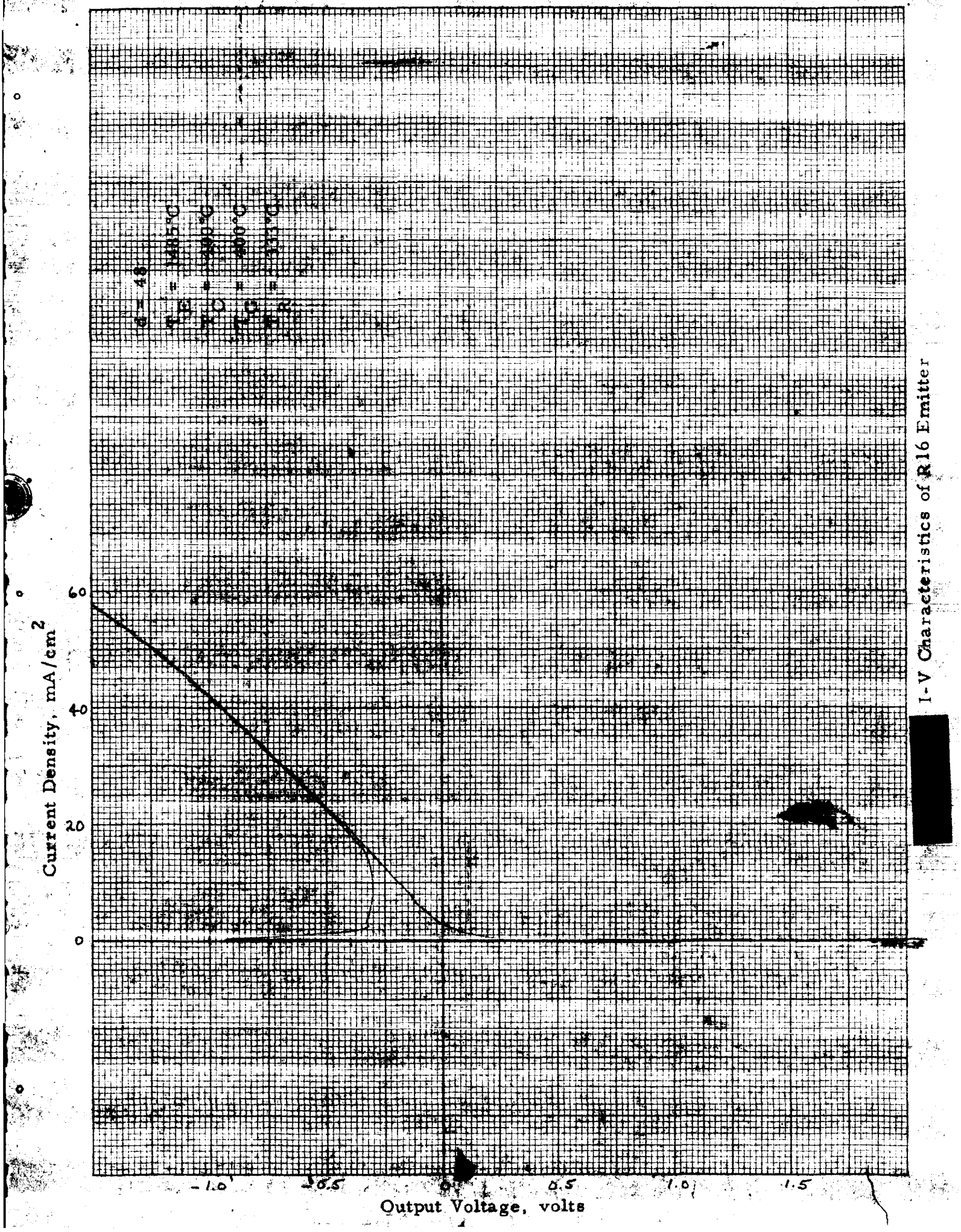

I-V Characteristics of R16 Emitter

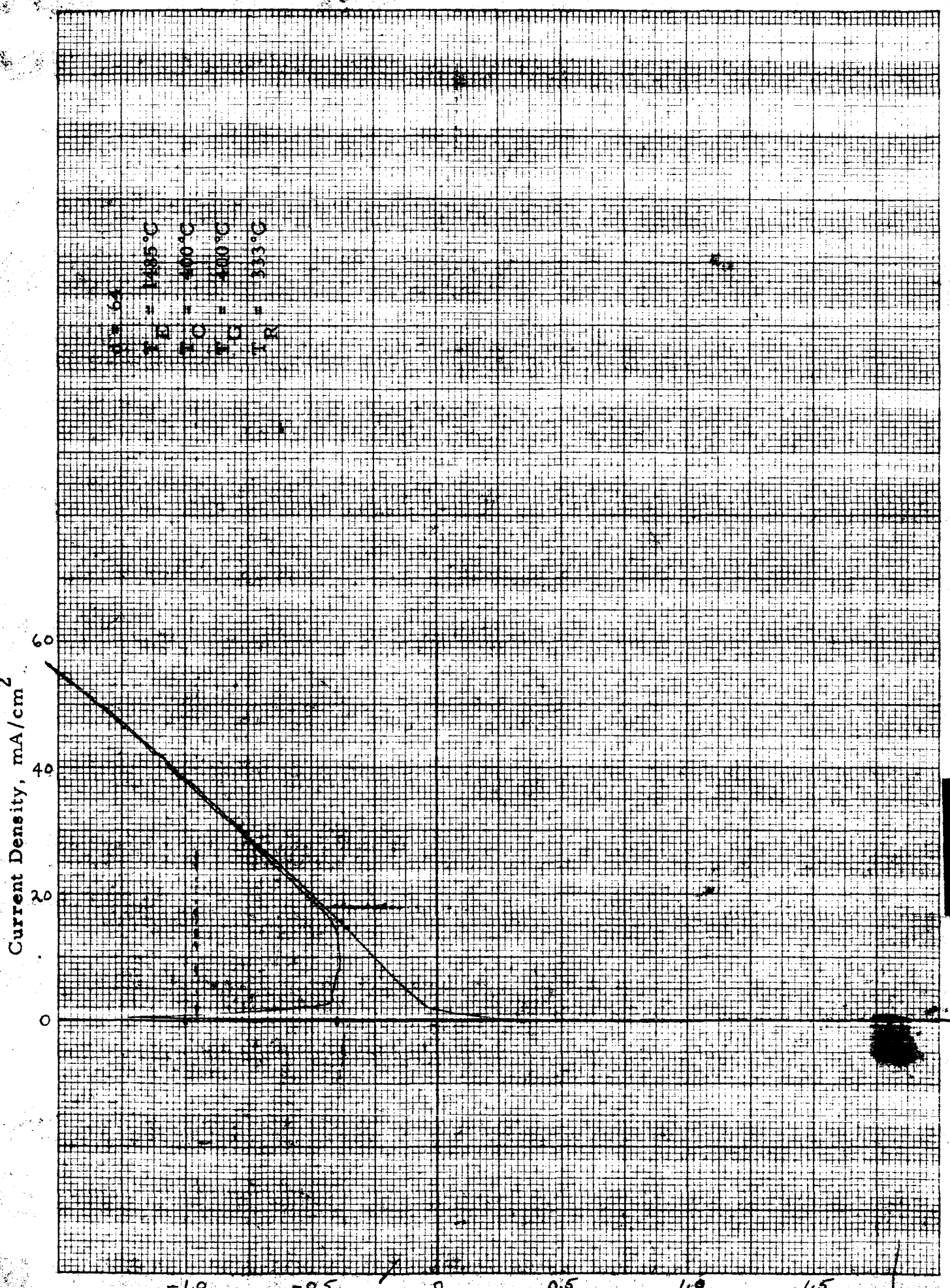

I-V Characteristics of R16 Emitter

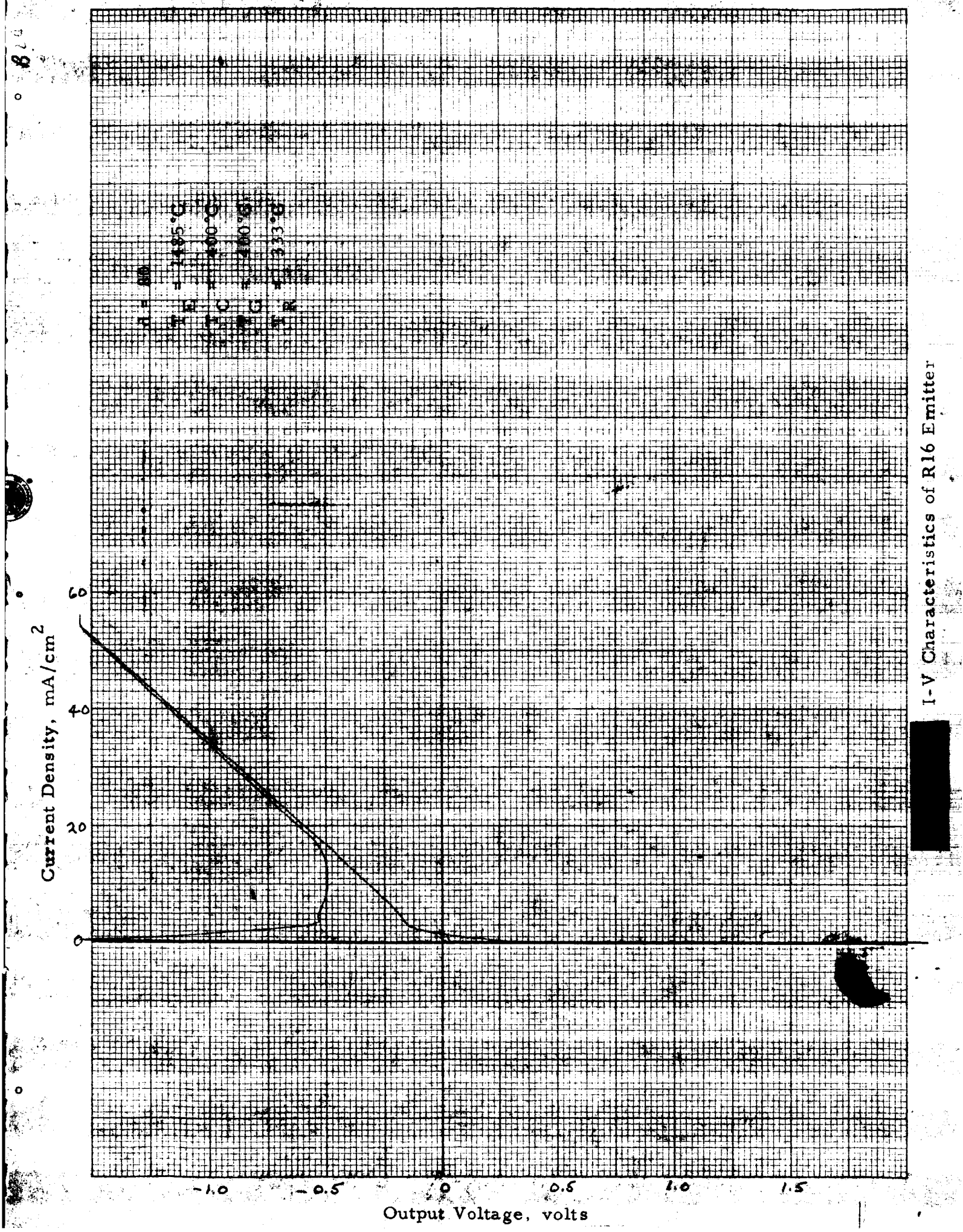

I-V Characteristics of R16 Emitter

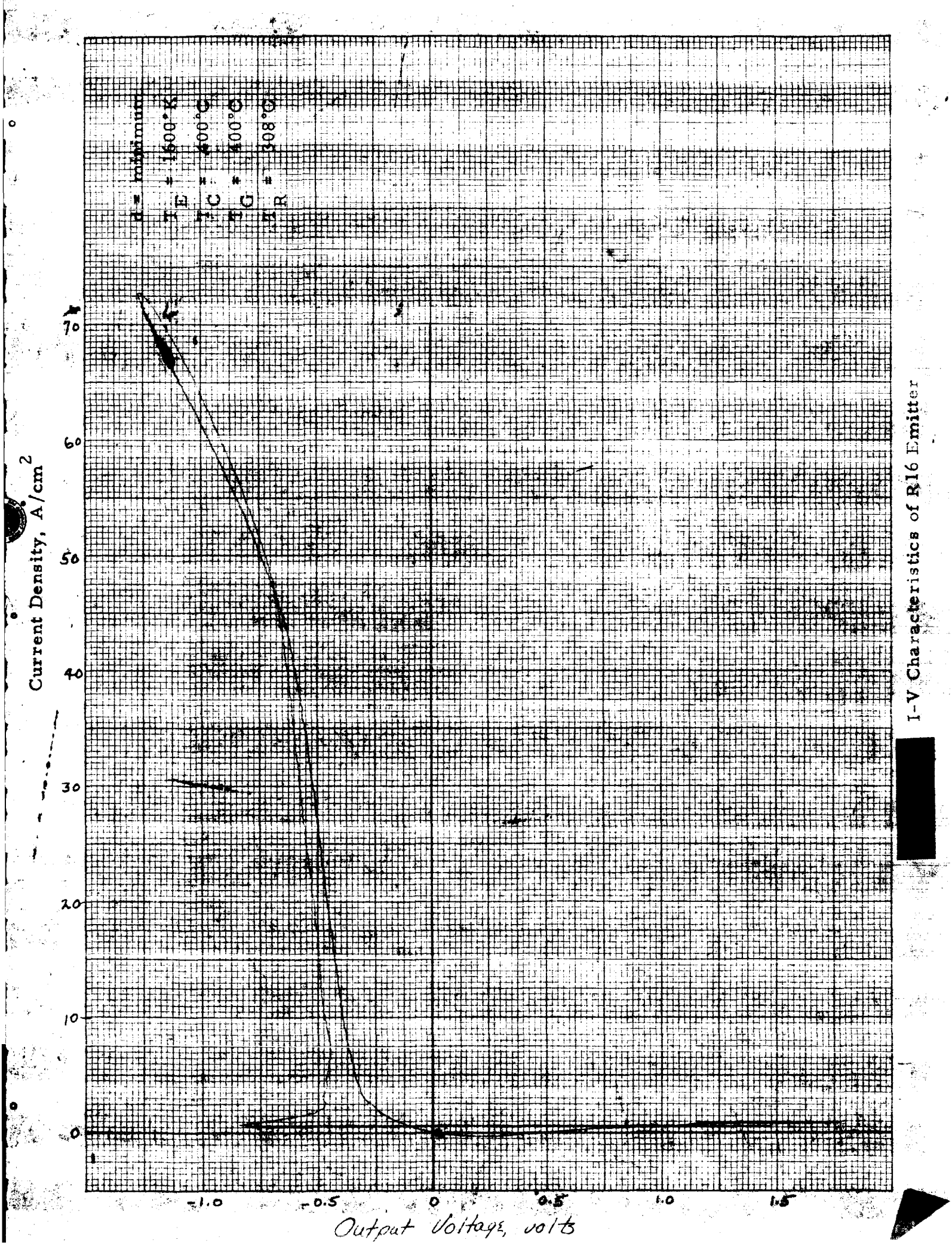

I-V Characteristics of R16 Emitter

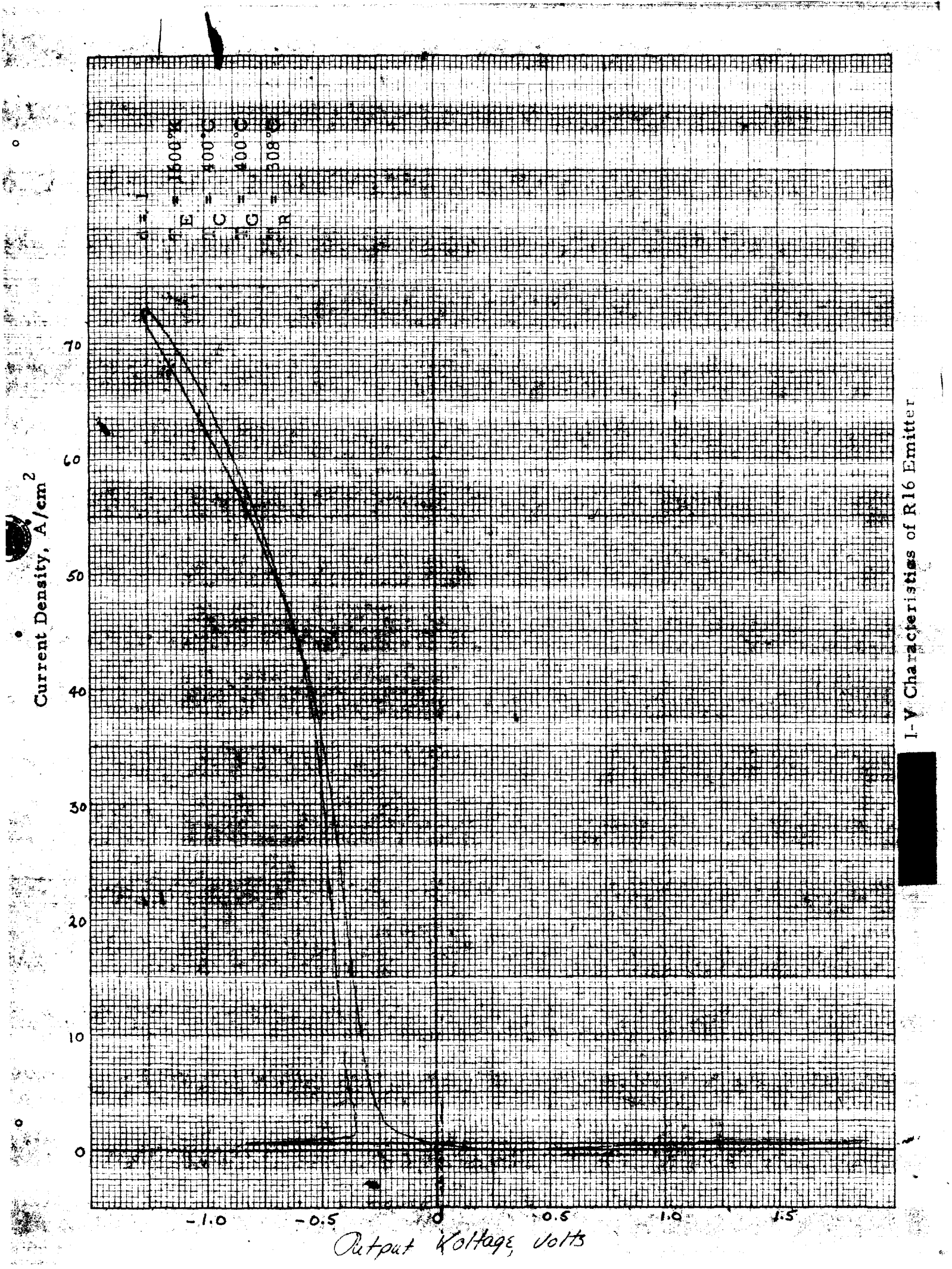

I-V Characteristics of R16 Emitter

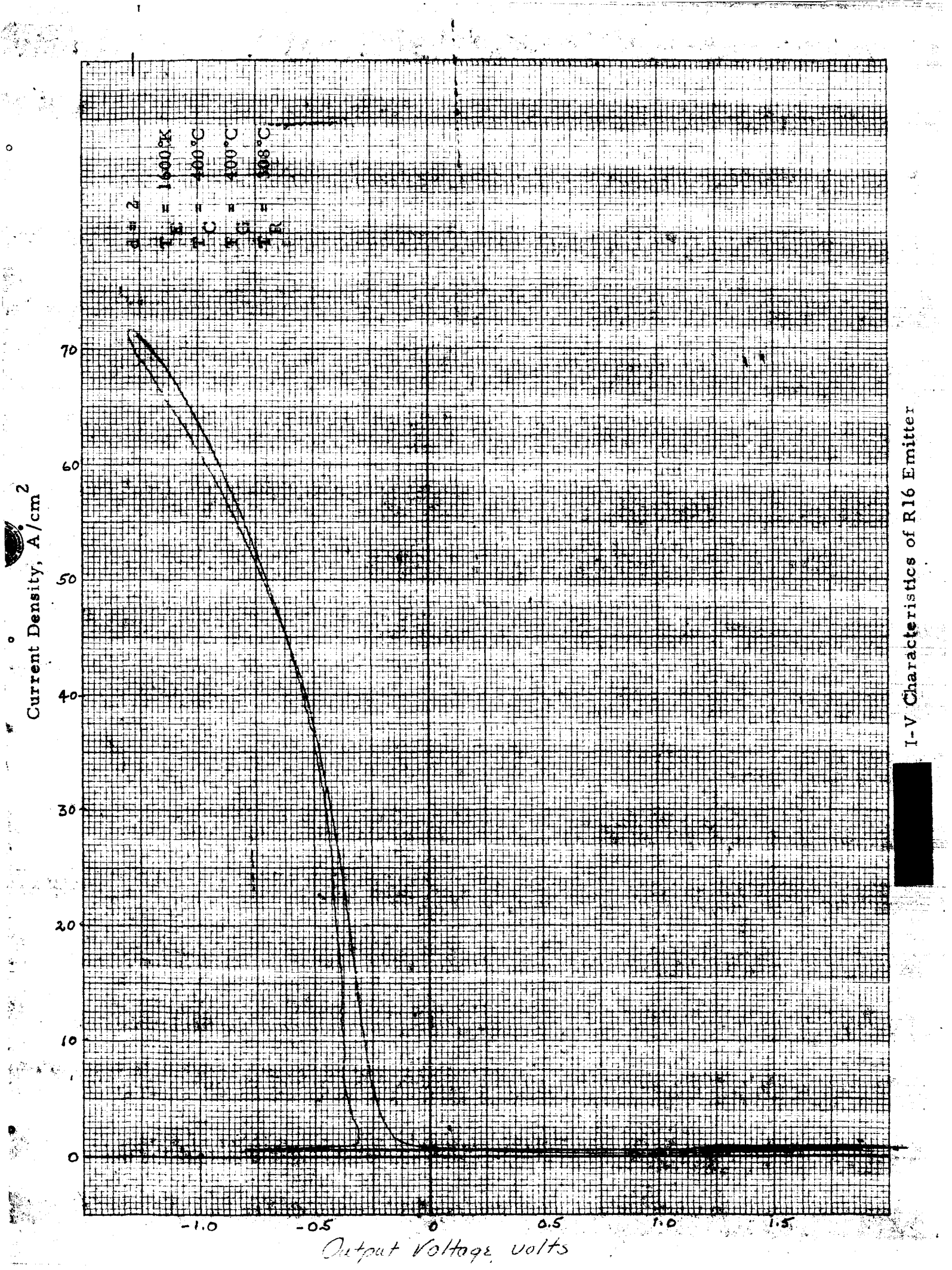

I-V Characteristics of R16 Emitter

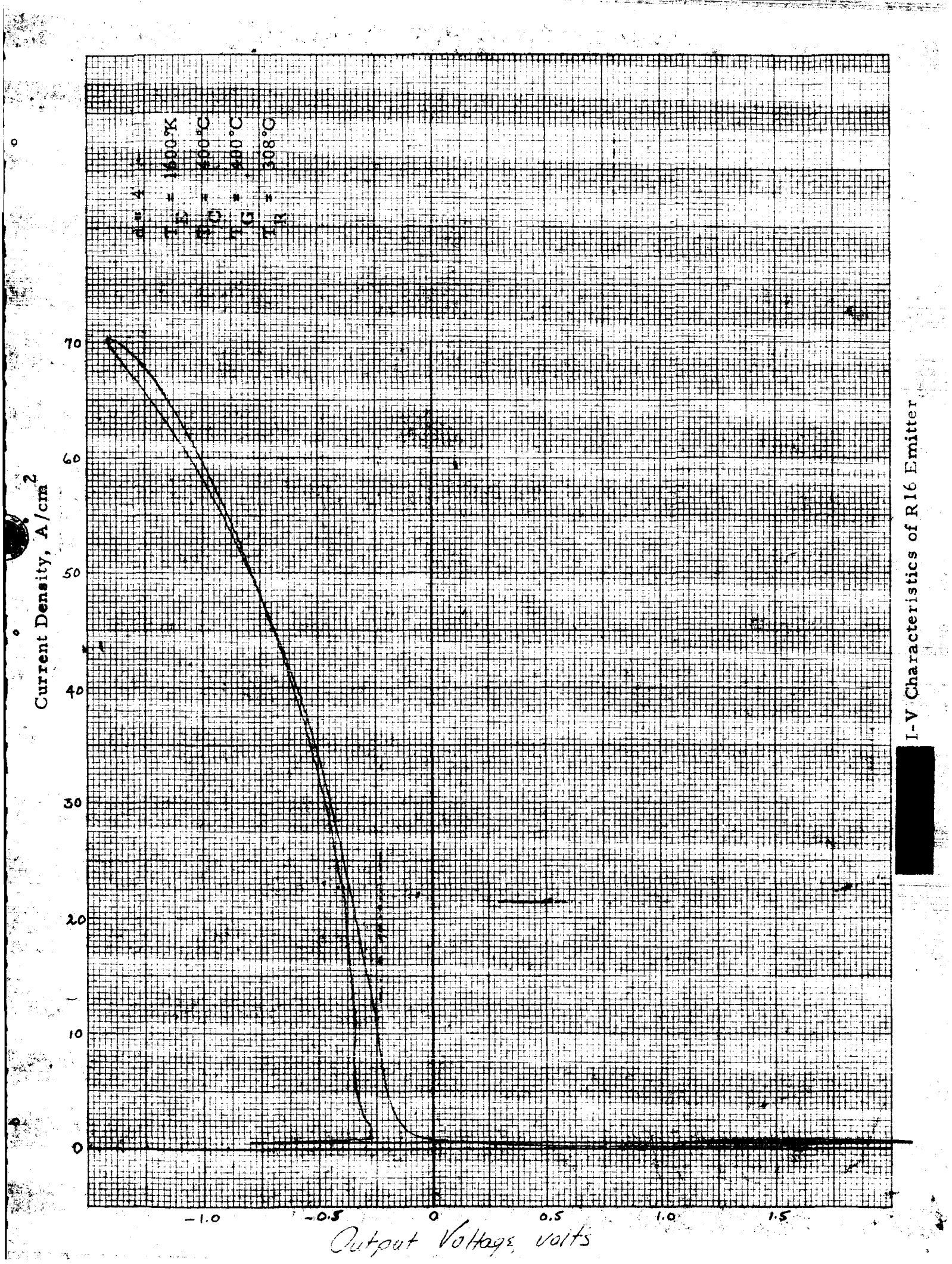

I-V Characteristics of R16 Emitter

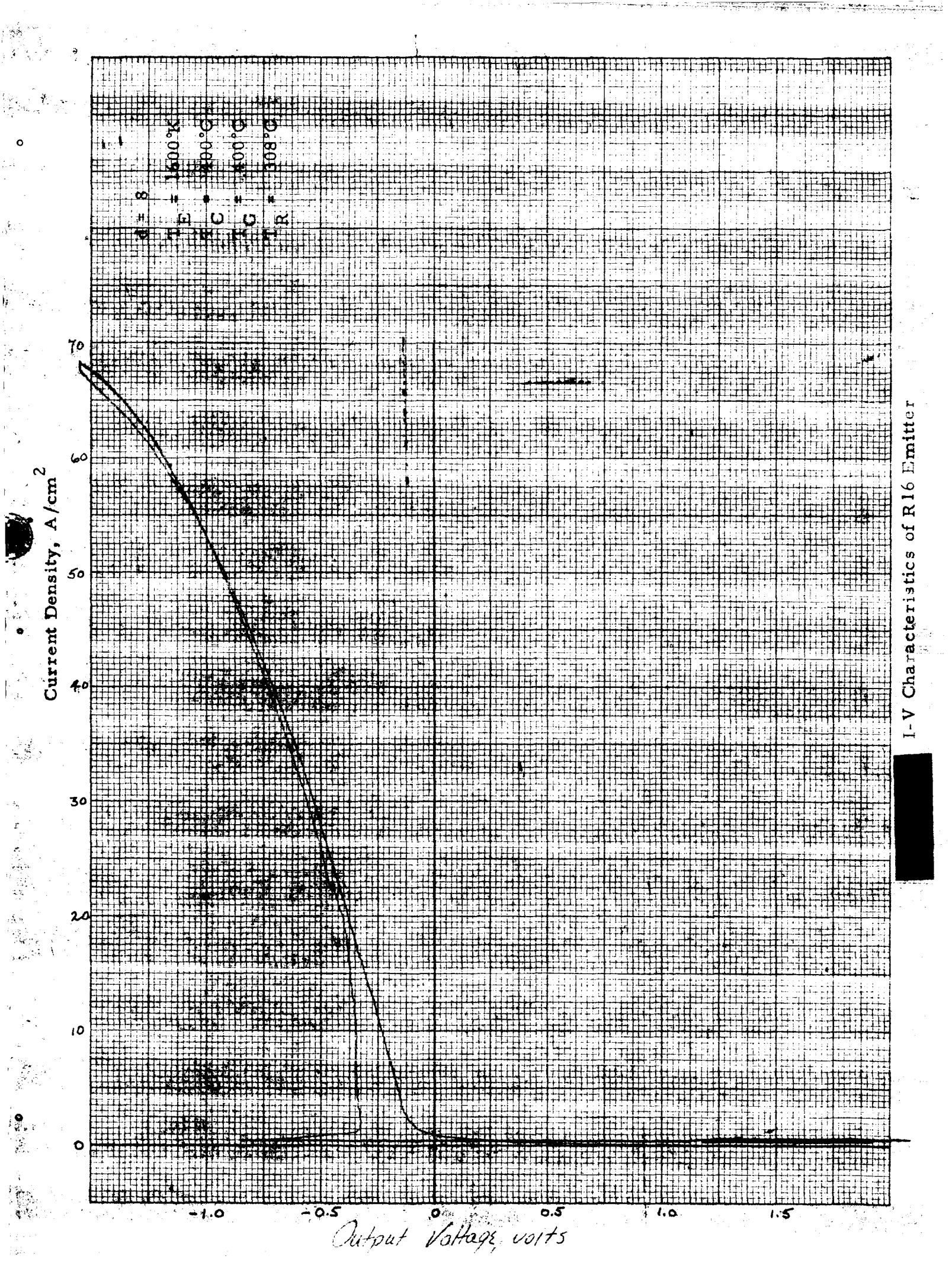

I-V Characteristics of R16 Emitter

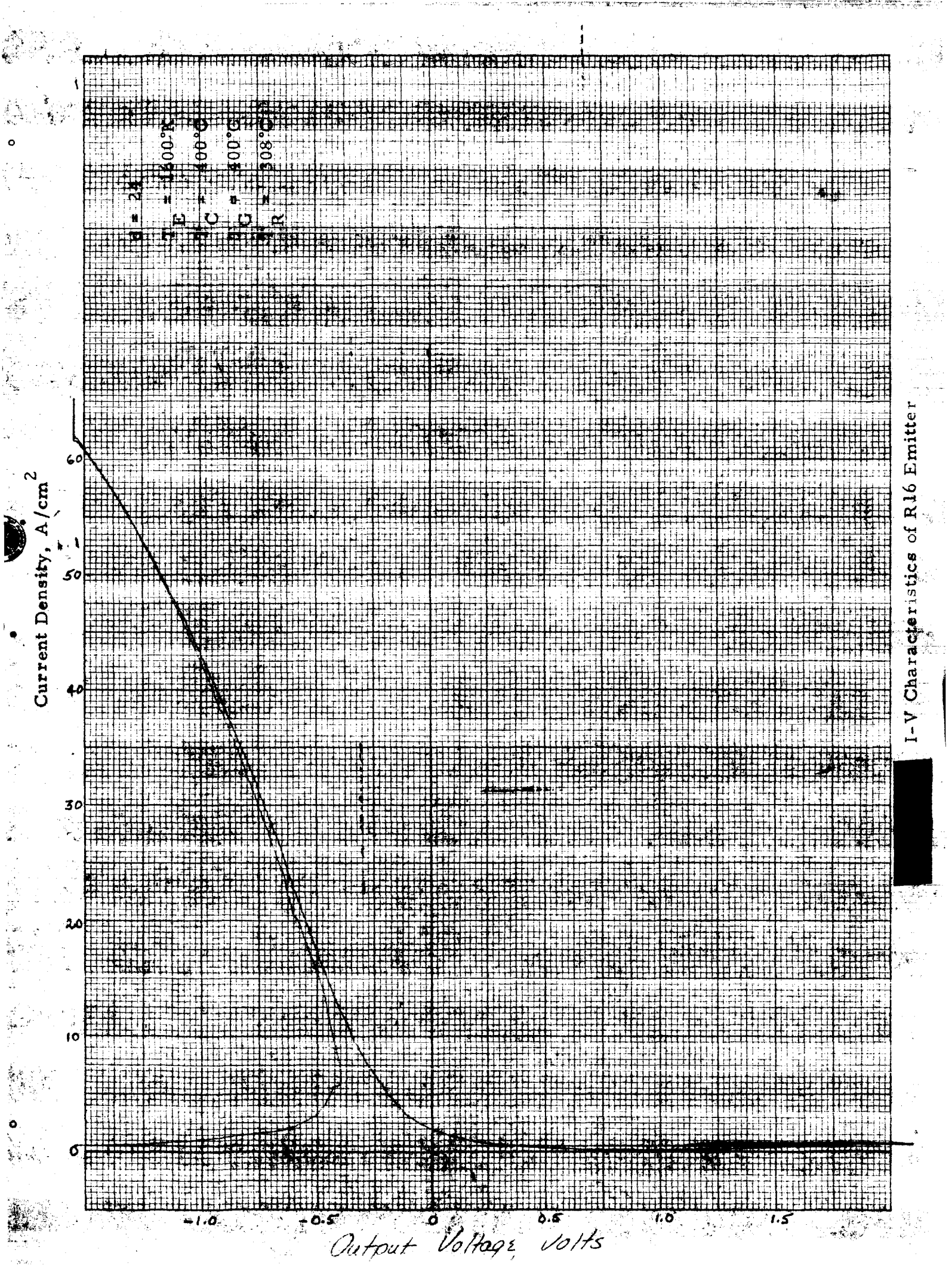

I-V Characteristics of R16 Emitter

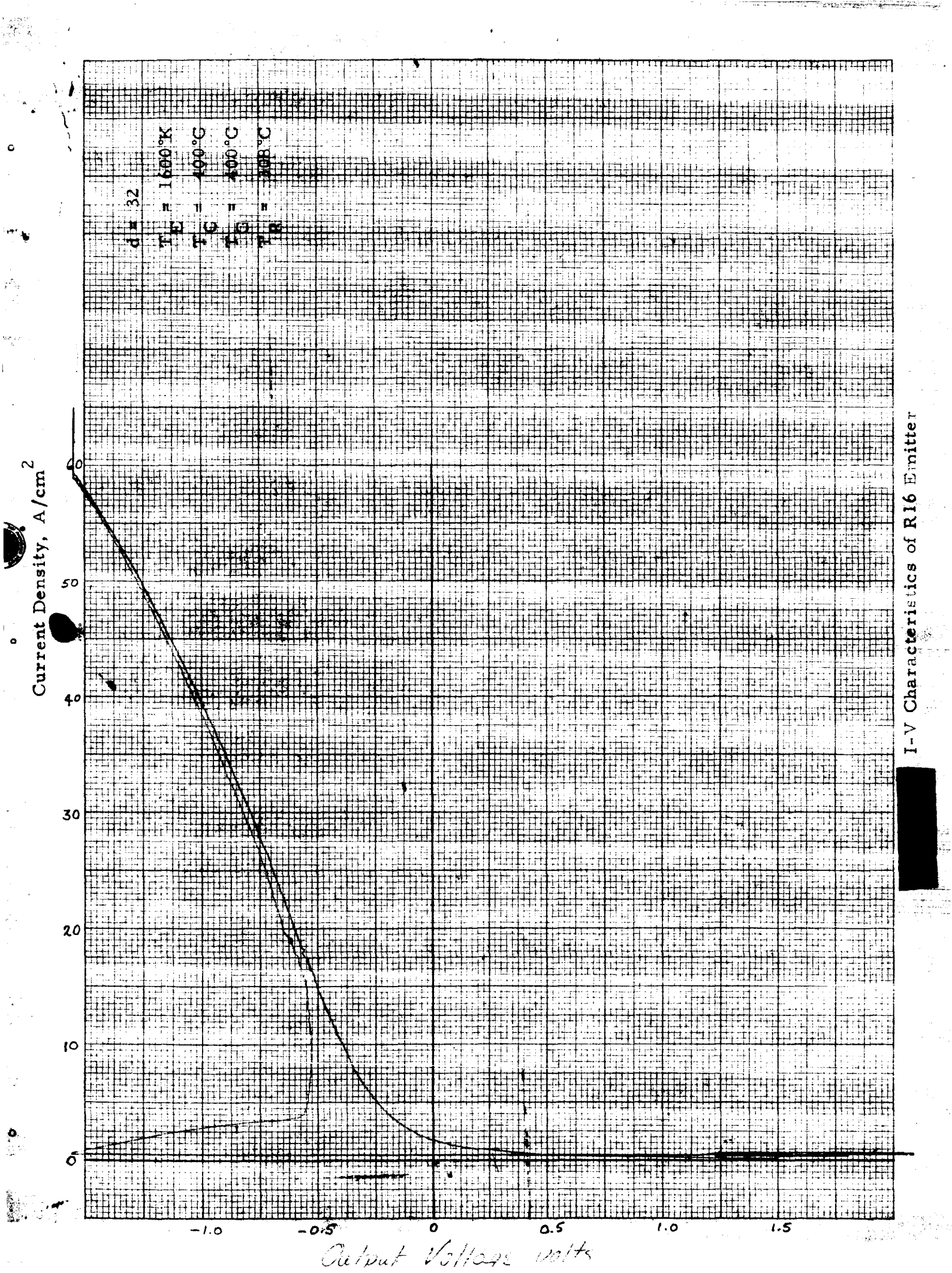

I-V Characteristics of R16 Emitter

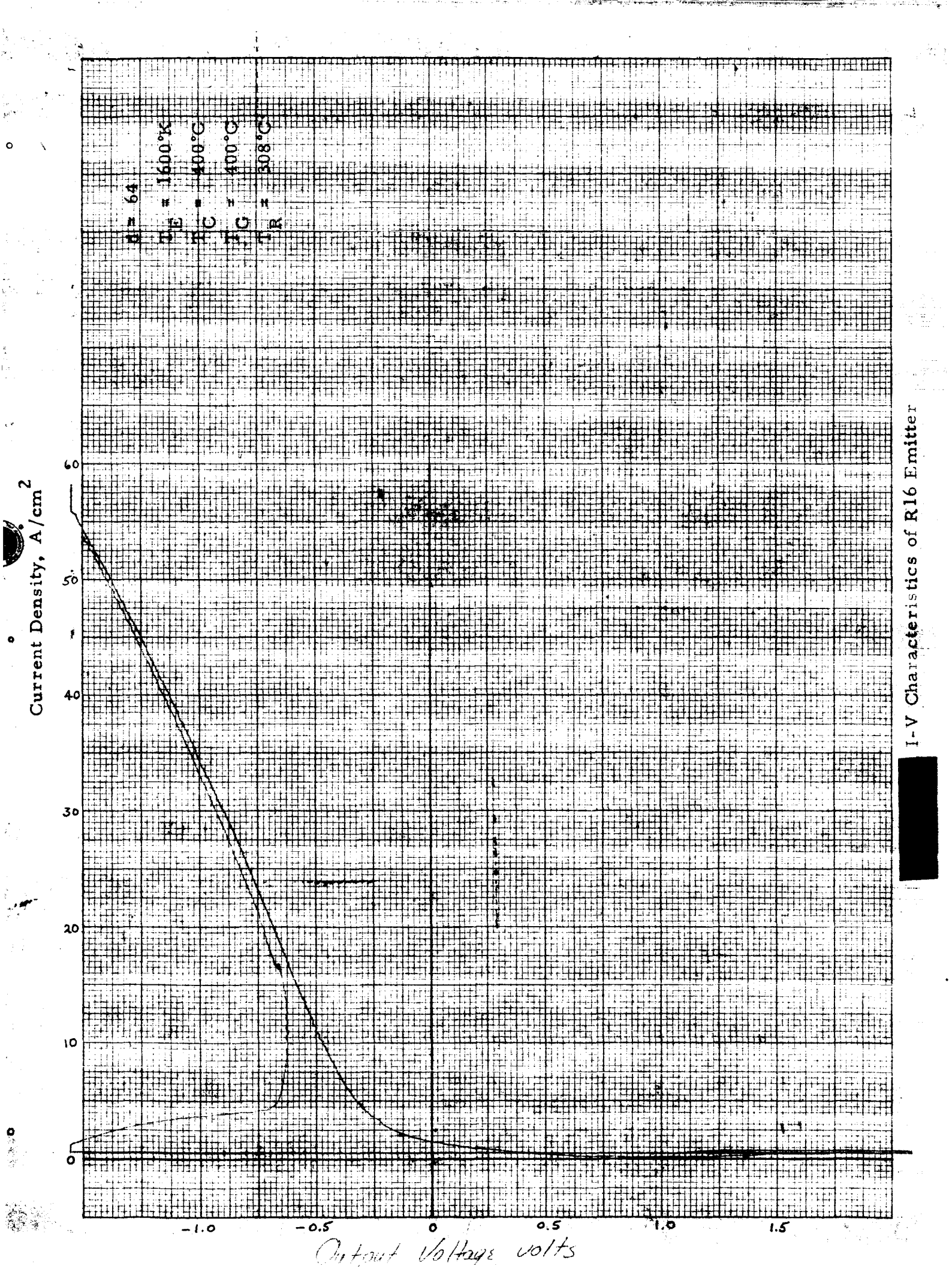

I-V Characteristics of R16 Emitter

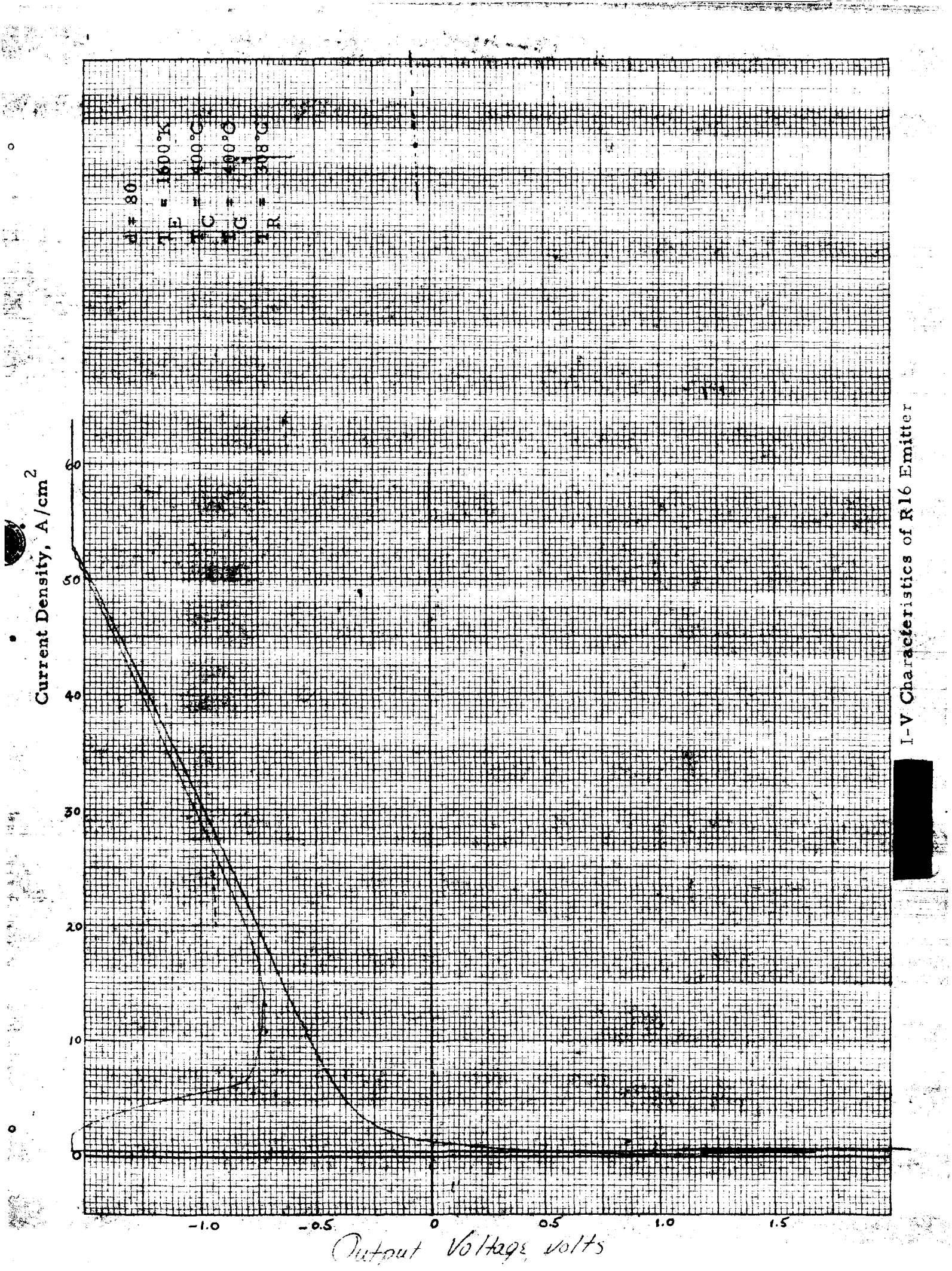

I-V Characteristics of R16 Emitter

APPENDIX G

SELECTED ORIGINAL DATA FROM CESIUM FLUORIDE EXPERIMENTS

This appendix contains selected I-V characteristics which were used to determine the surface work function of the tungsten emitter as described in Chapter IV. Those runs showing curves with alphabetical identification were taken over an interval of time beginning with the curve marked A.

new PURO #1

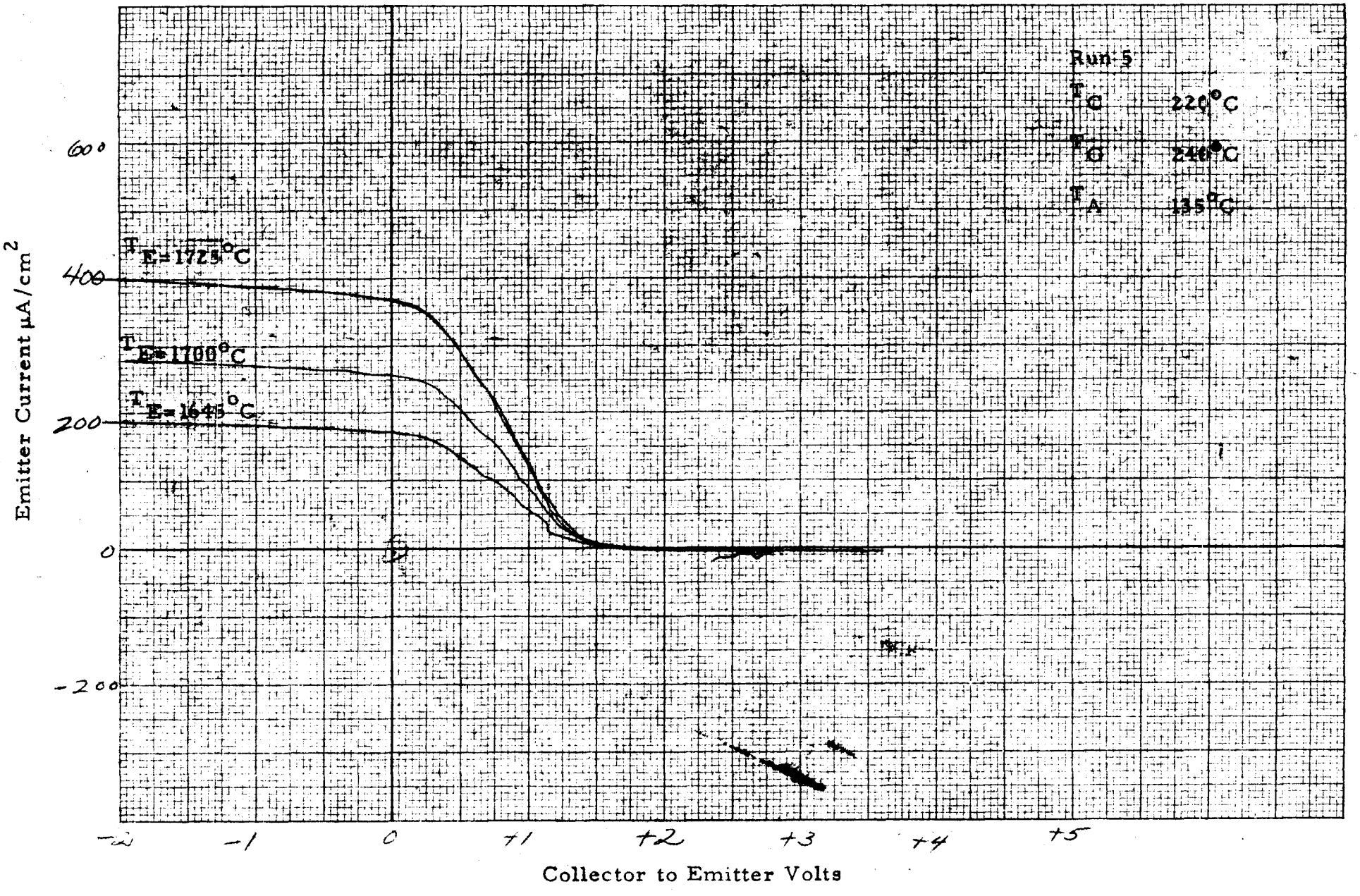
Run 5
T_C 220°C
T_G 240°C
T_A 135°C
T_E=1725°C
T_E=1700°C
T_E=1645°C
600
400
200
0
-200
-2
-1
0
+1
+2
+3
+4
+5
Emitter Current μA/cm²
Collector to Emitter Volts

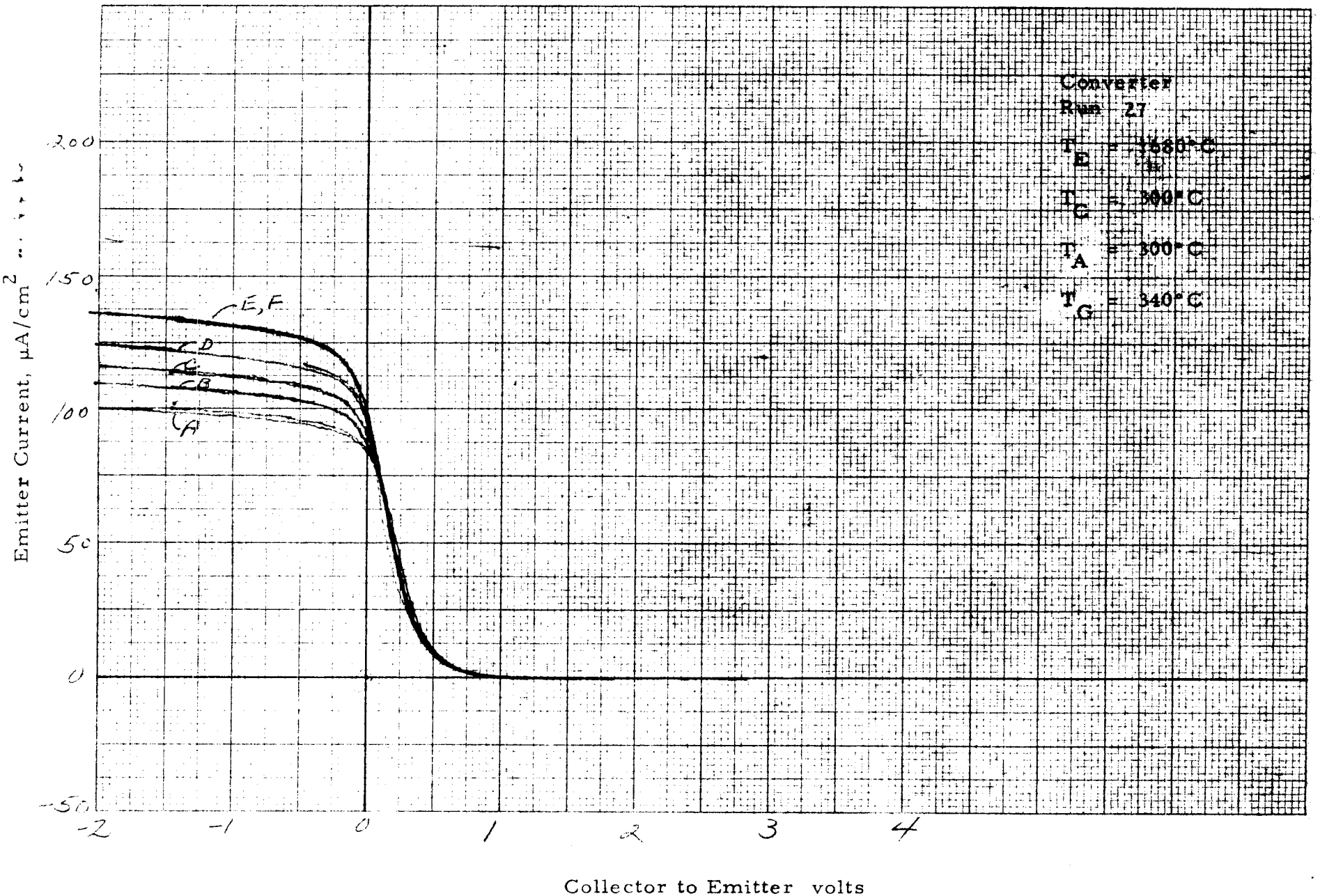
Converter
Run 27
T_E = 1660°C
T_G = 300°C
T_A = 300°C
T_G = 340°C
E, F
D
C
B
A
200
150
100
50
0
-50
-2
-1
0
1
2
3
4
Emitter Current, μA/cm²
Collector to Emitter volts

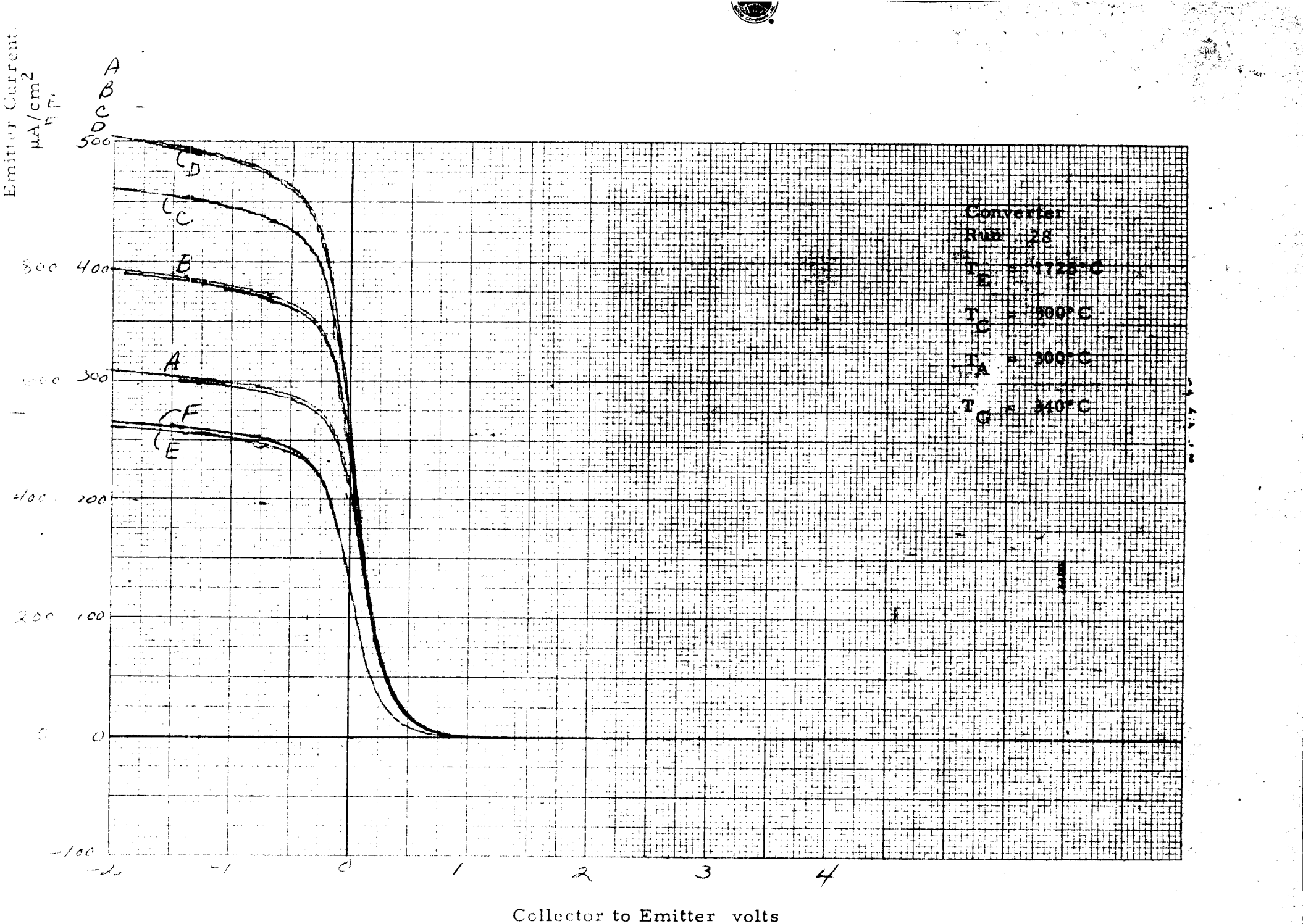
Emitter Current
μA/cm²
A
B
C
D
E
F
500
400
300
200
100
0
-100
-2
-1
0
1
2
3
4
Converter
Run 28
T_E = 1725°C
T_C = 1300°C
T_A = 1300°C
T_G = 1240°C
Collector to Emitter volts

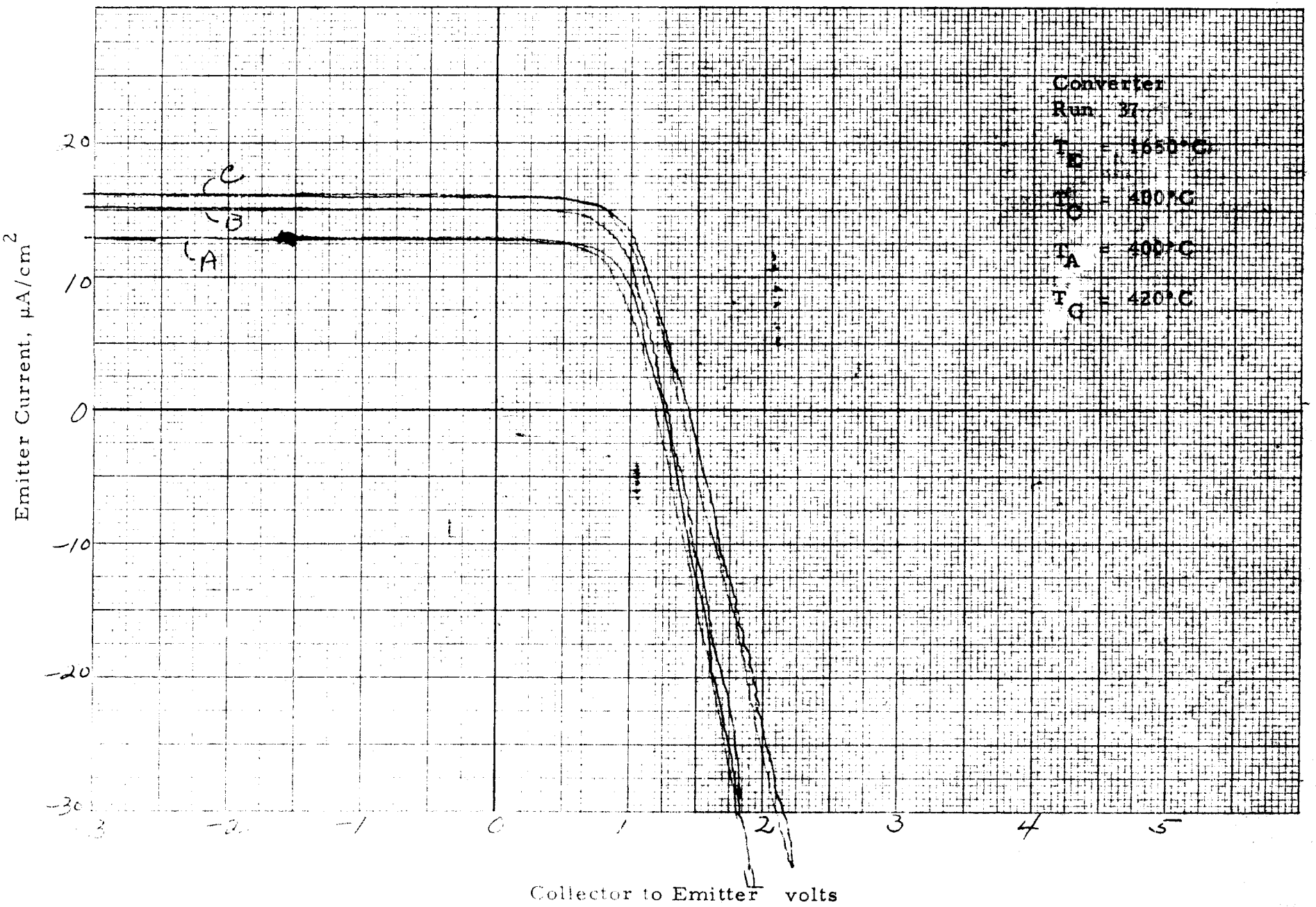
Converter
Run 37
T_E = 1650°C
T_C = 400°C
T_B = 400°C
T_A = 400°C
T_G = 420°C
C
B
A
20
10
0
-10
-20
-30
-3
-2
-1
0
1
2
3
4
5
Emitter Current, μA/cm²
Collector to Emitter volts

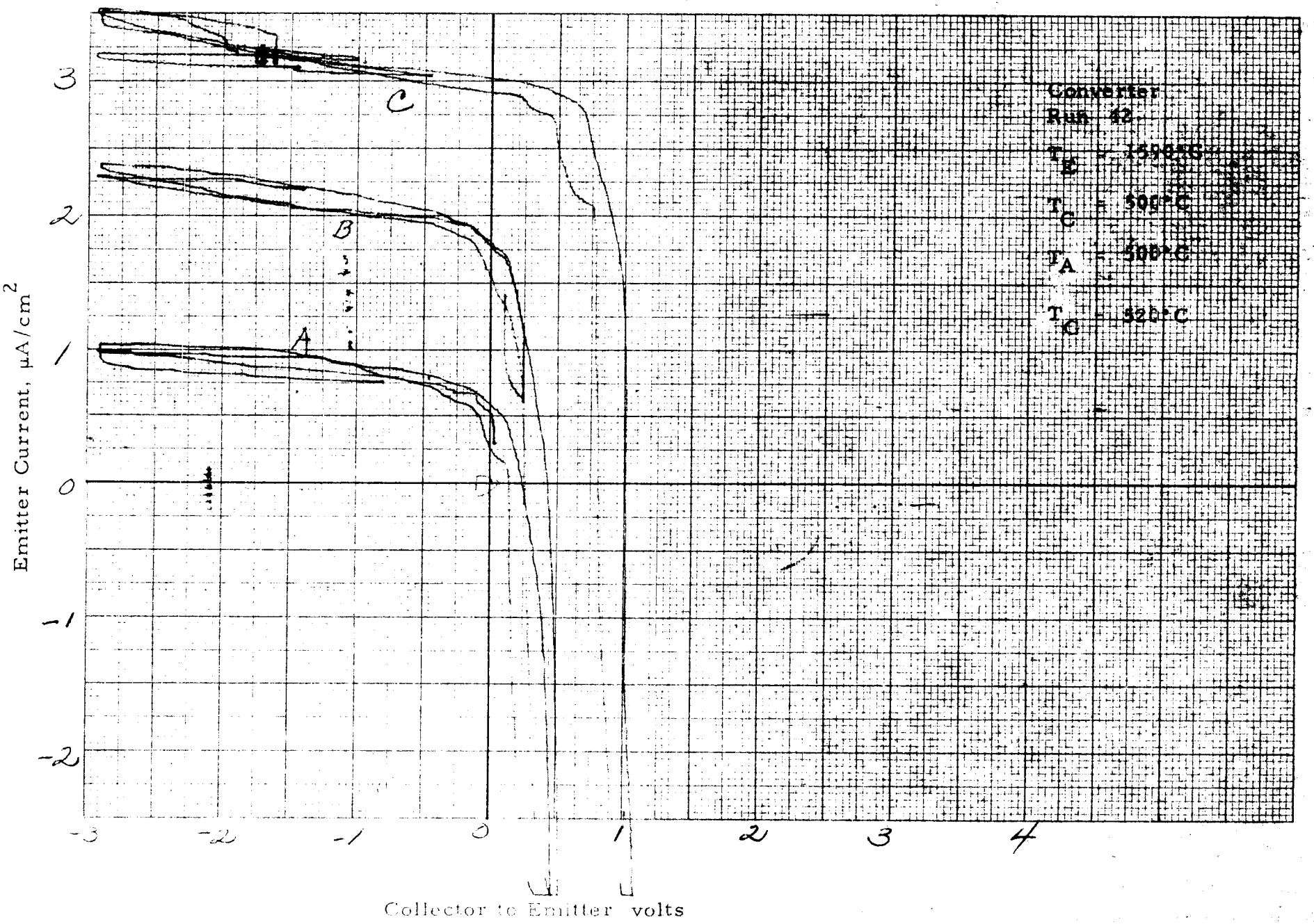
Converter
Run 42
T_E = 1590°C
T_C = 505°C
T_A = 500°C
T_C = 520°C
C
B
A
3
2
1
0
-1
-2
-3
-2
-1
0
1
2
3
4
Emitter Current, μA/cm²
Collector to Emitter volts

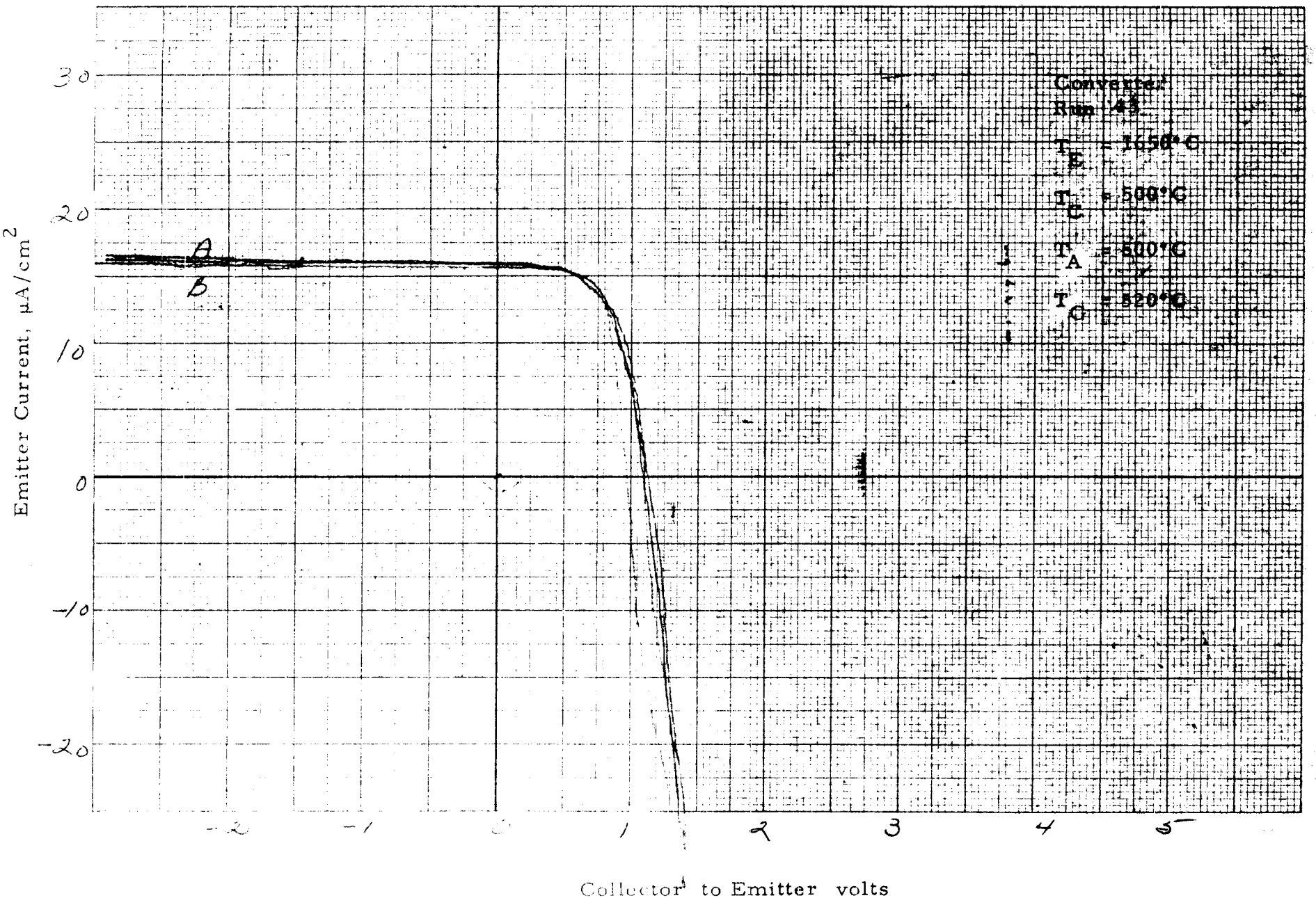
Converter
Run 43
T_E = 1650°C
T_C = 500°C
T_A = 800°C
T_G = 520°C
A
B
30
20
10
0
-10
-20
-2
-1
0
1
2
3
4
5
Emitter Current, μA/cm²
Collector to Emitter volts

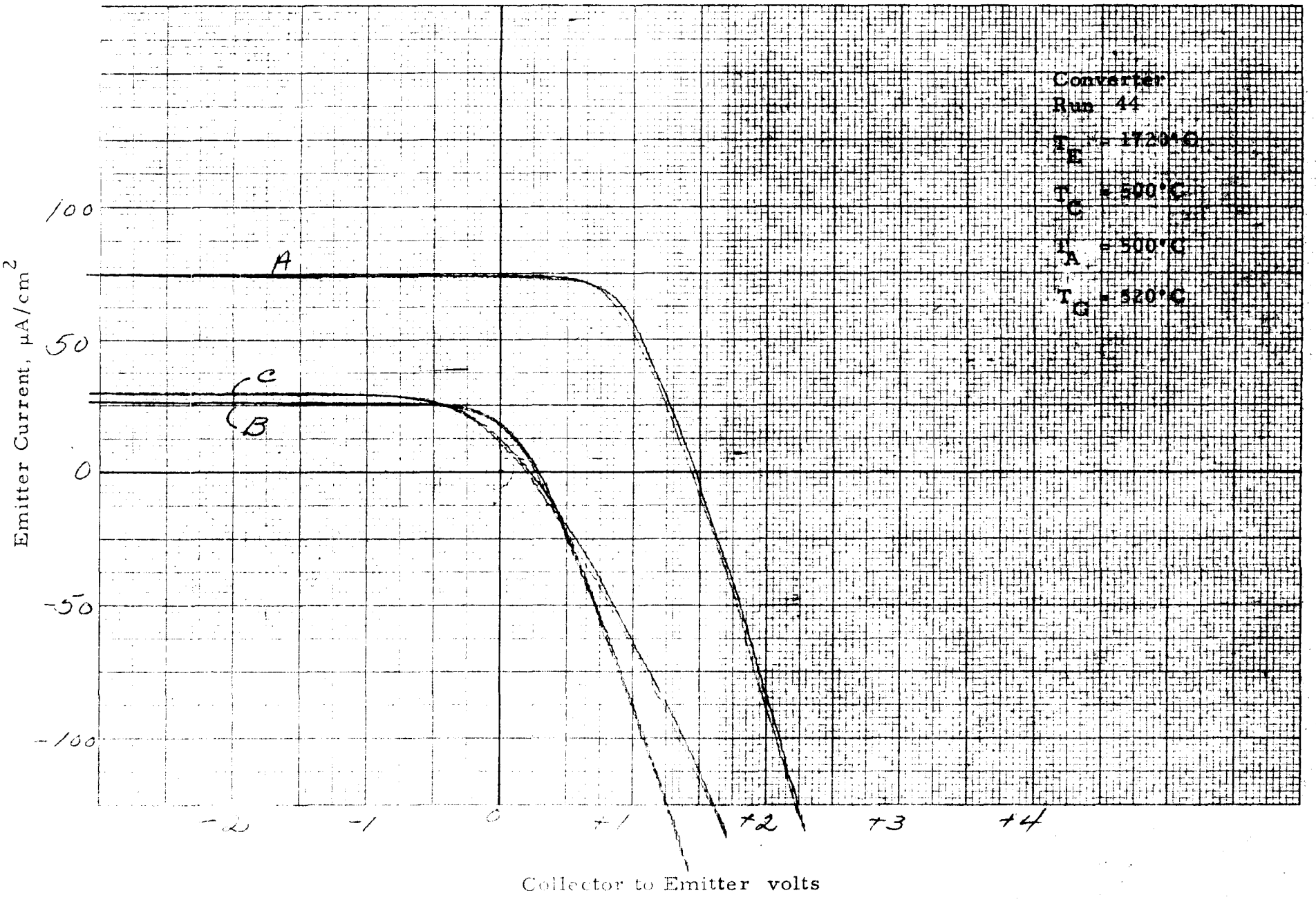
Converter:
Run 44
T_E = 1720°C
T_C = 500°C
T_A = 500°C
T_G = 520°C
A
B
C
100
50
0
-50
-100
-2
-1
0
+1
+2
+3
+4
Emitter Current, μA/cm²
Collector to Emitter volts